A STUDY ON THERMAL BEHAVIOR FOR ELECTRIC-POWERED AERIAL VEHICLES

A THESIS SUBMITTED TO
THE SCHOOL OF GRADUATE STUDIES.
OF
UNIVERSITY OF TURKISH AERONAUTICAL ASSOCIATION

BY

NADEAU IRAKOZE

IN PARTIAL FULFILLMENT OF THE REQUIREMENTS
FOR
THE DEGREE OF MASTER OF SCIENCE
IN
MECHANICAL AND AERONAUTICAL ENGINEERING

AUGUST 2024

A STUDY ON THERMAL BEHAVIOR FOR ELECTRIC-POWERED AERIAL VEHICLES

A THESIS SUBMITTED TO
THE SCHOOL OF GRADUATE STUDIES.
OF
UNIVERSITY OF TURKISH AERONAUTICAL ASSOCIATION

BY

NADEAU IRAKOZE

IN PARTIAL FULFILLMENT OF THE REQUIREMENTS
FOR
THE DEGREE OF MASTER OF SCIENCE
IN
MECHANICAL AND AERONAUTICAL ENGINEERING

SUPERVISOR: Assist. Prof. Dr. Erol GÜLTEKİN

AUGUST 2024

Approval of the thesis:

A STUDY ON THERMAL BEHAVIOR FOR ELECTRIC-POWERED AERIAL VEHICLES

Submitted by **NADEAU IRAKOZE** in partial fulfilment of the requirements for the degree of **Master of Science in Mechanical and Aeronautical Engineering**, University of Turkish Aeronautical Association by,

Assoc. Prof. Dr. Adnan GÜZEL
Dean, **The School of Graduate Studies, UTAA** _____

Assoc. Prof. Dr. Hamit TEKİN
Head of The Department,
Mechanical and Aeronautical Engineering _____

Assist. Prof. Dr. Erol GÜLTEKİN
Supervisor, Mechanical Engineering, UTAA _____

Examining Committee Members:

Assist. Prof. Dr. Erol GÜLTEKİN
Mechanical Engineering, UTAA _____

Assoc. Prof. Dr. Rahim JAFARI
Mechanical Engineering, UTAA _____

Assist. Prof. Dr. Muhammed ELMNEFI
Aerospace Engineering, Ostim Technical University _____

Date: 15.08.2024

I hereby state that the information contained in this document has been gathered and presented in accordance with academic regulations and ethical standards. Moreover, I affirm that I have fully acknowledged and referenced all non-original material and findings as required by these standards.

Nadeau IRAKOZE
Signature:

ABSTRACT

A STUDY ON THERMAL BEHAVIOR FOR ELECTRIC-POWERED AERIAL VEHICLES

Nadeau IRAKOZE
Master of Science, Mechanical and Aeronautical Engineering

Supervisor: Assist. Prof. Dr. Erol GÜLTEKİN
August 2024, 100 pages

This study introduces innovative battery protections specifically designed to enhance thermal regulation in small scale electric-aerial vehicles (EAVs). The system combines air cooling mechanisms with lattice-structured battery pack housings to overcome the limitations of conventional plain sheet battery pack designs. We have developed various novel lattice structures—3D Kagome, Honeycomb, Navtruss and Cross semicircle—that work in tandem with air cooling to improve temperature control. To validate the effectiveness of these designs, 3D kagome lattice was selected for experimental study comparing its thermal performance to that of a plain sheet metal battery pack housing. The battery pack performance was evaluated under different discharge rates of 1C, 2C, and 3C, in a standard room at approximately 28°C, and fan velocities set at 1 m/s, 2.5 m/s, and 5 m/s. The findings revealed that 3D kagome battery protection consistently outperforms the plain sheet by 7.4% at discharge rates of 2C and 3C when cooled at an air speed of 2.5 m/s, and by 3.7% at the same discharge rates with a cooling speed of 5 m/s. The Navtruss protection shows a 3.7% advantage over the plain sheet at discharge rates of 1C and 3C for both air speeds. The Honeycomb structure maintains equivalent performance to the plain sheet across all discharge rates and air speeds. The Cross-semicircle protection exhibits similar performance to the plain sheet at discharge rates of 1C and 2C, but achieves a 3.7% improvement at 3C with a cooling speed of 2.5 m/s.

Keywords: BTMS, Li-ion Batteries, Air Cooling, Lattice Structure, Additive Manufacturing.

ÖZ

ELEKTRİKLE ÇALIŞAN HAVA ARAÇLARININ ISIL DAVRANIŞI ÜZERİNE BİR ÇALIŞMA

Nadeau IRAKOZE
Yüksek Lisans, Makina Mühendisliği

Tez Yöneticisi: Dr. Öğr.Üyesi Erol GÜLTEKİN
Ağustos 2024, 100 sayfa

Bu çalışma, küçük ölçekli elektrikli hava taşıtlarında (EAV) termal düzenlemeyi geliştirmek için özel olarak tasarlanmış yenilikçi pil korumalarını tanıtmaktadır. Sistem, geleneksel düz sac pil takımı tasarımlarının sınırlamalarını aşmak için hava soğutma mekanizmalarını kafes yapılı pil takımı muhafazalarıyla birleştirir. Sıcaklık kontrolünü iyileştirmek için hava soğutmayla birlikte çalışan çeşitli yeni kafes yapıları (3D Kagome, Honeycomb, Navtruss ve Cross yarım daire) geliştirdik. Bu tasarımların etkinliğini doğrulamak için, termal performansını düz sac metal pil takımı muhafazasıyla karşılaştıran deneysel çalışma için 3D Kagome kafesi seçildi. Pil takımı performansı, yaklaşık 28°C'lik standart bir odada ve 1 m/s, 2,5 m/s ve 5 m/s'ye ayarlanmış fan hızlarında 1C, 2C ve 3C'lik farklı deşarj oranları altında değerlendirildi. Bulgular, 3D kagome pil korumasının 2,5 m/s hava hızında soğutulduğunda 2C ve 3C deşarj oranlarında düz levhadan sürekli olarak %7,4 ve 5 m/s soğutma hızında aynı deşarj oranlarında %3,7 daha iyi performans gösterdiğini ortaya koydu. Navtruss koruması, her iki hava hızı için 1C ve 3C deşarj oranlarında düz levhaya göre %3,7'lik bir avantaj göstermektedir. Honeycomb yapısı, tüm deşarj oranlarında ve hava hızlarında düz levhaya eşdeğer performansı korumaktadır. Çapraz yarım daire koruması, 1C ve 2C deşarj oranlarında düz levhaya benzer performans göstermektedir, ancak 2,5 m/s soğutma hızıyla 3C'de %3,7'lik bir iyileştirme sağlamaktadır.

Anahtar Kelimeler: BTMS, Li-ion Piller, Hava Soğutma, Kafes Yapısı, Katmanlı Üretim.

ACKNOWLEDGMENTS

I would like to express my sincere appreciation to my supervisor, Assist. Prof. Dr. Erol Gültekin, for his unwavering guidance, insightful recommendations, and constant encouragement during my research endeavors. I also wish to thank the government of Rwanda and the UTAA scientific research center for their financial backing, which was crucial for the execution of this project's experiments. Furthermore, I am thankful to Prof. Dr. Fatih Şahin for his significant contributions to the experimental setup at Gazi University, and to my colleagues for their daily support and encouragement.

TABLE OF CONTENTS

LIST OF TABLES

LIST OF FIGURES

LIST OF ABBREVIATIONS

BTMS	Battery thermal management system
BTM	Battery thermal management
TMS	Thermal management system
EAV	Electric-powered aerial vehicle
EV	Electric vehicle
SOC	State of charge
SOH	State of health
ECM	Equivalent circuit models
LIBs	Lithium-ion batteries
UAV	Unmanned aerial vehicles
HEVs	Hybrid electric vehicles
HEP	Hybrid electric propulsion
PCM	Phase change material
C-Rate	Discharge rate
CFD	Computational fluid dynamics
CAD	Computer-aided design
MCDM	Multiple criteria decisions making
$LiNiMnCoO_2$	Lithium nickel manganese cobalt (NMC) oxides
Al_2O_3	Alumina
AgO	Silver oxide
EAP	Electrified aircraft propulsion
PTC	Positive Temperature Coefficient
TPMS	Triply Periodic Minimal Surface

LIST OF SYMBOLS

T_{max}	Maximum temperature (˚C)
ΔT_{max}	Maximum temperature difference (˚C)
T_a	Ambient temperature (˚C)
T_i	Inlet temperature (˚C)
T_e	Outlet temperature (˚C)
T_m	Mean temperature (˚C)
T_s	Surface temperature (˚C)
ΔT_{ln}	Log mean temperature difference (˚C)
Pr	Prandtl number
R_e	Reynolds number
N_u	Nusselt number
V	Inlet velocity (m/s)
V_{max}	Maximum velocity (m/s)
D	Diameter of cell casing (m)
H	Height of cell (m)
K	Thermal conductivity (W/mK)
C_p	Specific heat (J/kgK)
N_{ud}	Average Nusselt number
$N_{uD,NL}$	Corrected Nusselt number
h_{air}	Convective heat transfer coefficient of air (W/m^2K)
h_w	Convective heat transfer coefficient of water (W/m^2K)
N	Number of cells
A_s	Surface area (m^2)
Q	Heat generation rate (W/m^3)
I	Battery current (Ampere)
R_i	Internal resistance of the battery (Ω)
ρ	Density (kg/m^3)
D	Diameter (m)
L	Length (m)

CHAPTER 1

INTRODUCTION

1.1 Motivation

Battery power usage is becoming increasingly prevalent, especially in the transportation industry, as systems shift from fuel to electric power to address environmental concerns and reduce greenhouse gas emissions. Maintaining effective temperature control in batteries is vital for maximizing the performance and longevity of EAVs, especially when faced with extreme weather conditions or aerial challenges. Li-ion batteries are designed to function within a range of -20℃ to 60℃, with the ideal operational temperatures being 15ºC to 35ºC as shown in Fig.1. Studies show that at temperatures above 50ºC, charging efficiency and battery lifespan decline significantly. Specifically, Li-ion batteries lose 60% of their capacity after 600 cycles at 50ºC and 70% after 500 cycles at 55ºC [1]

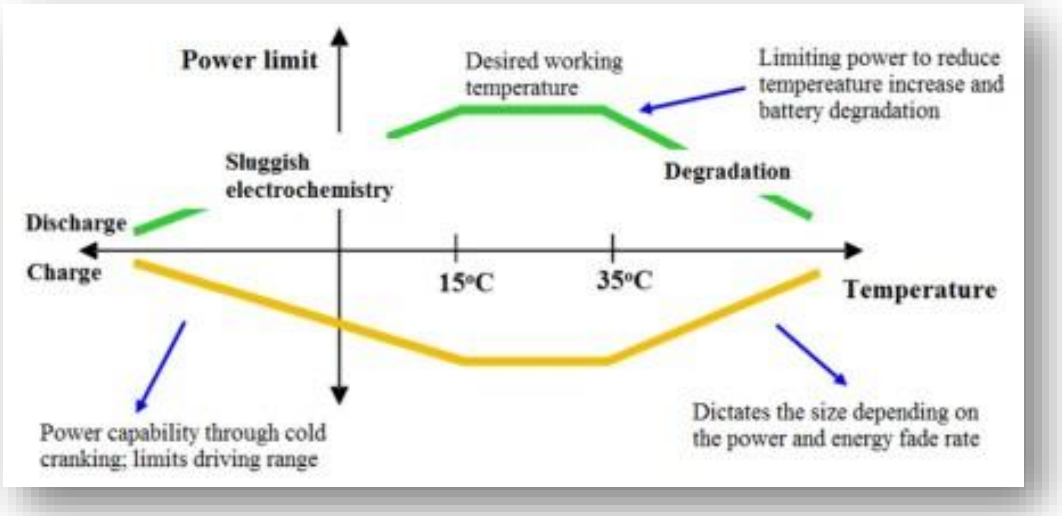

Figure 1. Optimum range for li-ion battery [2]

Without a BTMS, batteries are susceptible to overheating, leading to thermal runaway, fires, or explosions, posing significant safety risks. High temperatures can accelerate battery degradation, reducing lifespan and causing performance inconsistencies due to uneven cell aging. This research was motivated by the growing emphasis on clean energy and carbon footprint reduction in transportation, and the technological advancement on design of sophisticated Battery Thermal Management (BTM) solutions for Electric Vehicles (EVs). Through the implementation of the battery thermal solution proposed in this study, the batteries can be maintained within their ideal temperature range, thereby improving their overall performance, longevity, safety and efficiency. An effective BTMS extends battery longevity by minimizing thermal stress, maintaining uniform temperature distribution to prevent imbalances, and enabling batteries to function efficiently in diverse environmental conditions. [3]

1.2 Aim of Study

The aim of this study is to develop a BTM solution for EAVs with a specific emphasis on enhancing the battery pack protection design. The innovative design aims to enhance thermal dissipation by utilising air cooling method efficiently, without adding too much weight on the aerial vehicle. The analysed and proposed optimal BTMS for EAVs has a focus on enhancing safety of passengers, the vehicle itself, and its surroundings. This consequently contribute to the overall durability of the vehicle. Through a comprehensive review of existing literatures, coupled with analytical, computational and experimental analyses, This study seeks to offer a sustainable solution for air transportation problems usually caused by failures to properly manage excessive heat generated from battery during operations. The study will offer research orientation for engineers and designers who are involved in the development of EVs propulsion systems. The ultimate target is to contribute in the advancement of strategies for the reduction of greenhouse gas emission, dependable energy storage solutions that are being brought out into the aviation sector today. Given the reliance on balance and lightweight designs in aviation, the generated heat from battery cells must be effectively released using air cooling. The specific objectives being:

- Explore the influence of airflow velocity on battery cooling effectiveness.

- Model and produce lattice-structured battery pack protections using a Computer-Aided Design (CAD) tool and additive manufacturing respectively.
- Perform heat transfer simulations using a FEM tool.
- Analyze thermal performance of different lattice battery packs at different air velocities and different discharge rates.
- Compare each new design with the existing plainsheet battery pack.
- Calculate the power required to fly a specific fixed wing model selected.

1.3 Outline of Thesis

This thesis is made up of six chapters. In the initial chapter, the focus is on the motivation for the study and the presentation of the objectives and outline of the thesis. Chapter 2 provides a comprehensive review of the literature, which includes a brief discussion of battery theory, electric aerial vehicles, and BTMS. Chapter 3 describes the materials and methods used in the research, presenting relevant mathematical relations and modeling various lattice structures and a plain sheet metal battery pack in SOLIDWORKS and ANSYS Fluent. Chapter 4 presents and compares the simulation results, while Chapter 5 discusses findings from experimental studies and compares them with the simulations. Finally, Chapter 6 concludes the study and suggests future research directions based on the obtained results.

CHAPTER 2

LITERATURE REVIEW

2.1 Related Works

The swift advancement of electric vehicles has spurred a significant increase in research efforts. As a result, numerous theoretical, numerical, and experimental investigations have been carried out over the past decade to gain a deeper understanding of heat generation in battery packs, and thermal management of battery cells, modules and packs. Following are a summary of the reviewed related works.

The research conducted by Tahhan et al. presented a hybrid BTMS that integrates both air and liquid cooling strategies to improve thermal regulation in compact EV. Preliminary tests conducted without any cooling intervention revealed an uneven temperature profile, with a peak temperature at a discharge rate of 2C. The introduction of an air-cooling mechanism brought this peak down; however, it still led to the formation of localized hotspots due to the retention of heated air at the exhaust. The implementation of the hybrid BTMS markedly enhanced cooling performance and temperature consistency, achieving a 21.04% reduction in maximum temperature compared to natural convection methods. Tests at elevated ambient temperatures (up to 40°C) confirmed the system's robustness and adaptability, suggesting scalability to larger battery systems for broader implementation. The use of a glycol-water mixture and high-performance fans further enhanced thermal distribution and system efficiency, critical for extending battery lifespan and optimizing overall performance in EV applications. [4]

A paper conducted an analysis of 15-series battery modules (27 Ah capacity) to study factors influencing thermal management, such as coolant type, nanofluid ratios,

temperature, and fluid velocity. Researchers found that water (H_2O) exhibited superior thermal conductivity compared to other coolants, making it an effective medium for dissipating heat. Adding nanoparticles to the coolant further enhanced its thermal properties, improving heat dissipation. However, higher coolant temperatures and increased nanoparticle ratios led to higher battery module temperatures. Fluid velocity significantly affected module temperature, with higher velocities improving cooling efficiency but also introducing cost implications. The study highlights the need to balance coolant type, temperature, nanoparticle ratio, and fluid velocity to optimize battery cooling systems, ultimately contributing to enhanced battery performance and longevity. [5]

A study by Maria et al. delved into the thermal and electrical analyses of lithium-ion batteries, employing Al_2O_3 Nano-fluid as the coolant. The model they developed showcased a more effective cooling arrangement, leading to reduced bus bar temperatures. The study observed that augmenting the volume fraction of the coolant resulted in a decline in the temperature of the battery module. Furthermore, the study highlighted the escalating importance of the inlet velocity of the coolant, especially under higher discharge rates. This research underscores the significant influence that different cooling models can have on battery temperature, providing valuable insights for optimizing battery thermal management systems. [6]

Adler et al. explored the employment of thermo-acoustic refrigeration systems for cooling hybrid aircraft batteries, comparing it with conventional vapour cycle systems. They found that the thermos-acoustic system had a lower coefficient of performance than the vapour cycle system. Additionally, the mission profile of the hybrid aircraft did not significantly favour the thermo-acoustic system for battery cooling. The study concludes that further research is needed to fully evaluate the potential of thermo-acoustic refrigeration in this application. [7]

Chapman et.al's paper explores the evolution of Thermal Management System (TMS) for three distinct Electrified Aircraft Propulsion (EAP) concepts: Urban Air Mobility (UAM), regional, and single-aisle markets. The study outlines conventional liquid-based TMS designs tailored to both state-of-the-art and advanced electric component technology levels specific to each EAP concept. The paper aims to compare these TMS

designs, analyze the effects of changing requirements on TMS subcomponents, and develop generalized TMS sizing relations. Key findings indicate that cooling components with lower temperature limits increases TMS weight, and efficiency gains from specific technologies can reduce TMS weight despite stringent temperature limits. The research highlights the significant influence of electrical component efficiencies, vehicle cooling requirements, and operating temperatures on TMS design. [8]

This study by Kim explores the use of phase change materials (PCMs) for BTMSs in electric fixed-wing aircraft. The use of PCMs is essential for controlling the temperature of the battery pack, keeping it within the ideal range, and absorbing heat during take-off. The research emphasizes the significance of PCM's latent heat of fusion for BTMS performance, highlighting its potential as a low-mass solution for flight applications. A numerical model integrating a lumped equivalent circuit and a solid-liquid PCM model was developed to investigate PCM-based BTMS for electric aircraft. The findings suggest that PCMs are a promising solution for maintaining battery temperature in electric fixed-wing flight applications, offering a lightweight and effective thermal management approach. [9]

Benjamin et al discuss the importance of thermal management in hybrid- and all-electric aircraft design. They introduced thermal analysis extensions to open-concept, an open-source toolkit for optimizing aircraft design. This implementation included physics-based capabilities for analyzing and designing thermal management systems. The authors demonstrated how optimizing an aircraft's thermal management system can minimize fuel burn while maintaining component temperatures within acceptable limits. They highlighted that thermal constraints are often overlooked in conceptual aircraft design, and there is a notable lack of publicly available resources for integrating thermal considerations into electric aircraft studies. They showed how integration of time-accurate thermal models into the design optimization process is essential for accurately assessing the impact of thermal constraints on fuel burn and energy usage, and additionally, how different aircraft architectures are variably affected by thermal management system penalties, underscoring the importance of considering these constraints early in the design process.[10]

Gültekin and Mehmet's study investigates the crash resistance of different lattice structures designed to protect battery packs as compared to a standard plane sheet model with a thickness of 1.5mm. There were six different lattice designs which included a novel design cross-semicircular, semi-circular lattices and the topology-optimized model subjected to dynamic compression and impact loading conditions. The research revealed that honeycomb and plain sheet models were able to absorb energy well during dynamic compression while the plain sheet exhibited better specific energy absorption. However, 3D kagome lattice was found to be the best performing for protection against impact on the battery cells. Averaging two loadings, it offered good prospects unlike other types like this. [11]

This research by Gültekin and Yahşi, involved designing of six lattice structures using SolidWorks and their analysis in HyperWorks under static loading. The structure was subjected to a load of 0.2 MPa on the upper cover while the lower cover remained rigid. Each lattice has been assessed for compliance to evaluate its linear static response under the specified external load. The results show that the hexagonal honeycomb lattice is superior in terms of compliance, with a compliance value of 3.82 Nmm, twice as large as other designs, even though it weighs 23% more than plain sheet metal. In terms of mass reduction, the cross semicircle and 3D Kagome lattices have some advantages which suggest they can be quite suitable for weight loss while maintaining structural integrity. This study signifies that advanced lattice structures are very promising for further improvement of battery housing designs in terms of safety and efficiency across different sectors. [12]

Randon's paper provides an overview of the latest advancements and potential future developments in Hybrid-Electric Propulsion (HEP) systems for aviation. The integration of electric and hybrid technologies, such as regenerative fuel cell systems, electric fuel systems, and improved electric actuators, is highlighted as crucial for improving aircraft efficiency, safety, and environmental sustainability. Additionally, the paper discusses the importance of electric active laminar flow control systems in reducing fuel consumption and autonomous distributed air cooling systems for enhanced serviceability. Notably, the utilization of regenerated power during electric taxiing using flywheel batteries is emphasized for their durability and low maintenance requirements. The study also addresses the challenges associated with

implementing these technologies, including power and heat management, as well as the need for new infrastructure and regulatory frameworks to facilitate their adoption. Ultimately, the overarching goal is to significantly decrease fuel consumption and emissions, with the aim of achieving net-zero emissions by 2060. [13]

A study investigates the efficacy of ram-air TMS in the cooling processes of hybrid EVs. The study features a detailed TMS model, incorporating essential components and conducting sensitivity analyses to enhance fuel efficiency. Findings indicate that steady-state cooling during hot-day takeoffs can be achieved with a small puller fan or by oversizing the TMS. This research underscores the importance of well-designed TMS in reducing fuel consumption for hybrid-electric aircraft. By optimizing the TMS, it was discovered that raising the temperature of electric components can eliminate parasitic drag. [14]

The paper by Pesaran et.al, provided a comprehensive literature review of BMS technologies used in electric vehicles. It highlighted the critical functions of BMS, including battery monitoring, thermal management, and safety mechanisms, emphasizing their importance in maintaining battery performance, longevity, and safety. The review covered various state estimation techniques for determining State of Charge (SOC) and State of Health (SOH), discussing methods like Kalman filters, impedance spectroscopy, and neural networks. Additionally, the paper examined advancements in thermal management strategies to prevent overheating and ensure uniform temperature distribution across battery cells. It also explored fault detection and mitigation strategies, underscoring the role of BMS in preventing hazardous conditions like overcharge, over discharge, and short circuits. The review identified challenges in existing BMS technologies, such as the need for improved accuracy in state estimation and the integration of advanced materials for better thermal conductivity. [15]

The research conducted by Saqli et.al provided a comprehensive analysis, modeling, and simulation of a li-ion battery pack composed of three 18650 cylindrical cells, utilizing COMSOL Multiphysics. The investigation focused on two distinct cooling strategies: air-cooling and tube-cooling. Findings from the simulations indicated that tube-cooling demonstrated superior efficiency, effectively maintaining the

temperature of the cells within the optimal operational range at an inlet velocity of 0.1 m/s. The electrochemical-thermal model developed in this study was employed to formulate a second-order Equivalent Circuit Model (ECM) in Matlab, facilitating precise estimations of critical battery states, including SOC and SOH. The overarching objective was to design an effective TMS to guarantee suitable operating conditions for the battery pack. Additionally, the study proposed enhancements to the model, emphasizing the need to account for degradation factors such as hysteresis that influence battery performance. [16]

2.2 An Overview about Li-Ion Batteries

In the category of rechargeable batteries, Li-ion batteries stand out due to various advantages they offer. These batteries can be charged at a fast rate and possess a significantly high specific energy per weight. Furthermore, they are less toxic, boast a prolonged cycle life, and feature a high open circuit voltage. Fig.2 below illustrates chemistries for li-ion batteries.

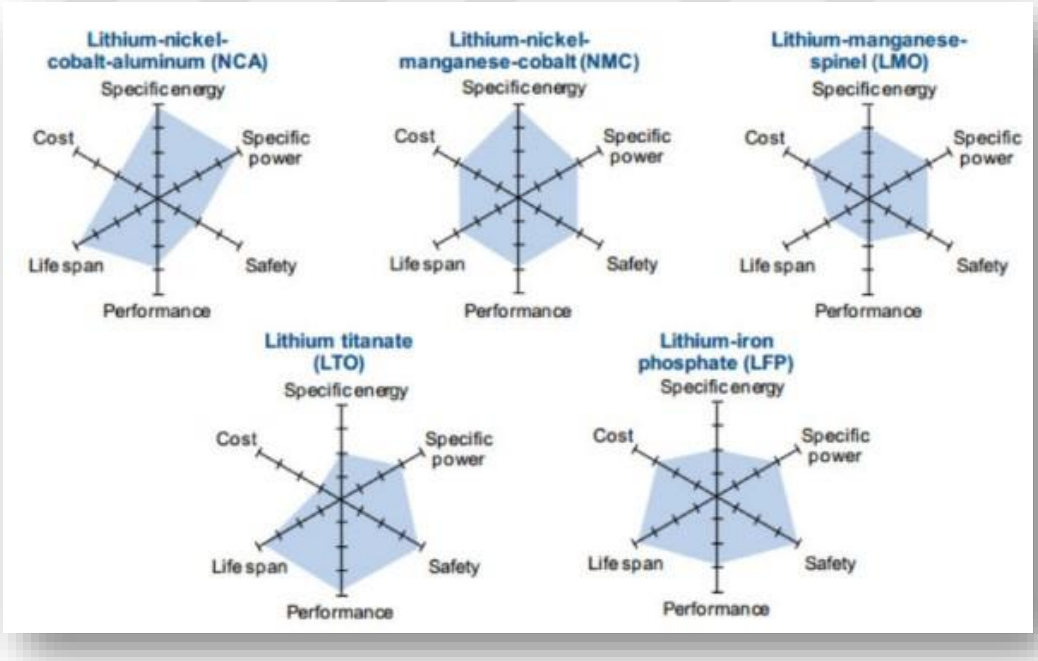

Figure 2. Li-ion chemistries for EV application. [17]

Lithium-ion cells can be categorized into three main shapes: cylindrical, prismatic, and pouch, with each shape having unique construction features.

2.2.1 Cylindrical Battery Cell

Cylindrical battery cells are a classic and widely used type of lithium-ion battery, with common sizes including 18650, 26650, and 21700. They are known for their high energy density, stable performance, and durability. Advantages include consistent output voltage, good mechanical stability, wide temperature tolerance, and mature technology. However, their cylindrical shape leads to inefficient space utilization in battery packs and challenges in battery management due to the need for managing multiple cells. Fig.3 shows parts of a cylindrical cell. [18]

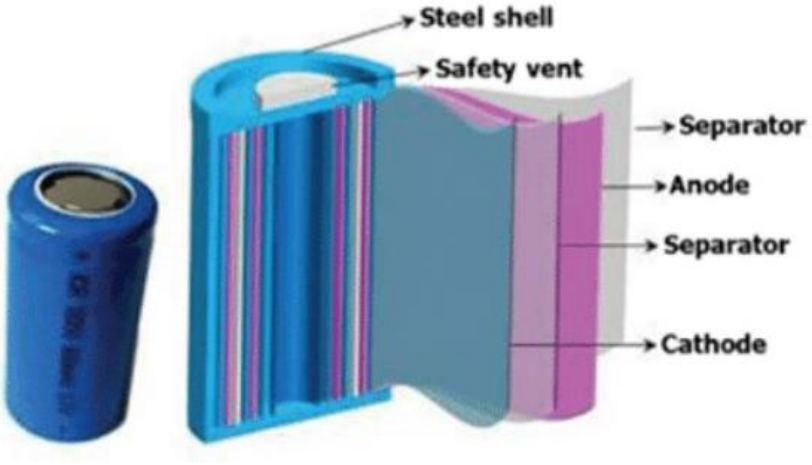

Figure 3. Cylindrical cell [19]

2.2.2 Prismatic Battery Cell

The prismatic battery cell, is a rectangular energy storage unit. This type of lithium-ion battery is made for saving space in electric and autonomous vehicles (EAVs), among others. It has a low-profile structure that resembles a flat box, which helps with thermal management and allows for better packaging within battery packs. There are many advantages to using prismatic cells. For one thing, they have high structural strength and mechanical load capacity, making them durable and reliable in various applications. Another benefit is their low internal resistance that ensures efficient

power transfer leading to prolonged life span of the batteries while minimizing any energy wastage through heat dissipation from the system components during charging or discharging cycles. Moreover, these cells are designed such that maximum volume utilization can be achieved thus resulting into higher storage capacities per given weight or size requirement.

On the other hand, there exist some drawbacks associated with prismatic cells too. The need for different space orientations calls for customization thereby making it difficult to establish universal production methods. In addition to this, although having bigger surface areas allows good air circulation around them hence improving cooling efficiency; still there can be problems related with heat dissipation management particularly when dealing with large number of such units within limited spaces where adequate ventilation may not be possible due to design limitations imposed by other system components' locations relative each other . Also, higher cost production processes accompanied by complex assembly procedures as well as potential increase over time in volume leading later on to weakened walls could compromise structural soundness among other things like swelling after exposure which might affect overall performance reliability characteristics expected from these types of batteries when subjected either intentionally or accidentally unto physical abuse impacts. The prismatic cell is shown in Fig.4 [20]

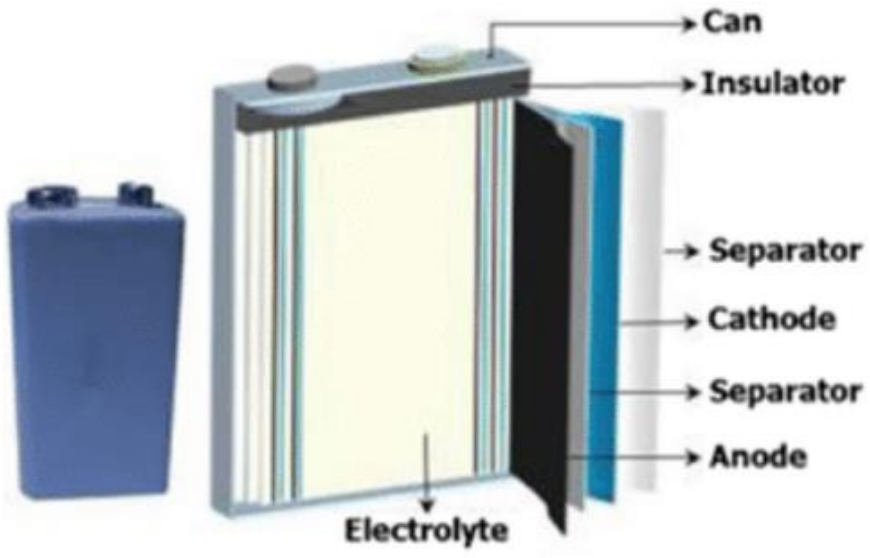

Figure 4. Prismatic cell [19]

2.2.3 Pouch Battery Cell

The pouch battery cell, also known as a laminate pouch cell, is a type of rechargeable lithium-ion battery characterized by its flat, flexible, and lightweight design. It features a laminate pouch or bag constructed from materials like aluminum and various polymers, which contains stacked electrodes (anode and cathode) and electrolyte in a flat configuration. This flexible and sealed design ensures that the electrolyte and electrodes are securely contained. Pouch cells offer several advantages due to their unique design. They are highly valued in applications where flexibility and a lightweight form factor are crucial, such as in portable electronics, electric vehicles (including specific applications like buses and drones), and energy storage systems. One of the significant benefits of pouch cells is their higher energy density compared to cylindrical cells. Additionally, they can be manufactured in various sizes and shapes, allowing for more efficient space utilization within battery packs. However, pouch cells also come with some drawbacks. Their flexible packaging, while advantageous in many respects, makes them more susceptible to physical damage. This vulnerability necessitates careful thermal management to prevent overheating during operation. Therefore, while pouch cells offer impressive design flexibility and energy density, they require attention to durability and thermal control to ensure reliable performance. A pouch cell and its parts is illustrated in Fig.5 [18],[20]

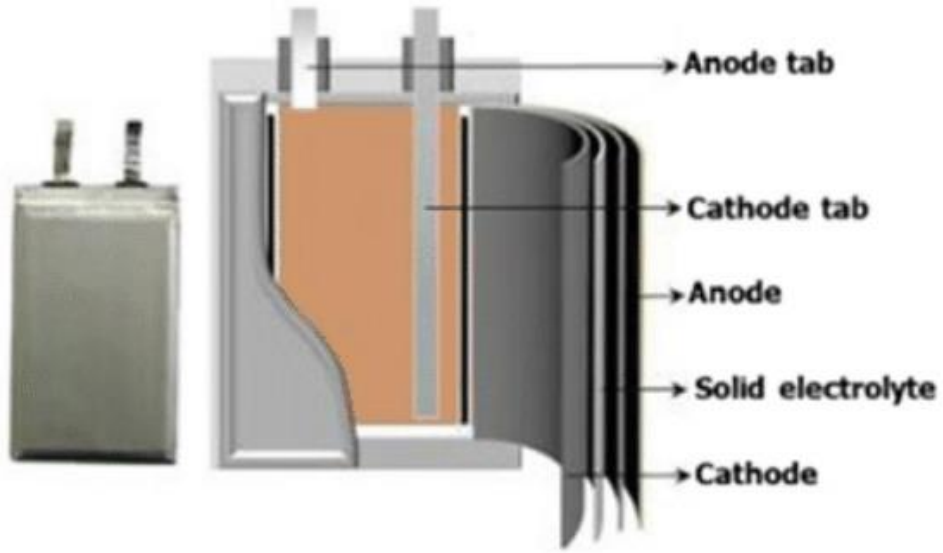

Figure 5. Pouch cell [19]

2.3 Heat Generation and Dissipation in Batteries

The generation of heat in batteries is a result of two main processes: Joule heating and electrochemical reactions that induce alterations in entropy. Joule heating, or resistive heating, arises from the internal resistance present in the battery as electric current passes through it. Electrochemical processes contribute to heat generation through changes in entropy during charge and discharge cycles. As the battery undergoes chemical reactions, there are changes in the state of the battery materials, which can either absorb or release heat, contributing to the overall thermal dynamics of the battery [21]. Eqn.1 illustrates the electrochemical reactions that take place within a lithium-ion cell when the battery is being charged or discharged.

$$\mathrm{LiCo_2} + \mathrm{C_6} \leftrightarrow \mathrm{Li_{1-x}CoO_2} + \mathrm{Li_x C_6} \quad (1)$$

A thorough understanding of battery dissipation mechanisms is crucial for comprehending the thermal behaviors of li-ion batteries. The standard battery structure typically comprises five key elements: the positive electrode (cathode), the negative electrode (anode), the separator, the electrolyte, and the casing. The anode is typically made up of carbon mixtures (e.g., Li_xC_6), while the cathode is commonly constructed from metal oxides (e.g. $LiMn_2O_4$). Lithium batteries, which are filled with electrolyte, exhibit high conductivity for li- ions, enabling their transfer between the cathode and anode, resulting in a series of chemical reactions that produce heat. [22]

2.4 BTMS for EAVs

Development and application of batteries for EVs faces several major challenges, including long charging times, overheating, high costs, in some occasions short circuits, and limited duration of a battery's functionality. It is essential to ensure battery operation within an optimal temperature range, monitor the state of the battery to detect potential failures and deliver alarm messages, and implement measures to suppress thermal runaway propagation. [23]

The process of controlling heat inside a system to maintain safe and reliable operation is known as thermal management. Thermal management helps regulate device or system temperature by eliminating or dissipating excess heat through strategies such

as conduction, convection, and radiation. BTMS are indispensable for EAVs as they ensure the maintenance of optimal battery working temperatures, enhancing safety and extending battery life. BTMS plays a key role in maintaining optimal battery performance by regulating temperatures during charging and discharging activities. Additionally, cooling the battery during fast charging is essential for handling high currents, which in turn supports the efficient and safe operation of the batteries. [24]

2.4.1 Battery Heating

In cold weather conditions, the temperature of battery packs in electric vehicles can fall below the optimal range for operation, which may negatively influence their performance and lifespan. To remedy this situation, a heating technique is utilized to promptly raise the battery pack to the suitable temperature. A common method involves the use of Positive Temperature Coefficient (PTC) heaters. These heaters are particularly efficient as they can quickly generate heat in low-temperature scenarios and automatically modulate their heating output as the temperature increases, ensuring both effective and safe heating of the battery pack. This technique is crucial for maintaining the battery pack within the optimal temperature range, thereby improving its performance and extending its longevity in colder climates. [25]

2.4.2 Battery Cooling

Battery cooling is typically categorized into three groups: air, liquid and PCM cooling methods.

The availability of air is widespread, and it is commonly employed in various industries for the cooling process. This method uses air to dissipate heat generated by electronic components in electrical devices and machines. By experimenting with different inlet velocities, optimal conditions can be determined to keep the cells within a safe temperature range. This method is highly influenced by heat capacity and thermal conductivity of the materials involved.

Air cooling proves to be highly efficient in the initial models of electric vehicles (EVs), yet encounters difficulties in maintaining consistent temperatures in hot climates and

under heavy loads. The process relies on convection, where heat is removed from the battery pack as air passes over it. This technique is straightforward and widely accessible. To improve air cooling for battery thermal management in EVs, key considerations include optimizing air flow channels for even distribution, strategically placing battery cells to maximize exposure to cooling air, and utilizing fans or blowers to increase air velocity for better convective heat transfer. Furthermore, incorporating heat sinks made of materials with high thermal conductivity and adding fins to expand surface area can boost the effectiveness of air cooling, ensuring the battery pack remains at optimal temperatures and extending its lifespan. [26]

Elevating the mass flow rate within air cooling systems results in a notable increase in the heat transfer coefficient, which in turn reduces the maximum temperature rise and enhances temperature uniformity. This boost in cooling efficiency helps maintain battery packs at optimal temperatures, which is crucial for their performance and longevity. However, this comes at a cost: the increased airflow results in higher parasitic power consumption (fans/blowers, etc.), and greater pressure drop, which can elevate operational costs and decrease overall battery efficiency. Balancing these trade-offs is essential for designing effective thermal management systems that maximize cooling benefits while minimizing associated costs and efficiency losses. This can be achieved by implementing structural modifications that do not compromise space utilization, such as using tapered manifolds, varying plenum angles, and incorporating pressure release ventilation. [27]

Air cooling can be achieved through natural convection (passive cooling), or through forced convection (active cooling) as shown in Fig.6. Natural convection relies on the natural rise of warm air and does not require any mechanical assistance. It is simpler and consumes no extra power but has limited cooling capacity and efficiency. In contrast, forced convection uses fans or blowers to actively move air over the battery cells, significantly enhancing heat transfer rates. Forced convection is more effective in maintaining lower and more uniform battery temperatures, especially under high thermal loads, but requires additional energy to operate the fans. [28]

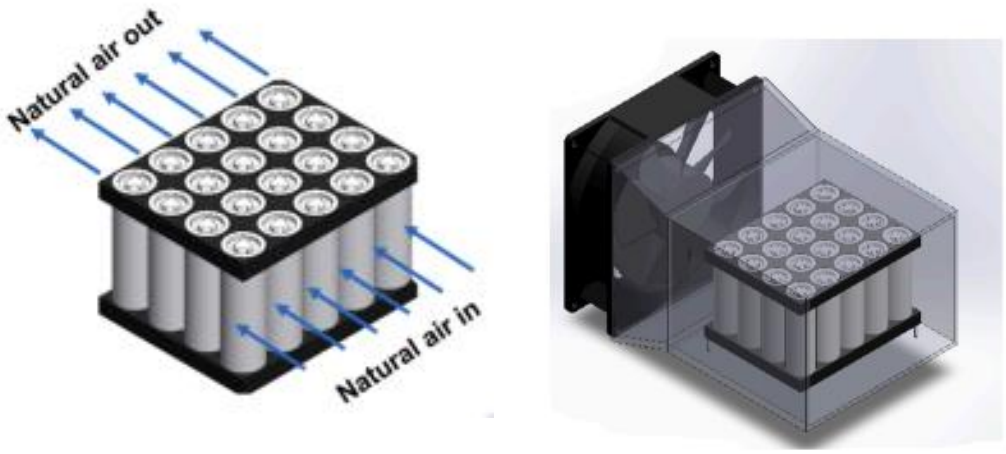

Figure 6. Natural (left) and forced air (right) cooling [29]

Liquid cooling involves passing a liquid coolant through cooling channels located between the cells, allowing it to absorb the heat produced by the cells. Subsequently, the heat is transferred to another heat sink, such as air, via a heat exchanger. There are two main methods of liquid cooling: Indirect and direct cooling.

Indirect liquid cooling uses a cooling medium that circulates through channels or plates near the battery pack, absorbing and dissipating heat through conductive materials like metals or thermally conductive composites, without direct contact with the battery cells. This approach minimizes the risk of electrical short circuits or chemical reactions, enhancing safety, particularly in the event of coolant leaks. It can be optimized by adjusting the inflow velocity and controlling the inlet coolant temperature. Higher inflow velocities improve cooling efficiency by reducing peak temperatures and temperature variations; conversely, higher inlet temperatures result in increased peak temperatures and temperature differences, highlighting reduced cooling efficiency under hot conditions. By combining these methods, the thermal efficiency and safety of the li-ion battery pack are optimized, resulting in reliable performance even in rigorous operating conditions. Fig.7 shows an example of liquid cooled battery by serpentine channels. [30]

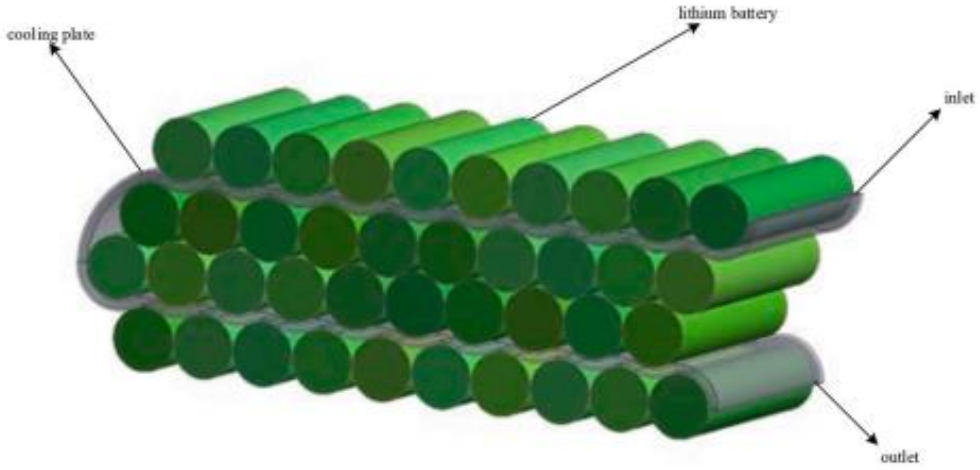

Figure 7. Liquid cooling through an indirect method. [31]

Direct liquid cooling is a technique used to cool batteries by surrounding them with a liquid-filled jacket that absorbs and dissipates heat directly from the battery surface. This method is highly efficient due to the superior heat transfer properties of liquids when compared to air. Cooling fluids like water, water/glycol mixtures, mineral oil, and fluorinated fluids are circulated around the battery to effectively decrease its temperature and ensure uniform thermal distribution. The direct liquid cooling method not only enhances cooling efficiency but also provides a fire suppression function, which is crucial for safety in electric vehicles. Optimizing factors such as gap spacing, flow rate, and the number of cooling pipelines can significantly impact the performance. Fig.8 illustrates a battery that is submerged in a cooling liquid.

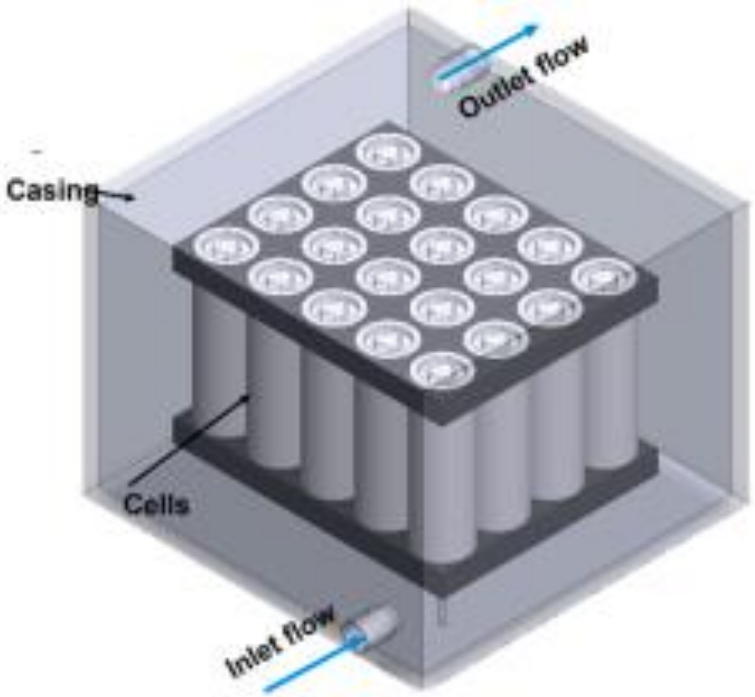

Figure 8. Direct immersion Cooling [29]

PCMs are unique substances that possess the ability to store and release considerable amounts of latent heat during the transition between solid and liquid phases. In battery systems, PCMs are generally integrated within the battery pack or situated in close proximity to the individual cells. As batteries function, they generate heat through the processes of charging and discharging; the PCM absorbs this excess heat, resulting in a phase transition from solid to liquid. This process allows the PCM to effectively dissipate thermal energy from the battery pack. When the heat generation decreases or halts, the PCM solidifies again, releasing the stored heat energy back into the environment or into a cooling mechanism as necessary. This cyclic process of phase change enables PCMs to regulate temperatures effectively and enhance the thermal management of battery systems. Incorporating thermally conductive particles, metal fins, foam, or expanded graphite matrices can help improve PCM performance. Multi-layer PCM configurations are highlighted for reducing system cost and mass, while PCM cooling with liquid is preferred for its efficiency and thermal uniformity. Depicted in Fig.9 is an illustration of a battery pack employing PCM for its cooling mechanism. [32]

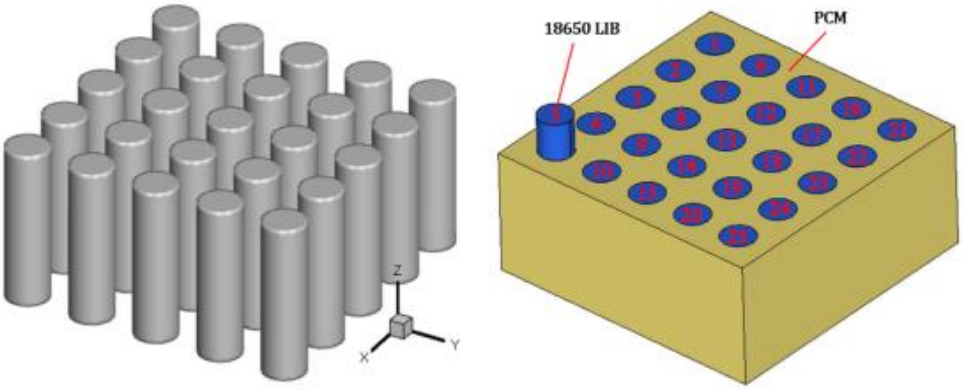

Figure 9. PCM cooling [33]

2.4.3 Design Optimization of the Battery Pack Structure

The novel battery pack design discussed in the article [36] introduces a unique design featuring hollow spoiler prisms. These prisms, comprising four baffles strategically positioned within the battery pack, aim to improve heat dissipation by altering airflow direction and extending flow channels. By increasing the contact area between cells and cooling air, this design enhances overall cooling performance. Moreover, the hollow structure of the spoiler prisms helps reduce material usage and decrease the weight of the battery pack, while also improving its load-bearing capacity. Through simulations, the optimal sizes for the spoiler prisms were determined, considering factors like average cell temperature, power consumption, and additional weight. This new battery pack structure targets the common issue of inadequate cooling in conventional battery packs, especially near the air outlet. Fig.10 is an example of spoiler-prism structured battery pack[34]

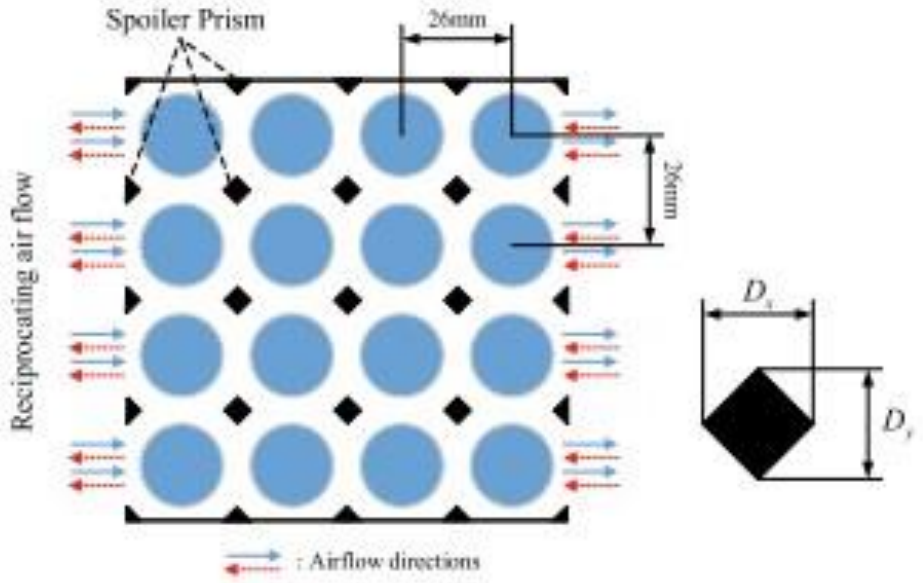

Figure 10. Spoiler prism battery structure [34]

2.4.4 Control Module in BMS

The Control Module within a BMS combines software and hardware to manage, monitor, and optimize battery performance. It focuses on key parameters like SOC, shown in Fig.11, and SOH crucial for reliability and safety in electric vehicles. The software controls operations and analyzes sensor data, while hardware components include sensors for measuring voltage, current, and temperature. Functions include balancing cell voltages, monitoring temperature and current, and ensuring communication between devices. Safety features like over-current and over-voltage protection are integrated. The BMS uses different architectures (modular, centralized, or distributed) to adapt to various needs and challenges. It employs predictive battery models such as ECM and electrochemical models to accurately estimate battery parameters and optimize performance. [35]

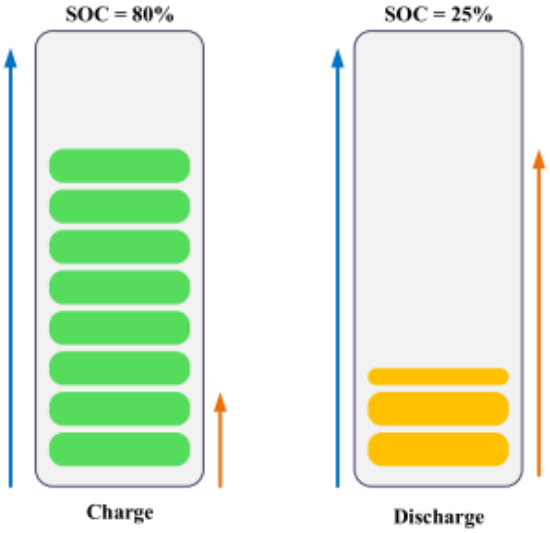

Figure 11. Charging and discharging process [36]

2.4.5 Use of Composite Materials for BTMS

Following studies indicate that using composite materials and novel structural designs can significantly improve the efficiency and effectiveness of BTMS, providing better thermal management for lithium batteries and enhancing their performance and safety.

The research findings from [37] highlight the progress in BTMS made possible by the innovative use of PCMs. The initial study introduces a multilayer composite material that incorporates paraffin wax, copper foils, and graphite to enhance heat dissipation and address the low thermal conductivity of conventional paraffin wax systems. This design leads to a significant reduction in battery temperature rise, especially at higher discharge rates, demonstrating its effectiveness in managing battery heat.

[38] Tackles the challenges of leakage, low thermal conductivity and volume expansion of paraffin based PCMs by developing a composite material that includes expanded graphite (EG) and LDPE. This composite enhances thermal conductivity, manages paraffin expansion, and prevents deformation, resulting in a notable reduction in battery temperature rise.

2.4.6 Battery Housing Design Alteration

Battery housing or battery protection for EVs is crucial for protecting the battery pack while meeting multidisciplinary engineering requirements. They provide several key functions: they shield the battery from external interference, such as impacts from crashes, prevent short circuits by keeping metal objects away from battery terminals, contribute to the battery's cooling system and protect the battery from water damage. The study by Wang et.al [39] introduces an innovative approach using lattice structures, specifically Triply Periodic Minimal Surface (TPMS), to design battery housings that balance mechanical stiffness and efficient thermal management. This method addresses the challenge of low thermal conductivity in traditional materials by embedding thermal convection and conduction considerations into a multi-objective topology optimization framework. Enhanced lattice structures contribute to superior mechanical properties and efficient heat dissipation, rendering them ideal for high energy density batteries essential for advanced applications such as EAVs. This methodology also promotes support-free additive manufacturing, which presents considerable advantages for the EV industry. An example of a lattice-based battery housing is illustrated in Fig.12. [39]

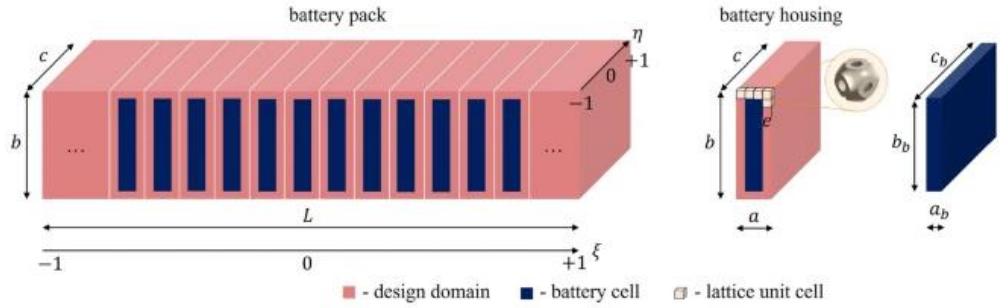

Figure 12. Lattice-based battery housing for EVs [39]

Incorporating aluminum-epoxy hybrid foam materials into battery pack housing design can improve BTMS due to aluminum's high conductivity and the foam's lightweight properties. A sandwich structure with aluminum face sheets and a hybrid foam core offers better heat dissipation and mechanical strength.[40] These materials act as effective heat sinks and provide insulation, preventing thermal runaway. In Fig.13, various classifications of lattice structures are depicted.

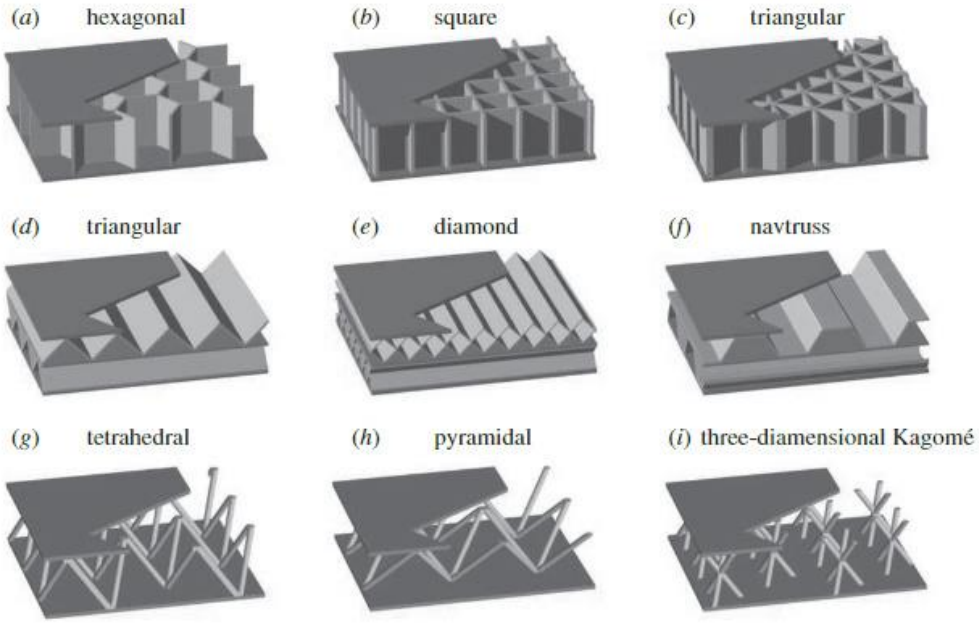

Figure 13. Lattice structure classifications.[11]

CHAPTER 3

MATERIALS AND METHODS

3.1 Material Selection

Heat transfer analysis was performed using ANSYS Workbench for the cylindrical li-ion battery with heat generation boundary condition. The battery pack system is organized in a 3x3 configuration, utilized air as the medium for cooling purposes. Air inlet temperature is 28˚C and the gap between batteries is 2 mm. Fig.14 and 15 shows dimensions of plain sheet and lattice-based battery packs, respectively.

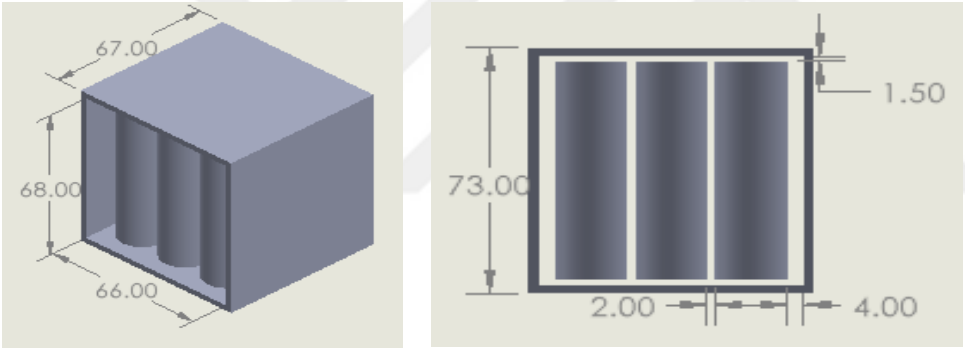

Figure 14. Plain sheet battery pack dimensions

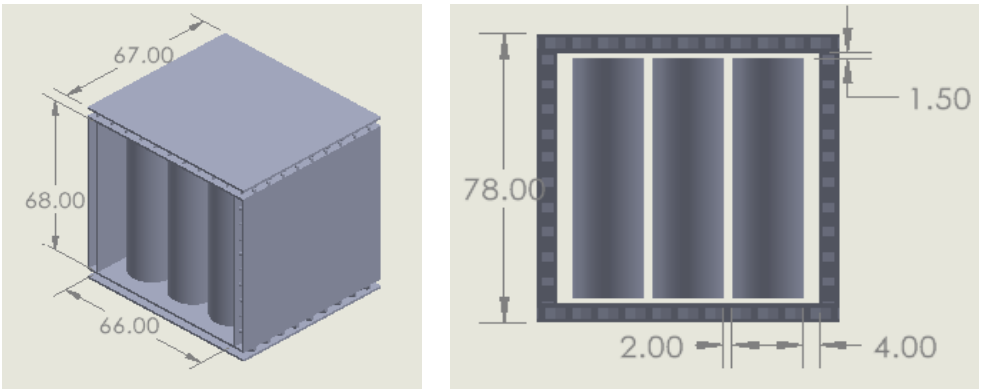

Figure 15. Lattice-based battery pack dimensions

Different types of lattice structures investigated in this study including prismatic, honeycomb, and truss-based designs are shown in Fig.16. Prismatic lattices are characterized by triangular or diamond corrugations, while honeycomb structures consist of webs forming triangular, square, or hexagonal cells. Truss-based lattices are composed of struts meeting at nodes with different cross-sections and angles, resulting in improved mechanical performance. The research specifically focused on evaluating 3D kagome, honeycomb, cross semicircle, and navtruss lattice structures, all with the same dimensions: 76mm width, 78mm height, and 67mm depth. Each lattice strut was designed with a strut diameter of 1.18mm and a joint angle of 45°, while the honeycomb structure had a wall thickness of 1.68mm. These lattices were arranged on a 1mm thick plate to create a sandwich panel, as opposed to a 2.5mm thick plain sheet metal used as a reference in the market.

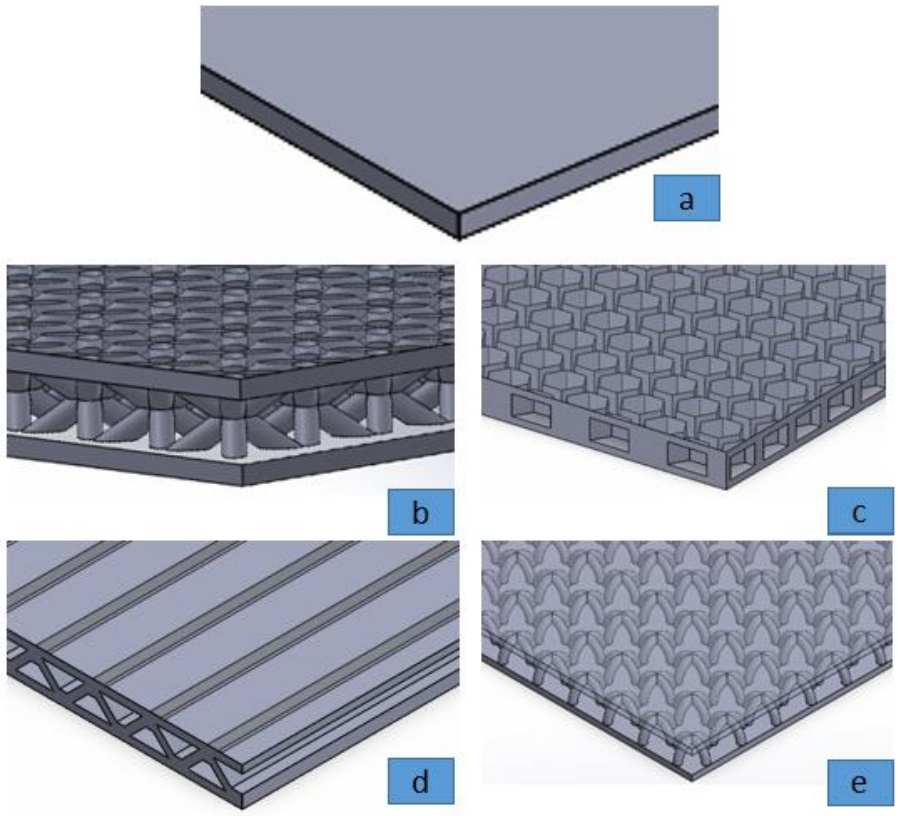

Figure 16. The various structures designed are as follows: (a) Plain sheet, (b) 3D Kagome lattice, (c) Honeycomb lattice, (d) Navtruss lattice, and (d) Cross-semicircle lattice.

Battery pack protection employs plain sheet aluminum made from 6061-T6. It is a strong, lightweight material used for controlling thermal conditions. Aluminum 6061-T6 has high thermal conductivity so it easily dissipates heat away from hot spots in the battery pack. Although plain sheets of aluminium conduct heat well they do not facilitate optimum air flow which may lead to inadequate cooling thereby causing some regions to become excessively hot if additional cooling methods are not put in place.

The 3D kagome lattice structure is a novel geometric framework aimed at enhancing thermal management of batteries packs. This design was selected because its unique arrangement consists interconnected triangular and hexagonal cells which significantly improves both airflow and thermal conductivity. The main objective behind this lattice system is to increase surface area that allows for more even distribution of cooling air throughout battery pack while maximizing heat dissipation through the same space.

Honeycomb battery pack protection system uses hexagonal cells arranged in a geometric pattern to improve safety and efficiency levels. Efficiency is increased by optimizing thermal management through enhanced airflow as well as improved heat dissipation towards maintaining safe operating temperatures within them. Moreover, honeycomb design provides lightness together with strength thus ensuring structural integrity without adding extra weight especially where there are high performance demands on safety standards.

The cross-semicircle battery pack protection adopts lattice design consisting interlinked semi-circular cells which greatly enhances thermal management capabilities. This particular structure increases the amount of surface area available for dissipation of heat within the battery packs while at the same time improving on internal circulation of air meant for cooling purposes. Its semicircular configuration encourages efficient transfer of heat between different parts through better convection current establishment around them hence leading to uniformity in terms of temperature distribution across these materials During high-performance applications such as these where lots energy needs to be supplied fast then there must be an optimization between dissipating power evenly over large areas or localized regions only.

Navtruss lattice battery protection system enhances thermal management through a complex arrangement of interlocking triangular trusses. These trusses create an open and rigid framework for efficient heat dissipation which prevents hot spots from occurring within the pack by promoting uniform cooling across all its parts. The lattice also helps to maintain safety levels in high performance applications where large amounts of energy are required thus ensuring that batteries operate within their optimal temperature ranges.

3.2 Numerical Modeling

In order to conduct a numerical heat transfer analysis utilizing ANSYS workbench software, a mathematical model is constructed to encapsulate the fundamental physics of the issue at hand. Different battery packs are used in ansys fluent to evaluate thermal performance of air cooled li-ion battery module using both natural and forced convection under various air inlet velocities and discharge rates.

Nonlinear thermal analysis accounts for temperature-dependent material properties, varying boundary conditions, and radiation effects, while transient analysis involves time-stepping to address dynamic thermal conditions. In contrast, the thesis focuses on linear, steady-state thermal analysis, where material properties are constant and radiation is excluded, assuming that the temperature distribution and thermal flows stabilize and remain constant over time. [41], [42]

The models incorporates the governing equations, relevant input variables, and their interrelations. It also addresses the initial and boundary conditions tabulated in Table 1, along with permissible variations in accordance with the governing equations Eqn.2 to Eqn.4. Additionally, the model is specifically designed to meet the objectives of the analysis by establishing constraints and outlining the appropriate methodology.

Table 1. Initial and boundary conditions for simulations

Parameter	**Value**
Ambient temperature T_a	28°C
Inlet air velocity for natural convection	0.001m/s
Inlet air velocity for forced convection	1, 2.5 and 5m/s
Convective heat transfer coefficient of air for natural convection	5W/m^{2}K
Convective heat transfer coefficient of air for forced convection	10W/m^{2}K

The finite volume method is employed to calculate numerical solutions for the governing equations under the following assumptions: the air flow is laminar and incompressible, the thermo-physical properties of materials are constant, heat transfer through radiation is neglected, and the vent assembly and battery cell coating materials are excluded from consideration.

Governing Equations:

Provided below are the equations for continuity, momentum, and energy conservation equations.

Continuity equation:

$$\frac{\partial \rho}{\theta t} + \nabla.(\rho \vec{u}) = 0 \tag{2}$$

Momentum conservation equation:

$$\frac{\partial \vec{u}}{\theta t} + (\vec{u}\nabla)\vec{u} = -\frac{\nabla \mathrm{p}}{\rho} + \frac{\mu}{\rho}\nabla^2 \vec{u} \tag{3}$$

Energy conservation equation:

$$\frac{\partial}{\partial t}\left(\rho C_p T\right) = \nabla.(\mathrm{k}\nabla \mathrm{T}) + Q_{gen} \tag{4}$$

where Q_{gen} is the heat generation of the battery, ρ is the density, k is the thermic conductivity, C_p is the heating capacity, and T is the temperature.

The heat generation in the battery Q voltage-based is defined by Eq.5: [22]

$$Q = \frac{1}{V}\left[I^2 R_i + IT\frac{dU_o}{dT}\right] \quad (5)$$

where Q is the rate of heat generation, V is the battery volume, I is current, R_i is the internal resistance of the battery, T is the battery temperature, and $T\frac{dU_o}{dT}$ is the entropic heat coefficient and its value could be set as 0.01116.

The heat generation rates and the heat fluxes used in the simulations, were calculated at different dicharge rates and the values are represented in Table 2. Cells are treated as the sole heat source.

Table 2. Heat generation rate and heat flux at 1C, 2C and 3C.

Parameters	**Values**		
Discharge rate (C-rate)	1	2	3
Battery Current (A)	2.9	5.8	8.7
Heat generation rate (W/m^3)	12131.8	44611.9	97440.25
Heat flux (W/m^2)	48	176.34	385.152

The research employs various battery discharge rates including 1C, 2C and 3C, along with air inlet velocities of 1, 2.5 and 5 m/s using a laminar model and SIMPLE algorithm for velocity-pressure coupling. The mesh is created in ANSYS with mesh size of 0.7mm. A PRESTO! scheme is selected to achieve greater accuracy in solving for natural convection.

The quality of the mesh in the simulations was assessed by analyzing the average skewness. Skewness indicates the extent to which the mesh cells deviate from their ideal shapes, which can have a significant impact on the accuracy and stability of the numerical solutions. By evaluating the average skewness throughout the mesh, we ensure that the computational grid was appropriately refined and well organized to accurately capture the physical phenomena being simulated. As shown in table 3, a

lower average skewness reflects a higher quality mesh, with cells that are more aligned with optimal shapes, thereby increasing the reliability of the simulation findings.

Table 3. Skewness range and the mesh quality

Skewness	Cell Quality
1	Degenerate
0.9 - 1.0	Bad
0.75 – 0.9	Poor
0.5 – 0.75	Fair
0.25 – 0.5	Good
> 0 – 0.25	Excellent
0	Equilateral

In Table 4, battery pack geometries are displayed alongside the average skewness values that were derived from the study.

Table 4. Battery packs and their average skewness values

Geometry	Skewness
Plainsheet	0.2
3D kagome	0.19
Honeycomb	0.2
Navtruss	0.22
Cross semicircle	0.23

Heat Transfer Performance Evaluation

Three dimensionless parameters, choosing the unit cell height (h) as the characteristic length, are defined in order to assess the heat transfer performance and flow resistance

of the truss-cored lattices over a wide range of airflow velocity. Such are: The Reynolds number , the Nusselt number , and the pressure drop coefficient .

The Reynolds number is defined by Eqn.6:

$$Re_H = \frac{\rho_f U_m h}{\mu_f} \tag{6}$$

The Reynolds number (Re) is a fundamental parameter for determining the flow regime of a fluid. Turbulent flow is characterized by its chaotic and irregular behavior, which results in considerable mixing and momentum transfer. In a transitional flow regime, the flow demonstrates properties that are intermediate between laminar and turbulent, indicating a potential transition to turbulence. In laminar flow, is characterized by the smooth movement of fluid in organized layers with minimal mixing and predictable behavior. Table 5 shows the flow types according to the Reynolds Number.

Table 5. Flow types and Reynolds Number

Reynolds number	**Fluid flow types**
Re > 4000	Turbulent
2300 < Re < 4000	Transitional
Re < 2300	Laminar

Based on the air property tables and charts, at 1 atm pressure air properties, the density and dynamic viscosity are calculated using linear interpolation and found to be 1.172 kg/m³ and 1.8628×10^{-5} kg/ms, respectively. The characteristic length is given by the height of the cell. Table 6, represents the relationship between fan produced air velocities and the calculated Reynolds Number.

Table 6. The dependence of the Reynolds Number on velocity

Velocity (m/s)	**Re_H**
1	1006.66
2.5	2516.64
5	5033.28

When the flow velocity is set at 1 m/s, it is identified as laminar flow, while at 2.5 m/s, the flow is categorized as transitional. At a higher velocity of 5 m/s, the flow becomes turbulent.

The Nusselt number is defined by Eqn.7:

$$Nu_H = \frac{d_p h}{k_f} \tag{7}$$

The pressure drop coefficient is given by Eqn.8:

$$f_H = \frac{\Delta P}{L} \frac{h}{\frac{\rho_f U_m^2}{2}} \tag{8}$$

where ρ_f, μ_f and k_f are the density, the dynamic viscosity and the thermal conductivity of air, respectively. U_m is inlet velocity, ΔP refers to the pressure drop and d_p is the heat transfer coefficient defined in Eqn.9 as:

$$d_p = \frac{Q}{A_{up} \Delta T} \tag{9}$$

where A_{up} is the area of the heating surface. For the iso-temperature boundary condition, Q is the heat flux the temperature difference ΔT is defined by Eqn.10 as:

$$\Delta T = \frac{(T_w - T_{in}) - (T_w - T_{out})}{\ln\{(T_w - T_{in})/(T_w - T_{out})\}} \tag{10}$$

where T_{in}, T_{out} and T_w are temperature at the inlet, outlet and bottom endwall.

Material Properties

Table 3 provides an overview of the specifications associated with the NMC cells that were employed.

Table 7. Specifications of NMC cell. [43]

Cell properties	**Specifications/Values**
Brand	Aspilsan
Chemistry notation	NMC
Chemistry	$LiNiMnCo0_2$
Weight (g)	45.9
Density ρ (kg/m^3)	2775
Specific heat capacity C_p (J/kg K)	880
Thermal Conductivity K (W/m K)	3
Maximum voltage (V)	4.2
Diameter of cell (mm)	18
Height of cell (mm)	65
Nominal capacity (mAh)	2900
Nominal voltage (V)	3.65

The characteristics of aluminum 6061-T6, which are utilized in the simulations pertaining to the battery pack, are detailed in Table 4.

Table 8. Properties of Aluminum 6061-T6 used. [44]

Battery housing	**Aluminum**
Brand	Aluminum 6061-T6
Specific heat capacity (J/kg K)	895
Density (kg/m^3)	2700
Thermal Conductivity (W/m K)	167

3.3 Experimental Validation

To validate the numerical solutions, an experimental investigation was conducted to measure the temperature of NMC cells during discharge.

The lattice parts were produced using the Concept Laser M2 Cusing shown in Fig.17, which employs Selective Laser Melting (SLM) technology with a 400W Ytterbium (Yb) fiber single laser. The system has a build volume of 250 mm x 250 mm x 230 mm (W x L x H) and operates in an inert atmosphere of argon or nitrogen. The metal powders used by the machine could be Ti6Al4V, AlSi10Mg, Stainless Steel 316L, Inconel 625, and Inconel 718. For this study's experiments, AlSi10Mg was used.

Figure 17. Concept Laser M2 Cusing production machine [45]

In the experimental setup shown in Fig.18, a DC power supply was utilized to charge the battery pack. Equipped with temperature sensors, the battery pack is then integrated into the system to monitor its thermal performance during operation, by reading temperatures at different pack spots. Data acquisition and control are managed by a computer, and a PID based control system supervising the entire discharge process. Varying air speeds of 1, 2.5, and 5 m/s were generated using a fan to cool the battery pack, with a motor driving the fan to ensure a steady airflow for efficient heat dissipation. Electrical parameters such as voltage and current were monitored using

multimeters throughout the experiment. To simulate load conditions for the battery pack, discharge lamps were employed.

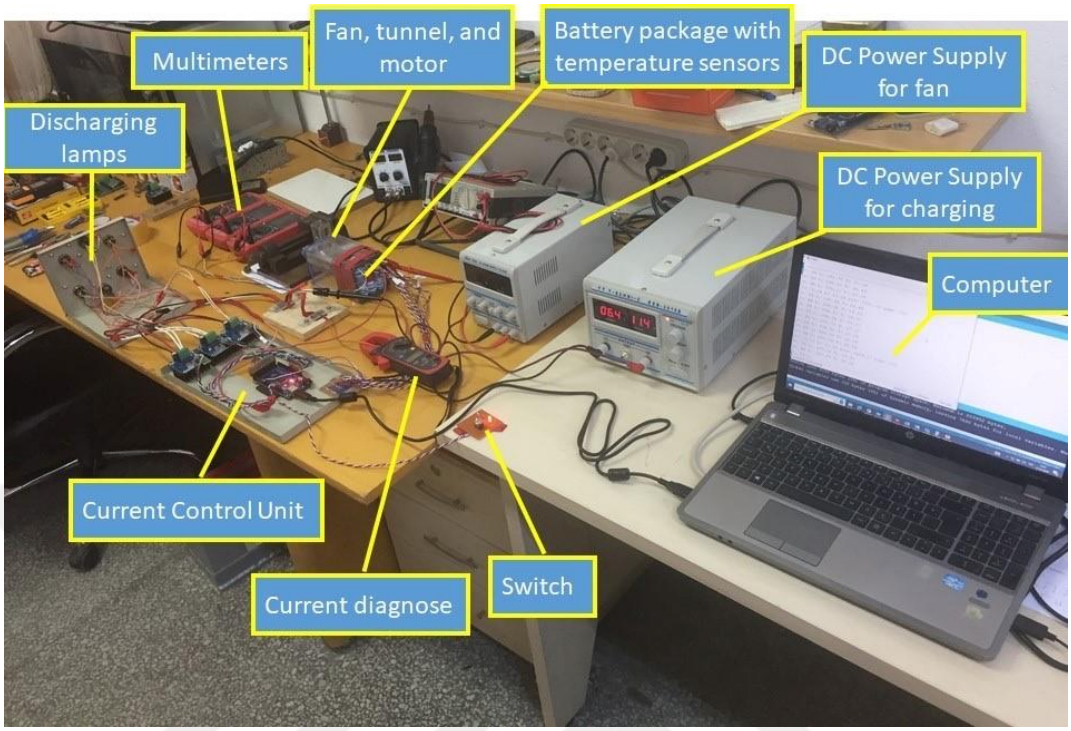

Figure 18. The setup for experimentional test of the models

Following in Fig.19 and Fig.20 are the produced model parts, using additive manufacturing. The models were used for experimentation.

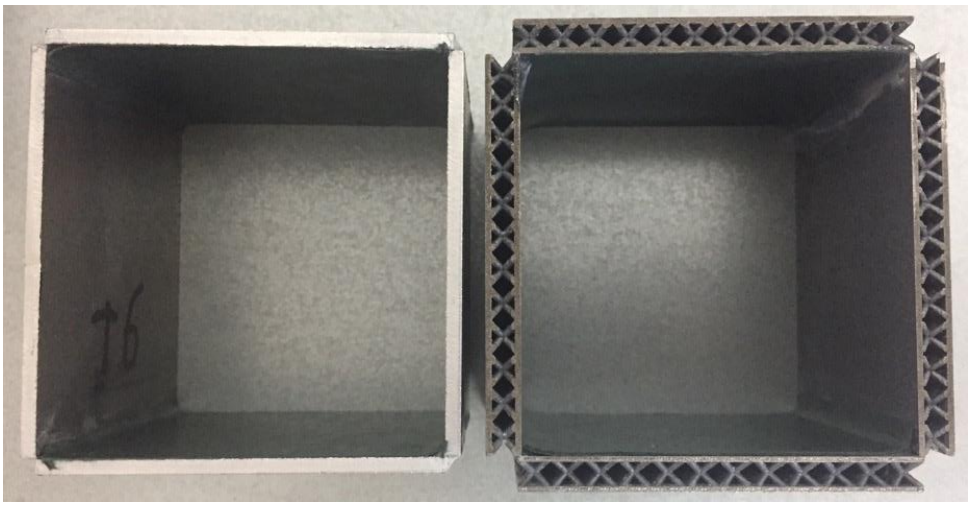

Figure 19. The produced plainsheet (left) and 3D kagome (right) battery packs.

Using additive manufacturing in fabricating lattice structures facilitates the production of intricate geometries that are challenging or unattainable using traditional

techniques. The reason to design and manufacture customized lattice configurations is that it enhances the performance of battery packs in terms of weight reduction, thermal management, and structural integrity.

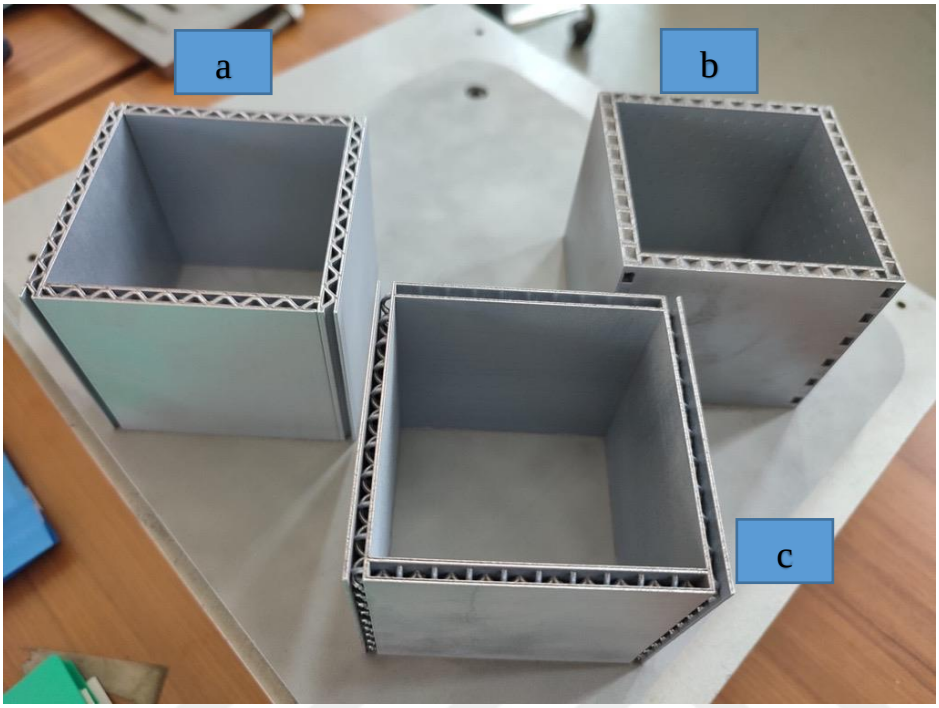

Figure 20. The produced are: (a) Navtruss, (b) Honeycomb and (c) Cross-semicircle battery packs.

The image shown in Fig.21 is known as a 3P3S configuration in which three parallel (3P) and three series (3S) connections have been made. This kind of arrangement helps to even out the capacity and voltage of the battery pack, thereby improving its performance and dependability. In this layout, every set of cells that are connected in parallel adds up to higher overall capacity as well as increased ability for current

delivery; at the same time, when these groups are connected using series links, they give desired output potential difference necessary for use in high power devices.

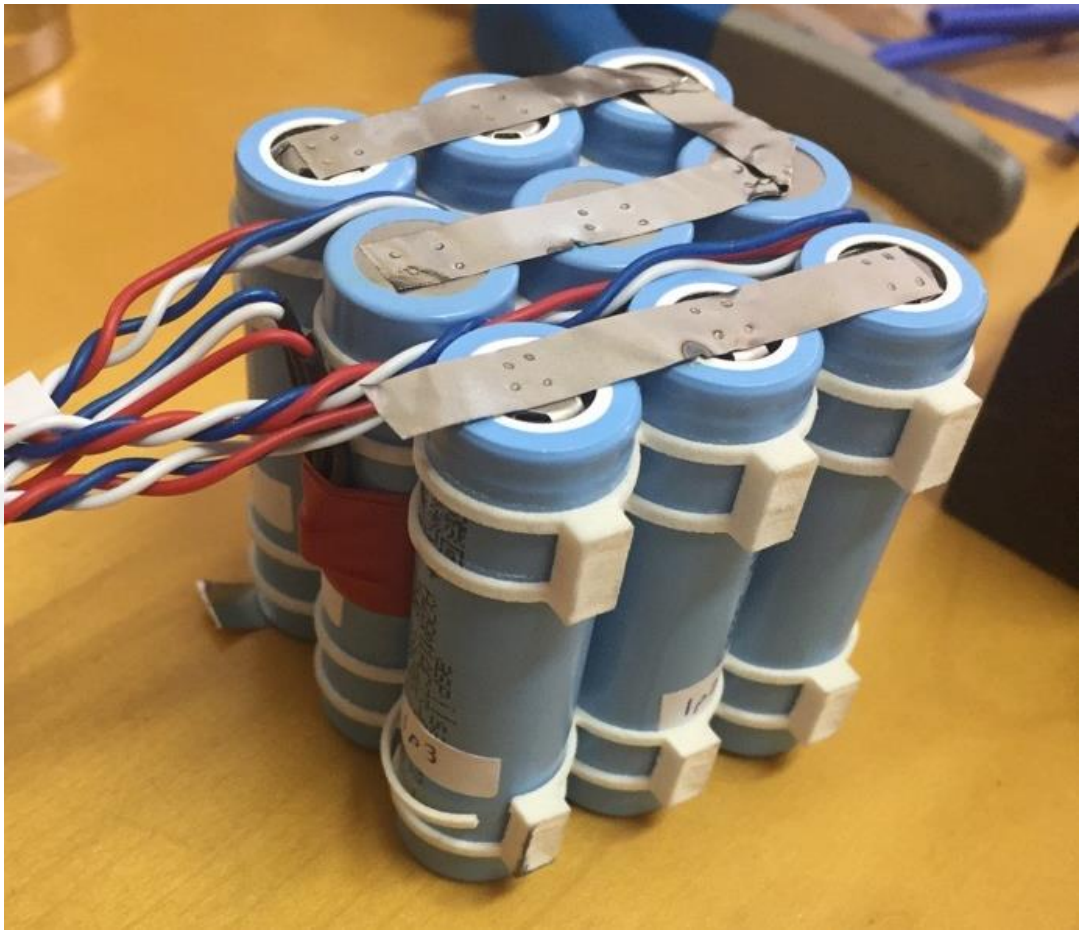

Figure 21. Cell pack in 3P3S configuration

The cell holders were produced in the additive manufacturing laboratory of the university, employing selective laser sintering (SLS) technology. These holders are made from PA2200, a material recognized for its lightweight characteristics. The SLS printer utilized for this process is the EOS FORMIGA P110 velocis, illustrated in Fig. 22.

Figure 22. EOS FORMIGA P110 Velocis used to produce cell holders [46]

The experiments were initiated with batteries at 95% SOC and were concluded at different SOC levels. Fig.23 illustrates the appropriate SOC values associated with varying discharge capacities at different voltages and temperatures.

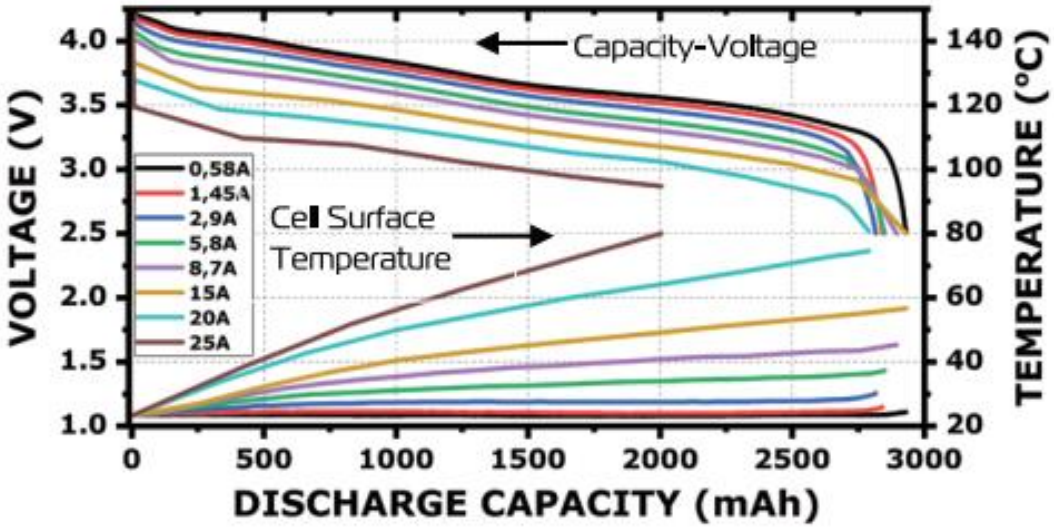

Figure 23. The characteristic curve of discharge capacity at different SOC [47]

3.4 Battery Package Integration to UAV

The Skywalker X8 shown in Fig.24, will be the model to test our best battery performance in real life application. It is a well known fixed-wing UAV (Unmanned Aerial Vehicle) that sees frequent use across different fields, notably in aerial photography, surveying and research.

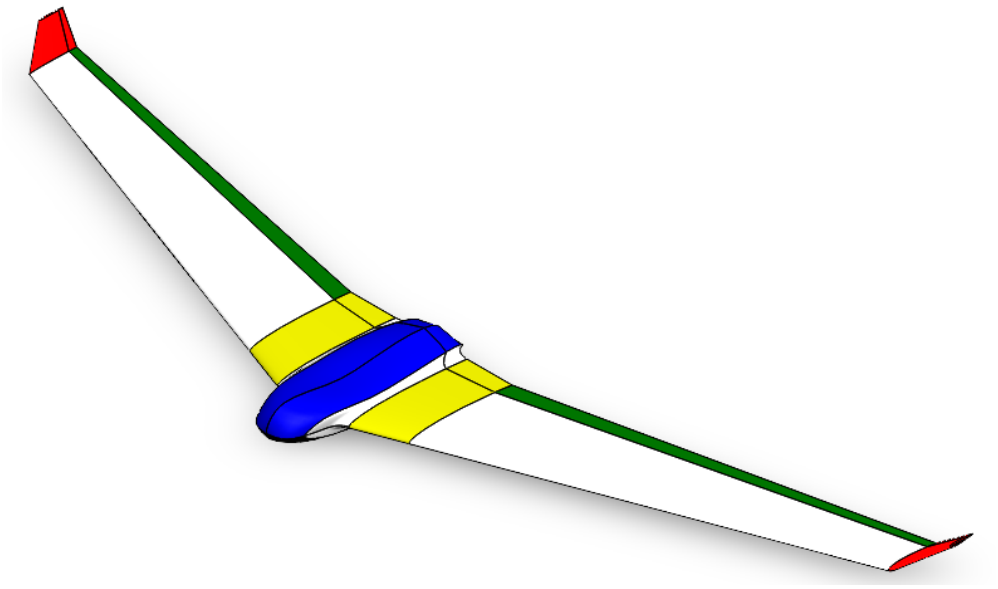

Figure 24. UAV fixed wing Skywalker X8 Model [48]

The primary determinant of flight time is the drone's battery capacity.

For 3C, each cell of our battery model can discharge up to 8700 mAh and 3.65V

For 3P3S configuration;

I = 26100 mAh

V = 10.95 V

The maximum discharge capacity is given by Eqn.11:

$$Q = V \times I \tag{11}$$

$Q = 10.95V \times 26.1Ah$

$Q = 285.8W$

Table 9 shown below outlines the type of motor and the battery capacity required for the skywaker x8 model.

Table 9. Motor and battery specifications of Skywalker UAV

Specifications	**Values**
Motor	3530 500KV – 5010 810KV
Propeller	12x6E
Servo	x2 17g
ESC	60A – 100A
Battery	6s 22.2V 5000 – 6000mAH

For such a UAV requiring the battery capacity of 22.2V and up to 6000mAh, we need three batteries of 3C connected in series for the voltage increment, and only 1 set of three batteries connected in parallel to meet the capacity requirement.

CHAPTER 4

RESULTS AND DISCUSSION

The initial stage of the analysis focused on determining the heat generation and heat flux applied in the numerical examination. Battery cells were discharged at rates of 1C, 2C, and 3C in controlled laboratory conditions at around 28^0C. Furthermore, a battery pack comprising nine cells was drawn using Solidworks, and the results obtained from the simulation were compared with experimental data for verification purposes. The comparative analysis revealed a high degree of consistency between the simulation outcomes and the experimental findings.

4.1 Natural Convection Heat Transfer Simulation Results

Simulation findings of thermal behavior for the battery pack structures under natural convection conditions are presented. Each structure is evaluated at 1C, 2C and 3C, respectively.

4.1.1 Plain Sheet Battery Pack at Natural Convection

The maximum temperatures observed in the cells and the plain sheet battery protection for natural convection are as shown in Fig.25. For a discharge rate of 1C, the temperatures recorded are 50°C for the cells and 37°C for the battery protection. When the discharge rate is increased to 2C, the temperatures rise to 106°C for the cells and 61°C for the battery protection. At a discharge rate of 3C, the temperatures peak at 190°C for the cells and 96°C for the battery protection.

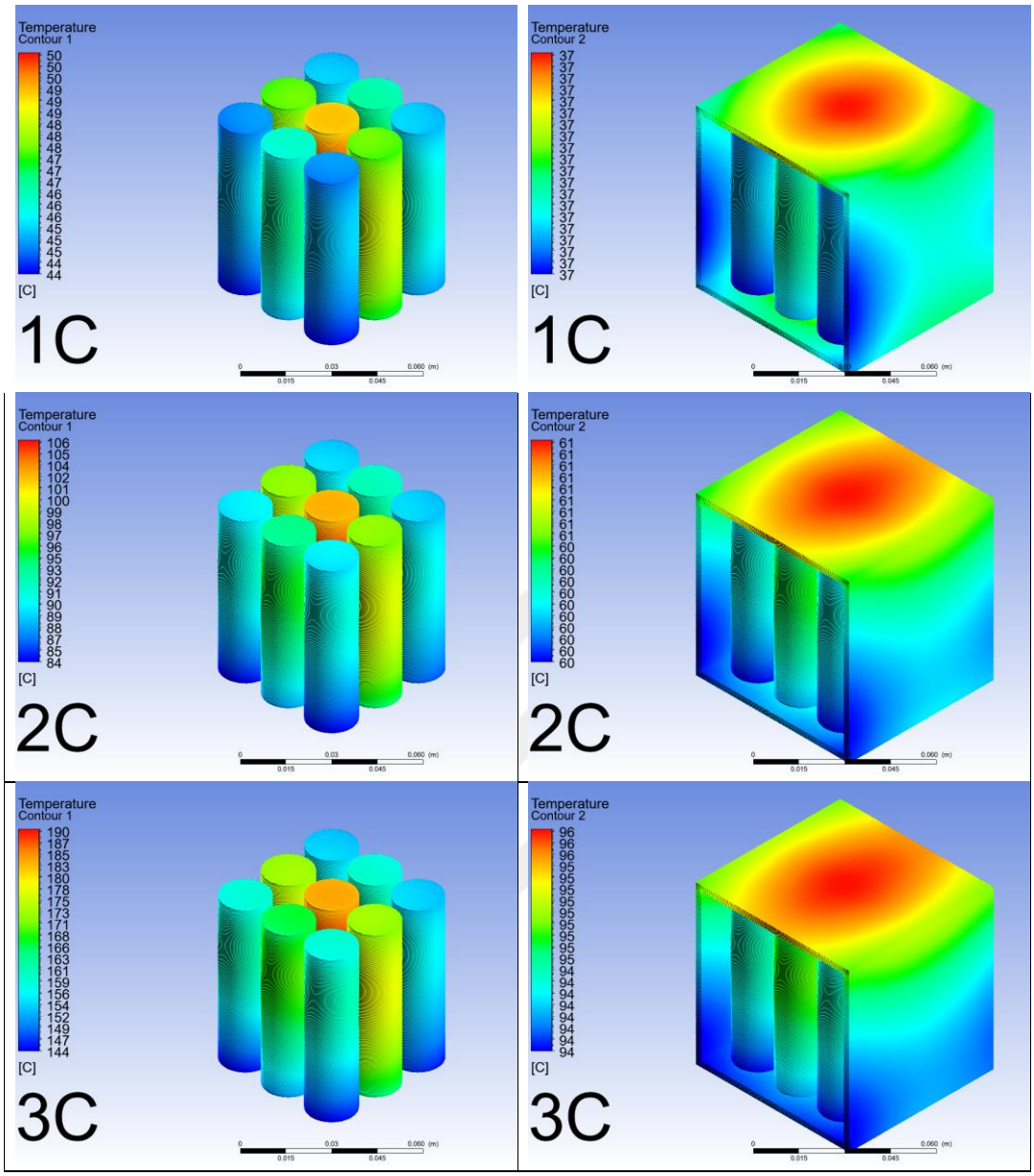

Figure 25. Cells and pack temperature distribution for plain sheet battery pack for natural convection at 1C, 2C and 3C

4.1.2 3D Kagome Battery Pack at Natural Convection

The 3D kagome battery pack at natural convection exhibits maximum temperatures of 31°C and 29°C at cells and battery protection respectively, during 1C discharge rate. When the discharge rate is increased to 2C, the maximum temperatures escalate to 41°C for the cells and 34°C for the protection. At a 3C discharge rate, the temperatures further increase to 56°C for the cells and 41°C for the protection, as shown in Fig.26.

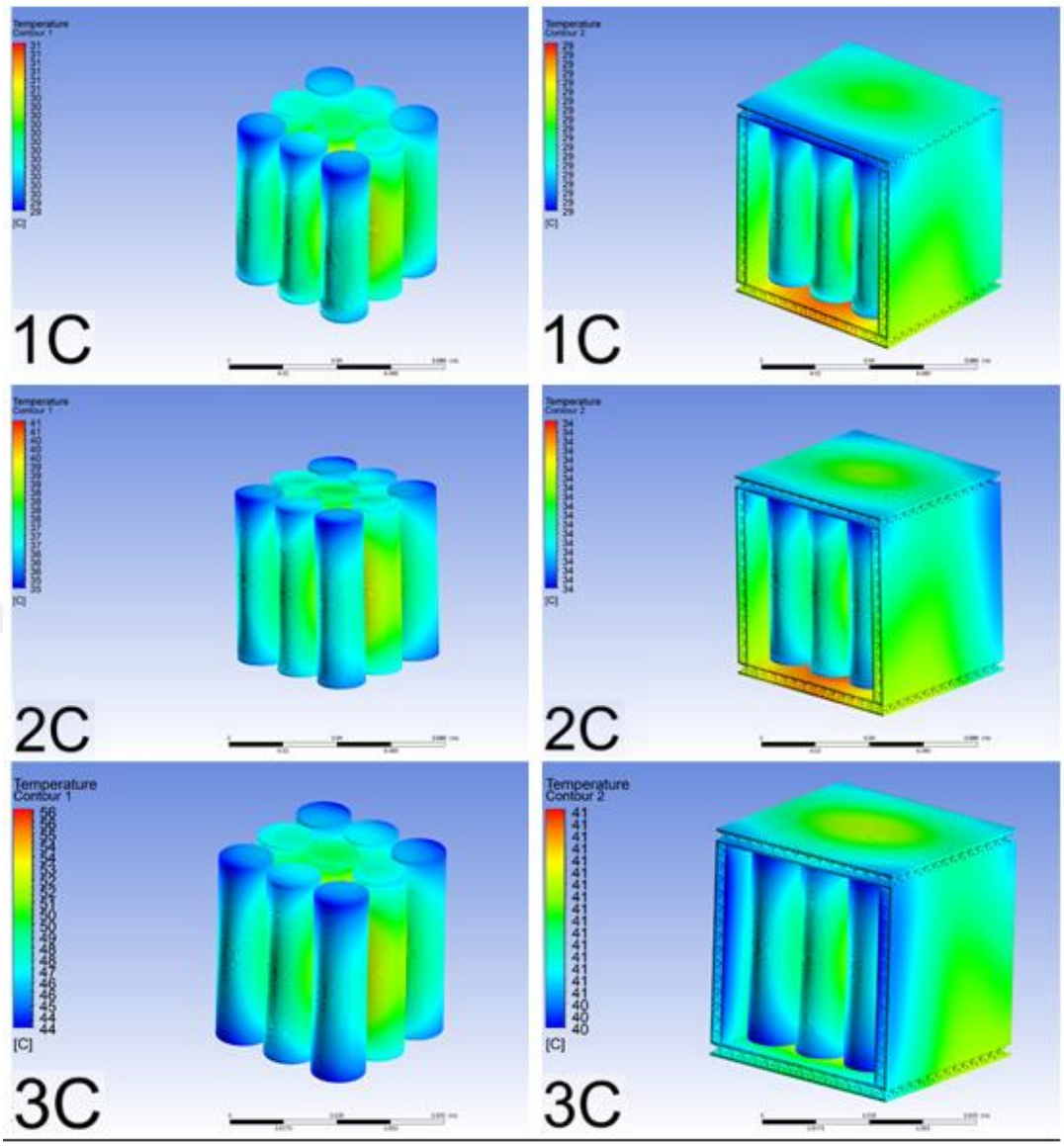

Figure 26. Cells and pack temperature distribution at natural convection for 3D kagome battery pack at 1C, 2C and 3C

It is observed that 3D kagome behaves 21.6% better than plainsheet at 1C, 44.3% at 2C and 57.3% at 3C, respectively at natural convection.

4.1.3 Honeycomb Battery Pack at Natural Convection

The simulation of honeycomb battery pack subjected to natural convection, as shown in Fig.27, indicated that the maximum temperatures recorded at the cells and battery protection were 52°C and 31°C, respectively, at the discharge rate of 1C. With the discharge rate of 2C, these maximum temperatures increased to 107°C for the cells

and 51°C for the battery protection. At the discharge rate of 3C, the temperatures further rise to 109°C for the cells and 77°C for the battery protection.

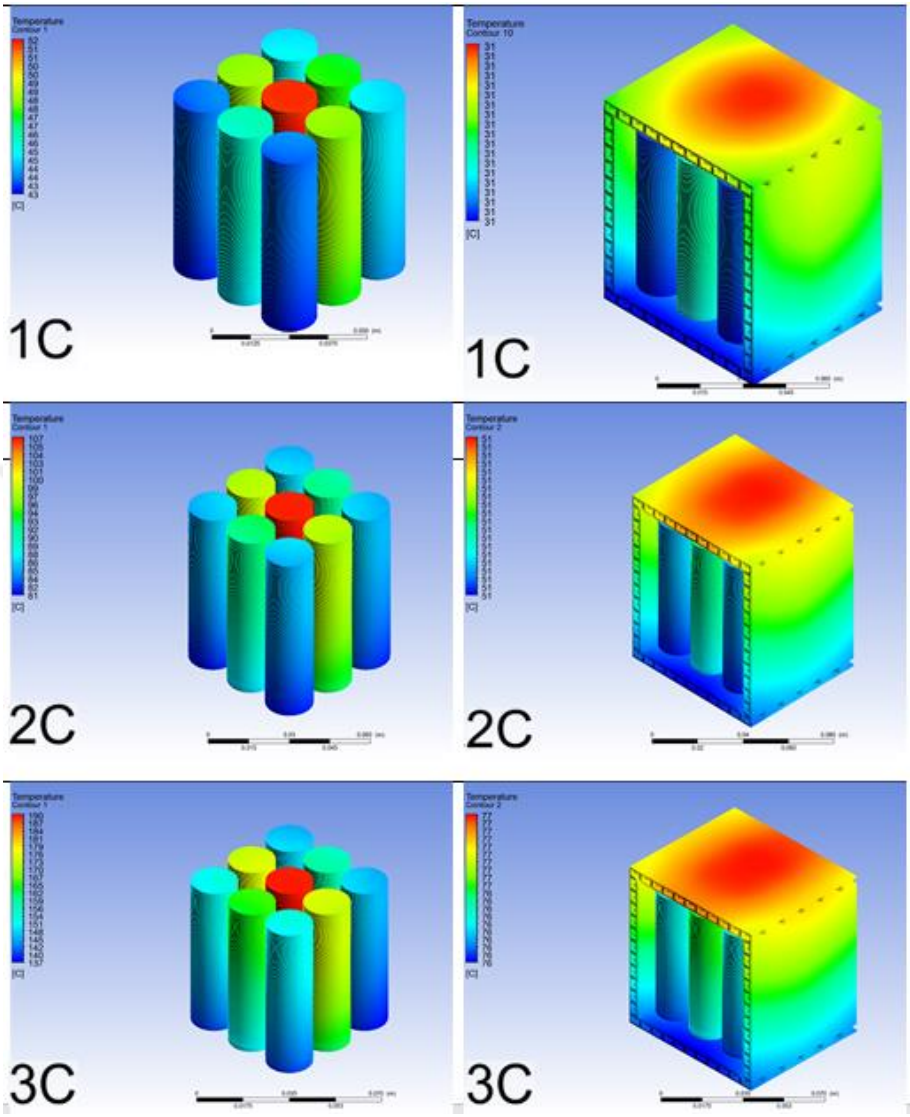

Figure 27. Cells and pack temperature distribution at natural convection for Honeycomb at 1C, 2C and 3C

It is observed that honeycomb behaves 16.5% better than plainsheet at 1C, 16.4% at 2C and 19.8% at 3C, respectively at natural convection.

4.1.4 Navtruss Battery Pack at Natural Convection

The Navtruss battery pack under natural convection, recorded maximum temperatures are 44°C in the cells and 30°C in the battery protection at a discharge rate of 1C. Upon

increasing the discharge rate to 2C, the maximum temperatures rise to 84°C for the cells and 34°C for the protection. At a discharge rate of 3C, these values further surged to 153°C for the cells and 52°C for the protection, as shown in Fig.28.

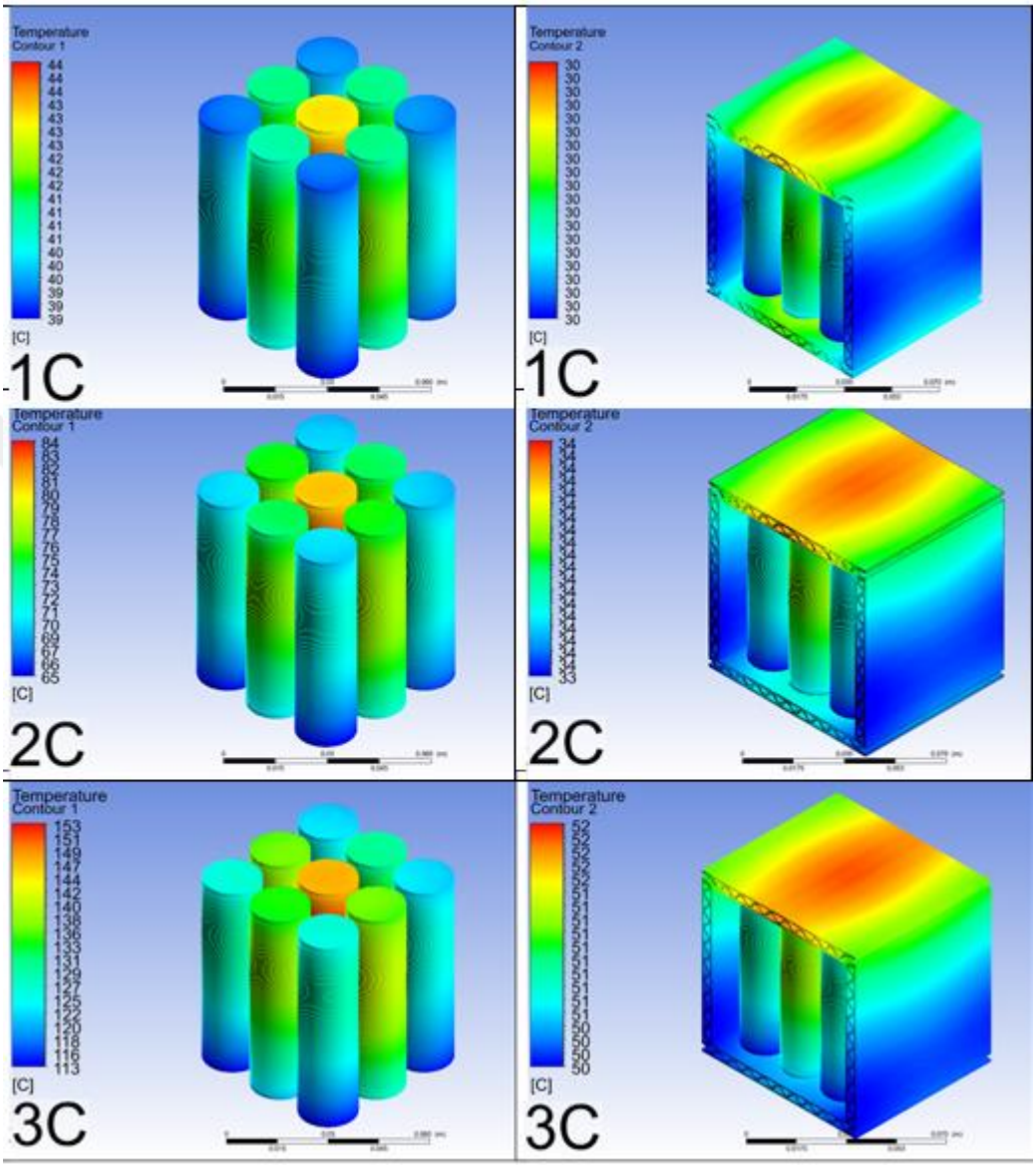

Figure 28. Navtruss cells and pack temperature distribution for natural convection at 1C, 2C and 3C

It is observed that navtruss behaves 18.9% better than plainsheet at 1C, 44.3% at 2C and 45.8% at 3C, respectively at natural convection.

4.1.5 Cross-semicircle Battery Pack at Natural Convection

The cross-semicircle battery pack under natural convection, recorded maximum temperatures are 44°C in the cells and 30°C in the battery protection at a discharge rate of 1C. Upon increasing the discharge rate to 2C, the maximum temperatures rise to 88°C for the cells and 39°C for the protection. At a discharge rate of 3C, these values further surged to 153°C for the cells and 53°C for the protection, as shown in Fig.29.

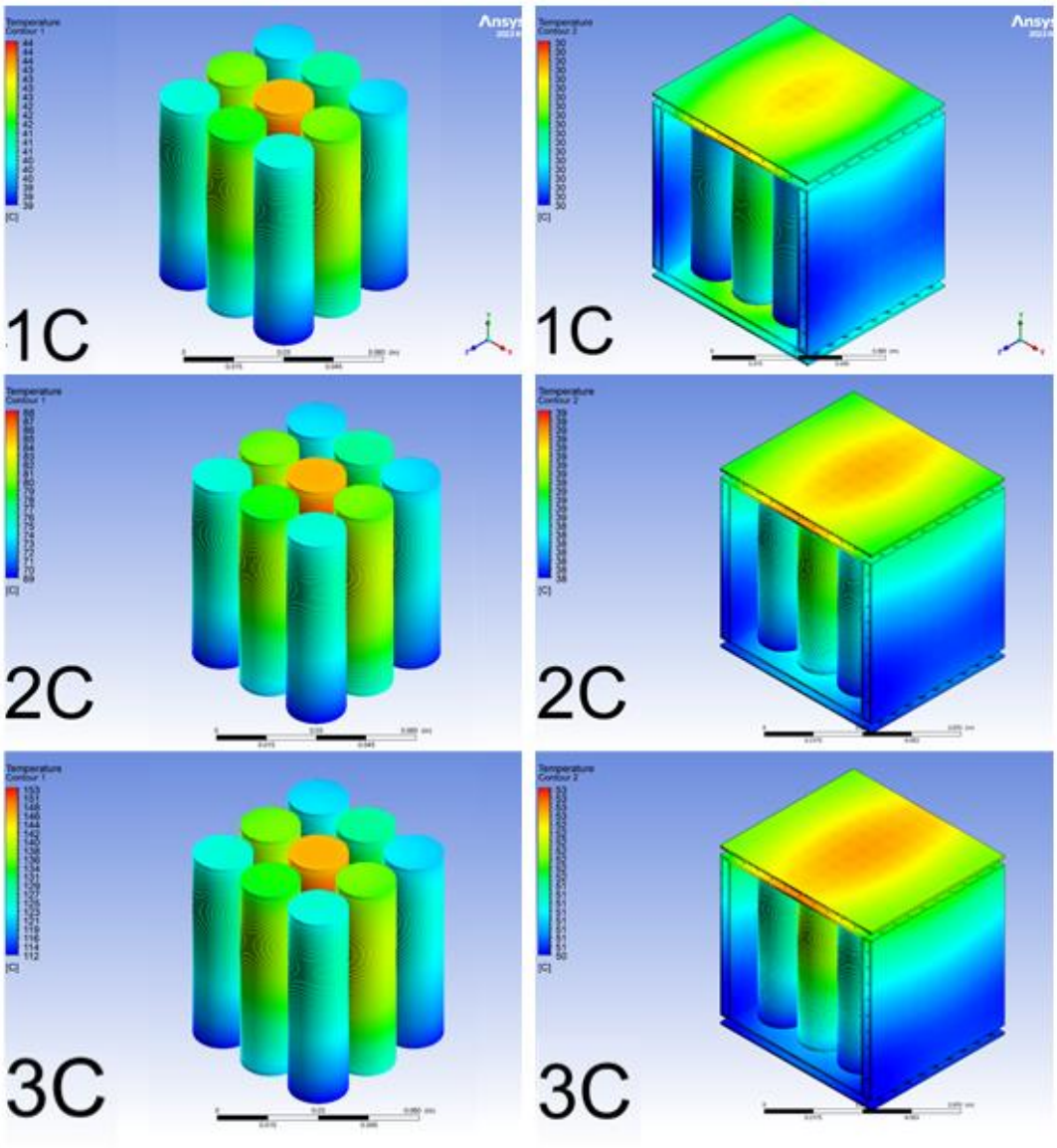

Figure 29. Cross-semircircle cells and pack temperature distribution for natural convection at 1C, 2C and 3C

It is observed that cross-semicircle behaves 18.9% better than plainsheet at 1C, 44.3% at 2C and 45.8% at 3C, respectively at natural convection.

A summary of the natural convection simulation results for all battery packs is presented in Table 10.

Table 10. Natural convection heat distribution summary

C-rate	Location	Plain Sheet (°C)	3D kagome (°C)	Honeycomb (°C)	Navtruss (°C)	Cross-semicircle (°C)
1C	Cell	50	31	52	44	44
	Pack	37	29	31	30	30
2C	Cell	106	41	107	84	88
	Pack	61	34	51	34	39
3C	Cell	190	56	190	153	153
	Pack	96	41	77	52	53

4.2 Forced Heat Transfer

Simulation findings of thermal behavior for the battery pack structures under forced convection conditions are presented. Each structure is evaluated at 1,2.5 and 5m/s respectively.

4.2.1 At velocity 1m/s

Presented are the results obtained when batteries are cooled at 1m/s.

4.2.1.1 Plain Sheet Battery Pack at 1 m/s

The maximum temperatures observed in the cells and the plain sheet battery protection for fan velocity of 1m/s are as shown in Fig.30. For a discharge rate of 1C, the

temperatures recorded are 28°C for the cells and 27°C for the battery protection. When the discharge rate is increased to 2C, the temperatures rise to 31°C for the cells and 27°C for the battery protection. At a discharge rate of 3C, the temperatures peak at 37°C for the cells and 28°C for the battery protection. This implies that the cooling process is effective for all three discharge rates at the specific velocity of 1m/s for plain sheet battery pack.

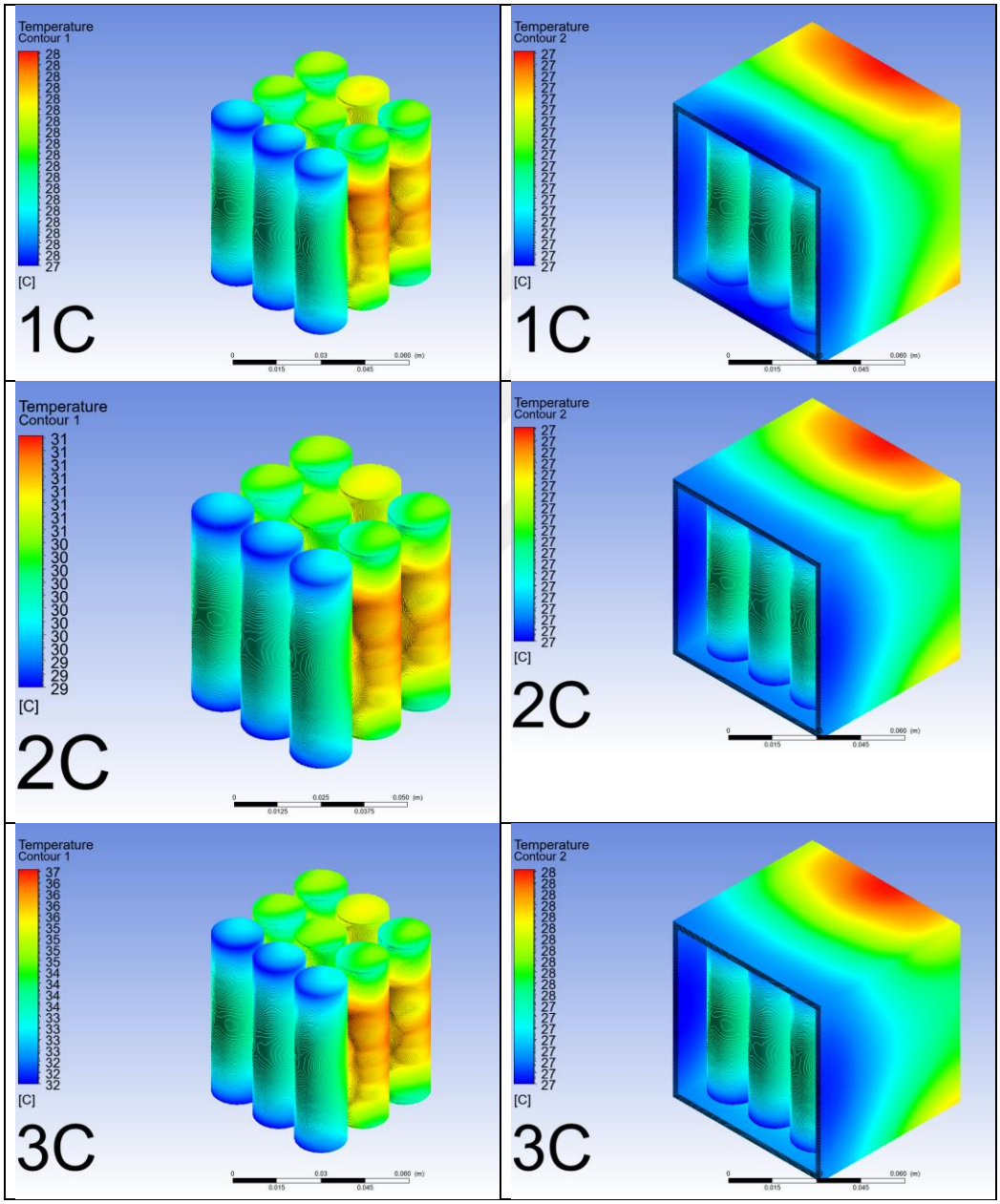

Figure 30. Cell and pack temperature distribution for plain sheet battery pack at 1m/s for 1C, 2C and 3C

4.2.1.2 3D Kagome Battery Pack at 1 m/s

The 3D kagome battery pack at fan velocity of 1m/s exhibits maximum temperatures of 29°C and 28°C at cells and battery protection respectively, during 1C discharge rate. When the discharge rate is increased to 2C, the maximum temperatures escalate to 30°C for the cells and 29°C for the protection. At a 3C discharge rate, the temperatures further increase to 33°C for the cells and 29°C for the protection, as shown in Fig.31.

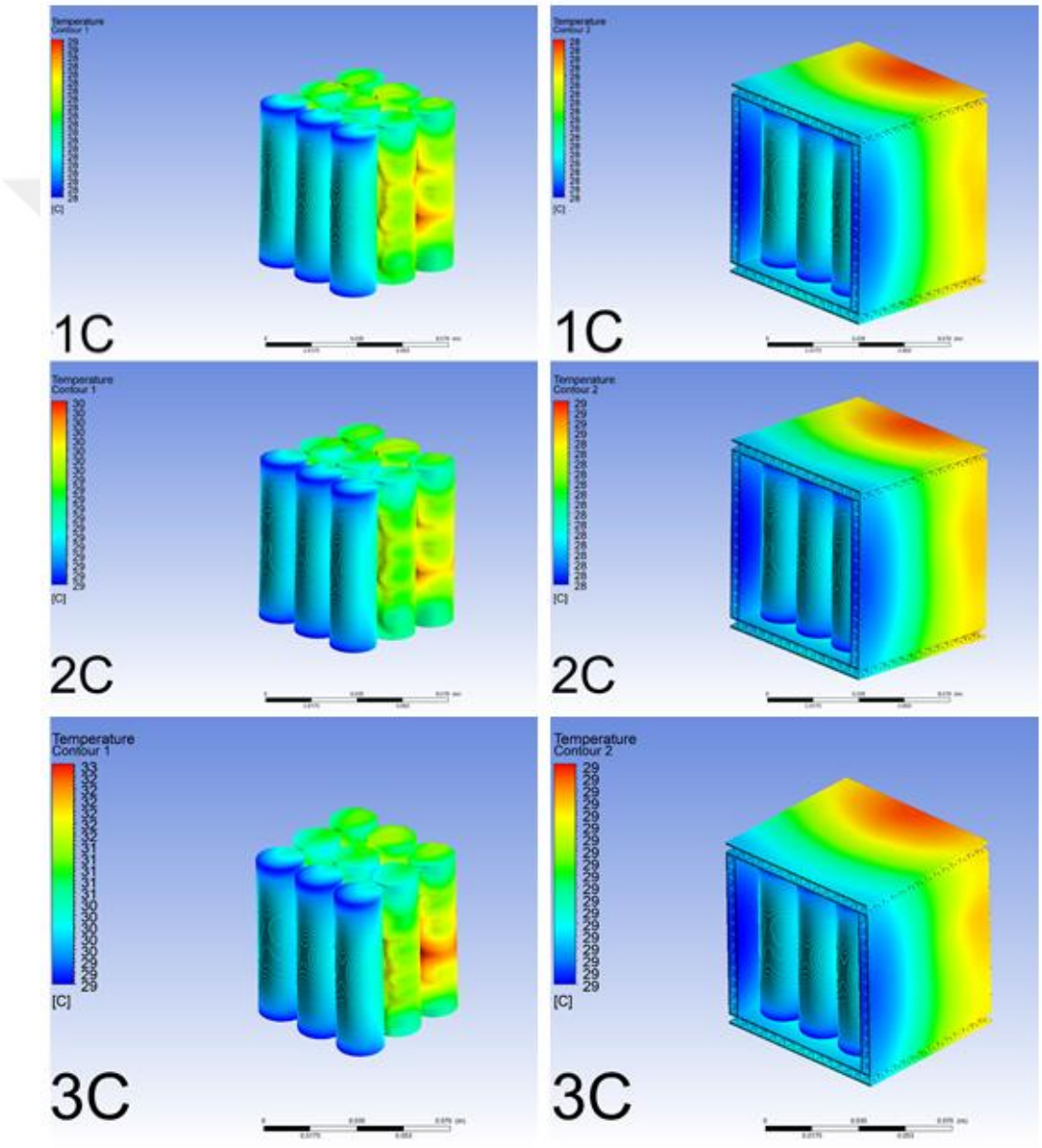

Figure 31. Cells and pack temperature distribution at 1 m/s for 3D kagome battery pack at 1C, 2C and 3C

It is observed that 3D kagome behaves 3.7% better than plainsheet at 1C, 7.4% at 2C and 3.6% at 3C, respectively when cooled with 1m/s air speed.

4.2.1.3 Honeycomb Battery Pack at 1 m/s

The simulation of honeycomb battery pack subjected to fan velocity of 1m/s, as shown in Fig.32, indicated that the maximum temperatures recorded at the cells and battery protection were 29°C and 27°C, respectively, at the discharge rate of 1C. With the discharge rate of 2C, these maximum temperatures increased to 34°C for the cells and 27°C for the battery protection. At the discharge rate of 3C, the temperatures further rise to 43°C for the cells and 28°C for the battery protection.

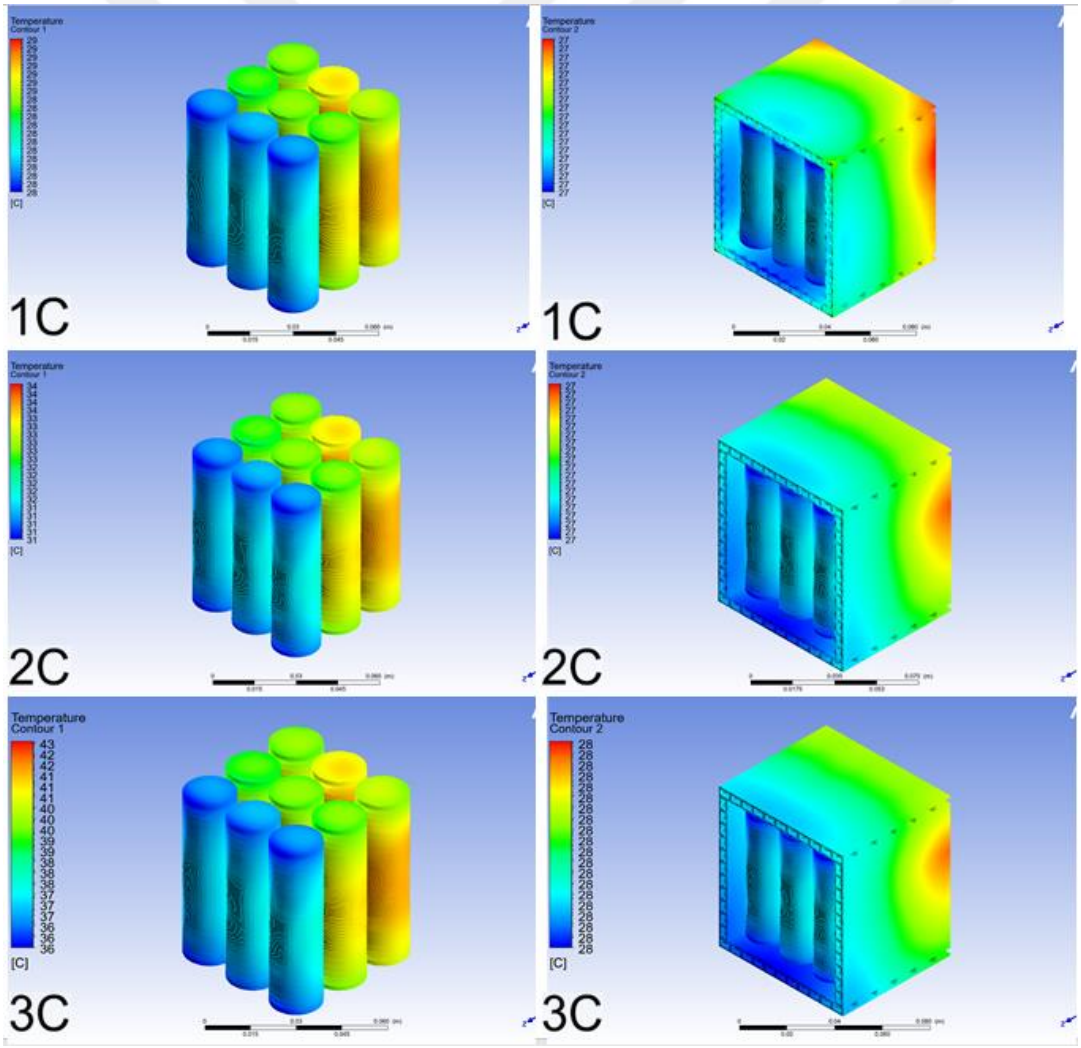

Figure 32. Cells and pack temperature distribution at 1 m/s for honeycomb battery pack at 1C, 2C and 3C

It is observed that honeycomb behaves similar as plainsheet battery pack at 1C, 2C and 3C discharge rates when cooled with 1m/s air speed.

4.2.1.4 Navtruss Battery Pack at 1 m/s

The Navtruss battery pack under 1m/s fan velocity recorded maximum temperatures of 30°C in the cells and 28°C in the battery protection at a discharge rate of 1C. Upon increasing the discharge rate to 2C, the maximum temperatures rise to 33°C for the cells and 28°C for the protection. At a discharge rate of 3C, these values further surged to 40°C for the cells and 28°C for the protection, as shown in Fig.33. The battery pack temperature remains consistent at 28°C across all discharge rates. This indicates that navtruss battery pack is effectively handling heat distribution across the battery.

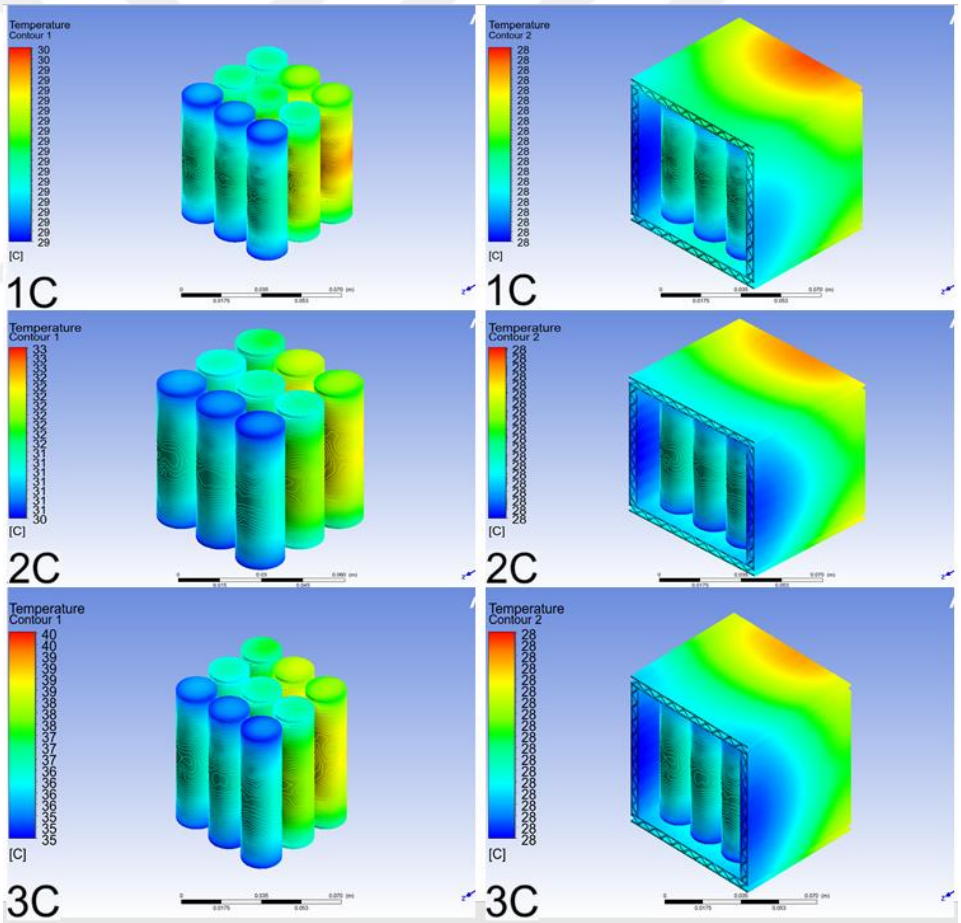

Figure 33. Cells and pack temperature distribution at 1 m/s for navtruss battery pack at 1C, 2C and 3C.

It is observed that navtruss behaves 3.7% better than plainsheet at 1C and 2C discharge rates, and behaves similar at 3C when cooled with 1m/s air speed.

4.2.1.5 Cross-semicircle Battery Pack at 1m/s

The Cross-semicircle battery pack under 1m/s fan velocity recorded maximum temperatures of 29°C in the cells and 27°C in the battery protection at a discharge rate of 1C. Upon increasing the discharge rate to 2C, the maximum temperatures rise to 34°C for the cells and 28°C for the protection. At a discharge rate of 3C, these values further surged to 43°C for the cells and 28°C for the protection, as shown in Fig.34.

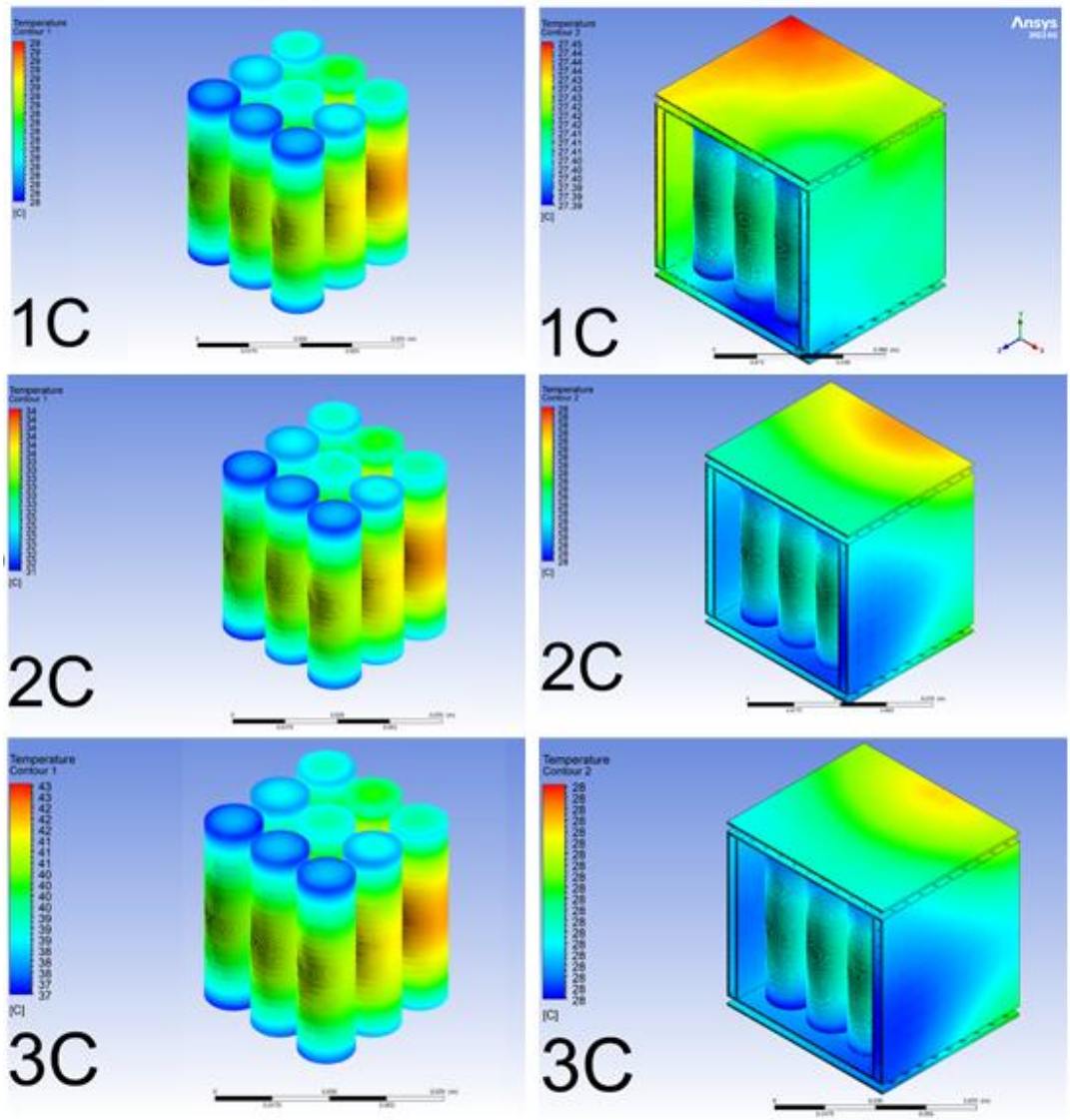

Figure 34. Cells and pack temperature distribution at 1 m/s for cross-semicircle

battery pack at 1C, 2C and 3C

It is observed that cross-semicircle behaves similar to plainsheet at 1C and 3C, but behaves better by 3.7% at 2C when cooled with 1m/s air speed.

From simulations results, for air velocity of 1m/s for all discharge rates (1C, 2C and 3C) is summarized in Table 11.

Table 11. Heat transfer at 1m/s summary

C-rate	Location	Plain Sheet	3D Kagome	Honeycomb	Navtruss	Cross Semicircle
1C	Cell	28	29	29	30	29
	Pack	27	28	27	28	27
2C	Cell	31	30	34	33	34
	Pack	27	29	27	28	28
3C	Cell	37	33	43	40	43
	Pack	28	29	28	28	28

4.2.2 At velocity 2.5 m/s

Presented are the results obtained when batteries are cooled at 2.5 m/s.

4.2.2.1 Plain Sheet Battery Pack at 2.5 m/s

The maximum temperatures observed in the cells and the plain sheet battery protection for fan velocity of 2.5m/s are as shown in Fig.35. For a discharge rate of 1C, the temperatures recorded are 28°C for the cells and 27°C for the battery protection. When the discharge rate is increased to 2C, the temperatures rise to 30°C for the cells and 27°C for the battery protection. At a discharge rate of 3C, the temperatures peak at 33°C for the cells and 27°C for the battery protection. This implies that the cooling process is effective for all three discharge rates at the specific velocity of 2.5m/s for plain sheet battery pack.

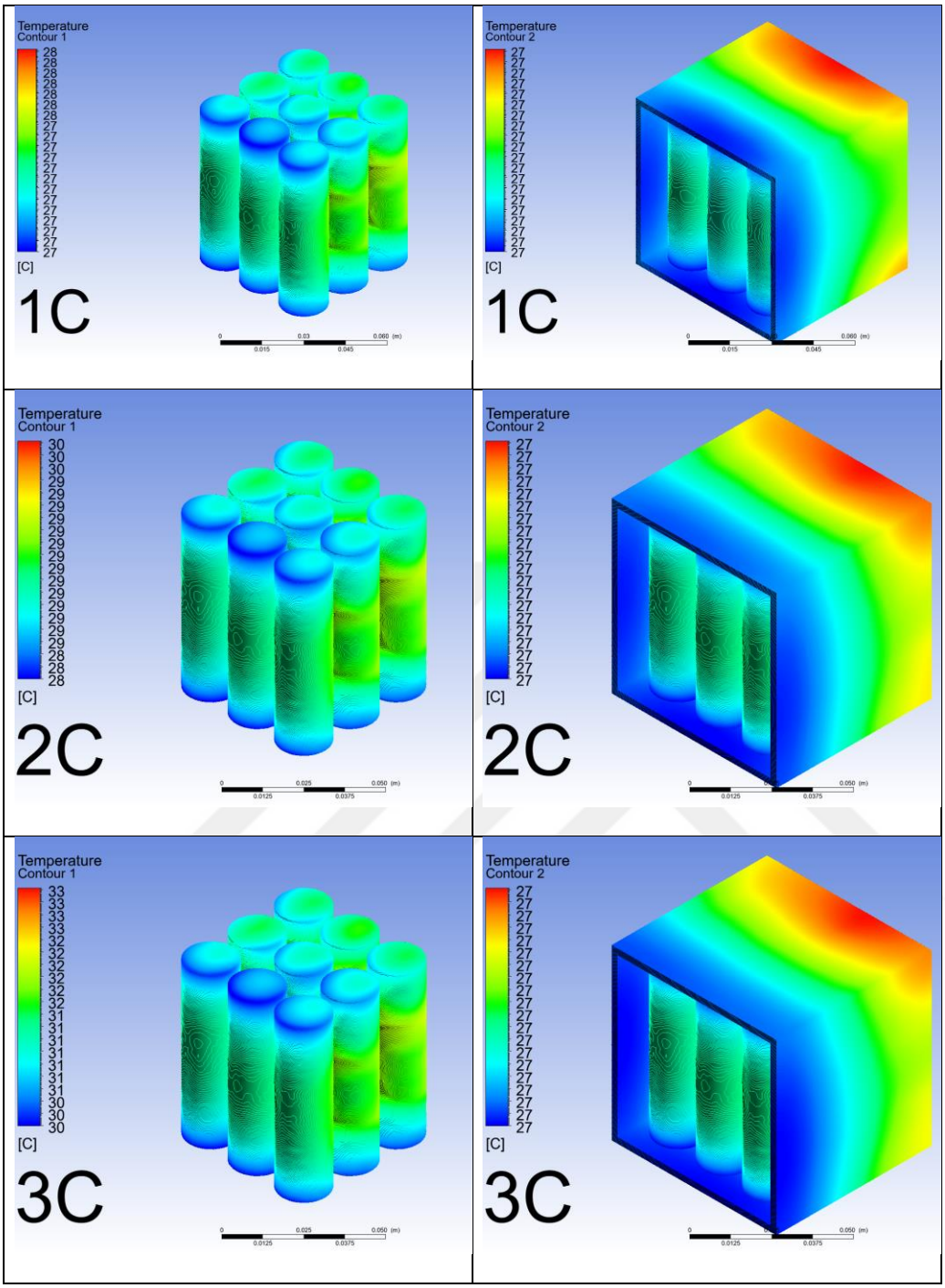

Figure 35. Plain sheet cells and pack temperature distribution at 2.5m/s for 1C, 2C and 3C

These findings suggest that the cooling rate of 2.5m/s is effective in maintaining the battery pack within the optimal temperature range.

4.2.2.2 3D Kagome Battery Pack at 2.5 m/s

The 3D kagome battery pack at fan velocity of 2.5m/s exhibits maximum temperatures of 28°C and 27°C at cells and battery protection respectively, during 1C discharge rate. When the discharge rate is increased to 2C, the maximum temperatures escalate to 30°C for the cells and 29°C for the protection. At a 3C discharge rate, the temperatures further increase to 31°C for the cells and 29°C for the protection, as shown in Fig.36.

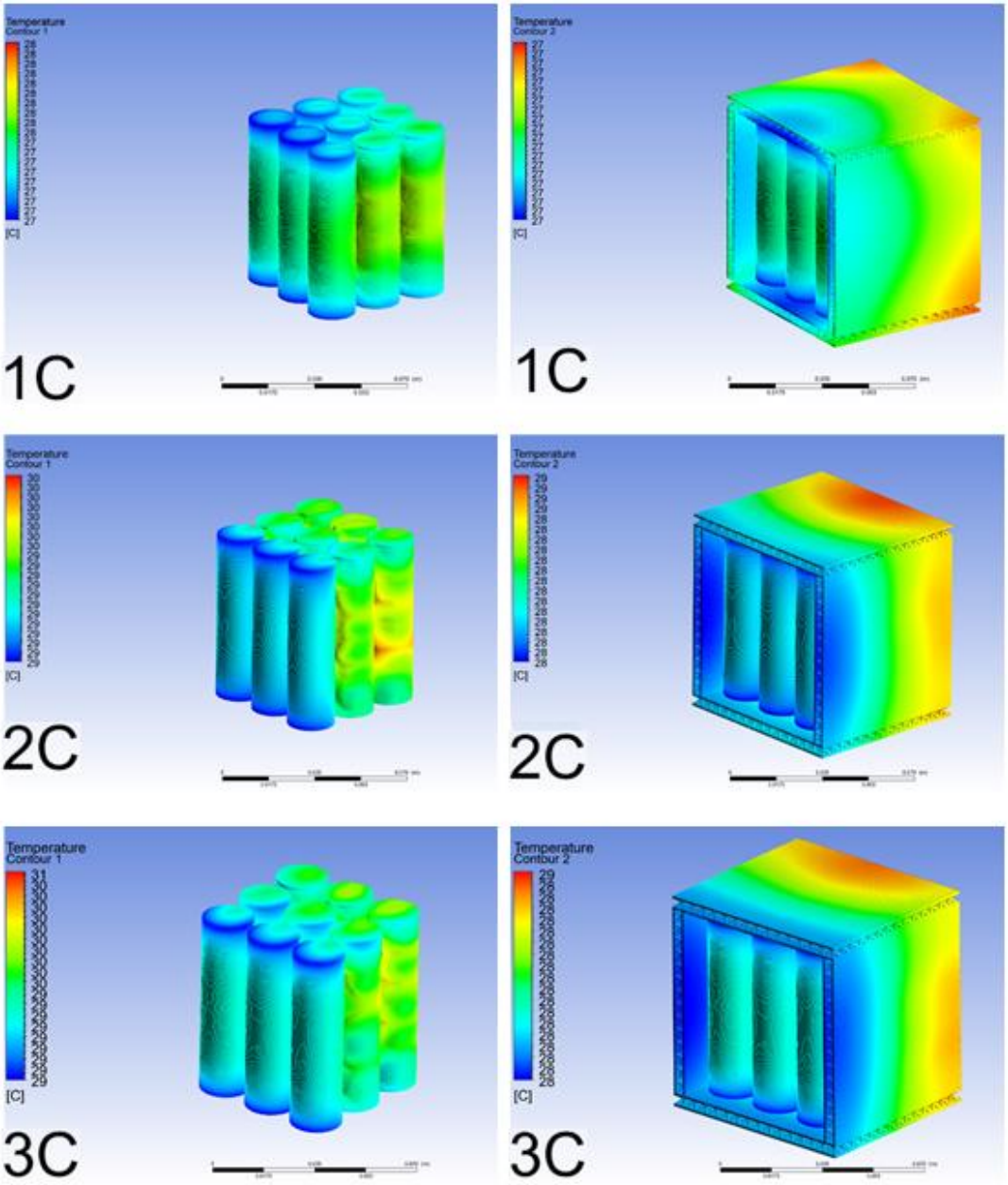

Figure 36. Cells and pack temperature distribution at 2.5 m/s for 3D kagome battery pack at 1C, 2C and 3C.

It is observed that 3D kagome behaves similar to plainsheet at 1C, and 7.4% at both 2C and 3C when cooled by 2.5 m/s air speed.

4.2.2.3 Honeycomb Battery Pack at 2.5 m/s

The simulation of honeycomb battery pack subjected to fan velocity of 2.5m/s, as shown in Fig.37, indicated that the maximum temperatures recorded at the cells and battery protection were 28°C and 27°C, respectively, at the discharge rate of 1C. With the discharge rate of 2C, these maximum temperatures increased to 32°C for the cells and 27°C for the battery protection. At the discharge rate of 3C, the temperatures further rise to 39°C for the cells and 27°C for the battery protection.

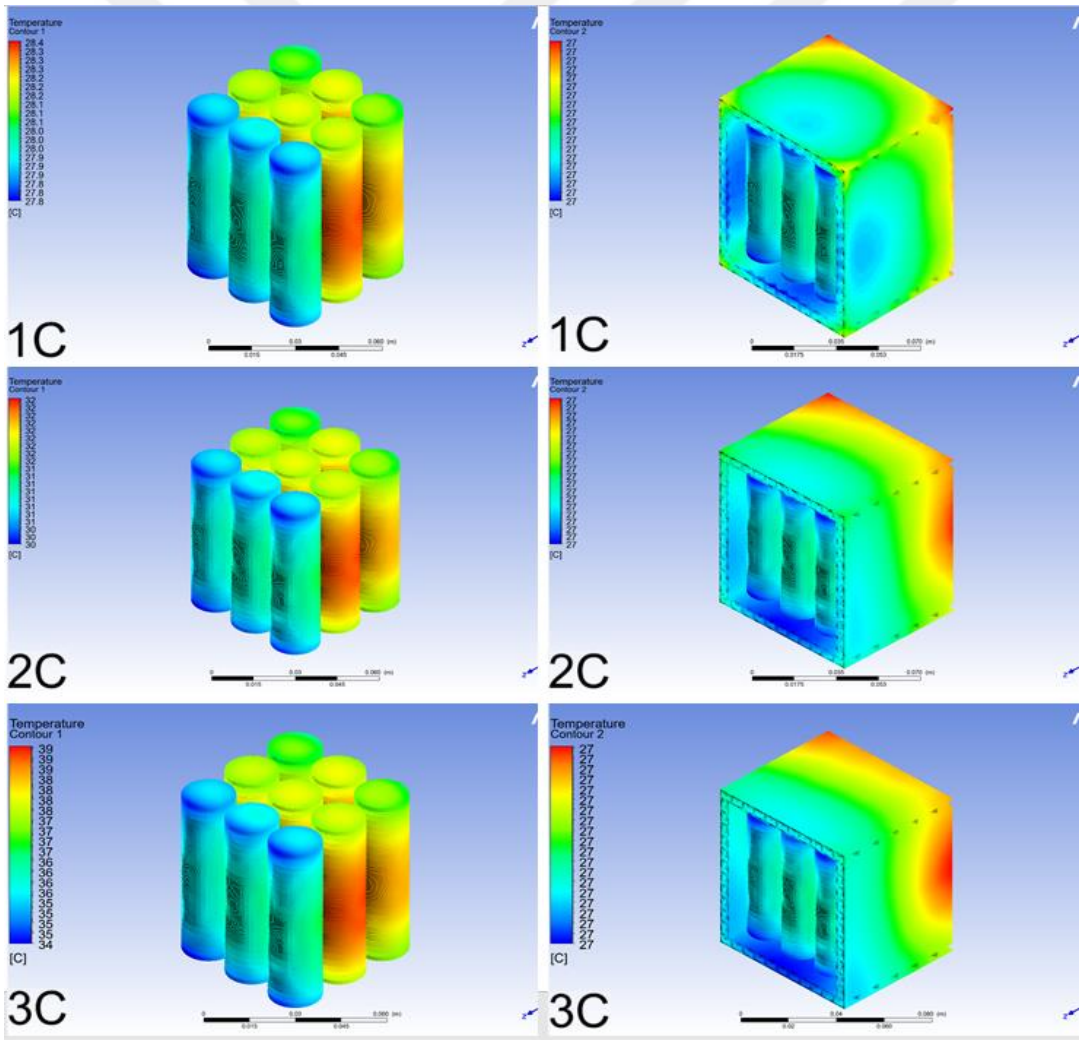

Figure 37. Cells and pack temperature distribution at 2.5 m/s for honeycomb battery pack at 1C, 2C and 3C

Overall, the honeycomb battery pack is managing temperature effectively across different discharge rates at 2m/s. The cells experience increased temperatures at higher discharge rates, and these temperatures are within acceptable limits. It is observed that honeycomb behaves similar to plainsheet when cooled by 2.5 m/s air speed at all three discharge rates (1C, 2C and 3C).

4.2.2.4 Navtruss Battery Pack at 2.5 m/s

The Navtruss battery pack under 2.5m/s fan velocity recorded maximum temperatures of 29°C in the cells and 28°C in the battery protection at a discharge rate of 1C. Upon increasing the discharge rate to 2C, the maximum temperatures rise to 31°C for the cells and 27°C for the protection. At a discharge rate of 3C, these values further surged to 37°C for the cells and 28°C for the protection, as shown in Fig.38.

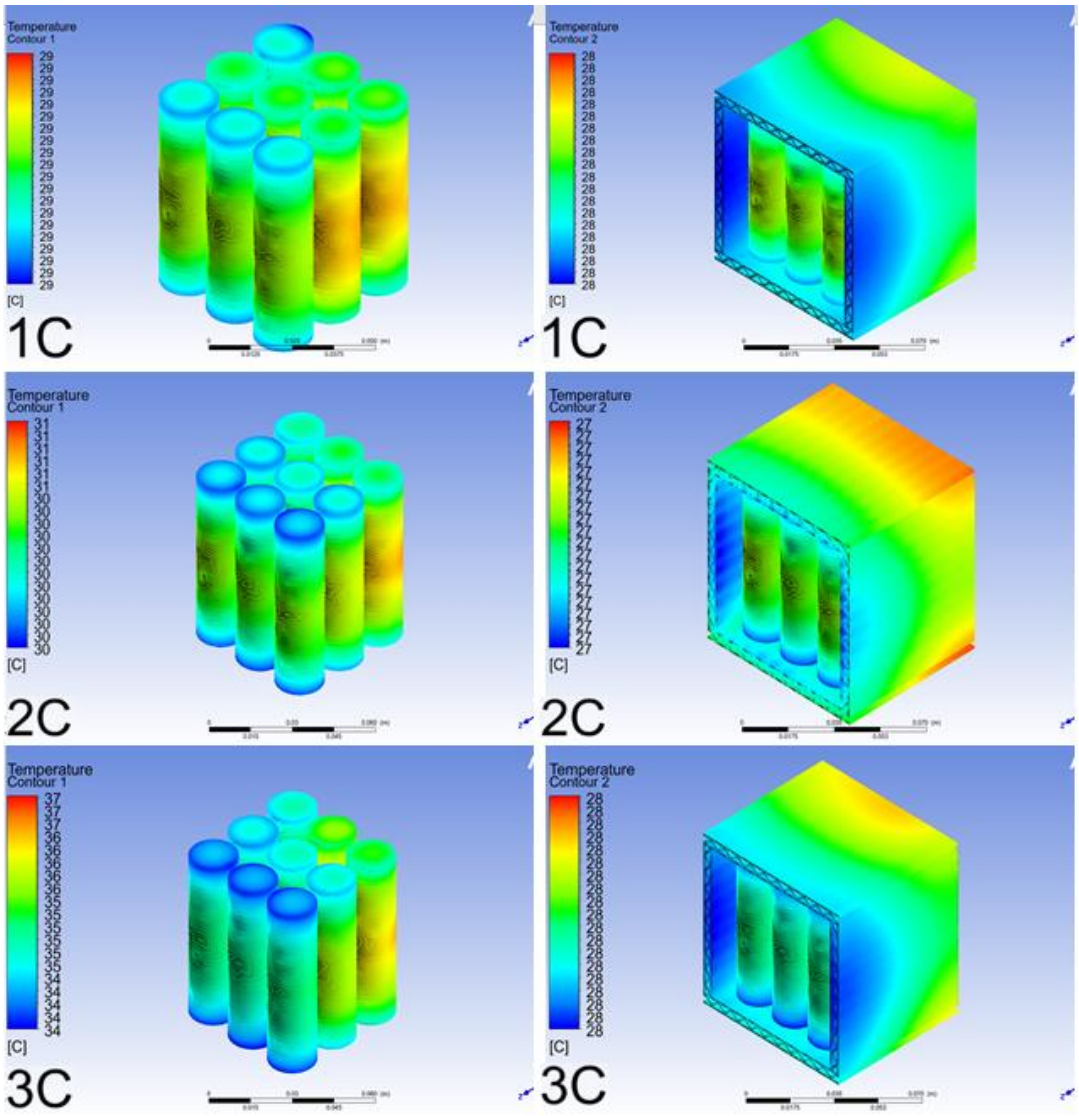

Figure 38. Cells and pack temperature distribution at 2.5 m/s for navtruss battery pack at 1C, 2C and 3C

It is observed that navtruss behaves better than plainsheet by 3.7% at 1C and 3C, but behaves similar to it at 2C when cooled by 2.5 m/s air speed.

4.2.2.5 Cross-semicircle Battery Pack at 2.5m/s

The Cross-semicircle battery pack under 2.5m/s fan velocity recorded maximum temperatures of 28°C in the cells and 27°C in the battery protection at a discharge rate of 1C. Upon increasing the discharge rate to 2C, the maximum temperatures rise to 33°C for the cells and 27°C for the protection. At a discharge rate of 3C, these values further surged to 40°C for the cells and 28°C for the protection, as shown in Fig.39.

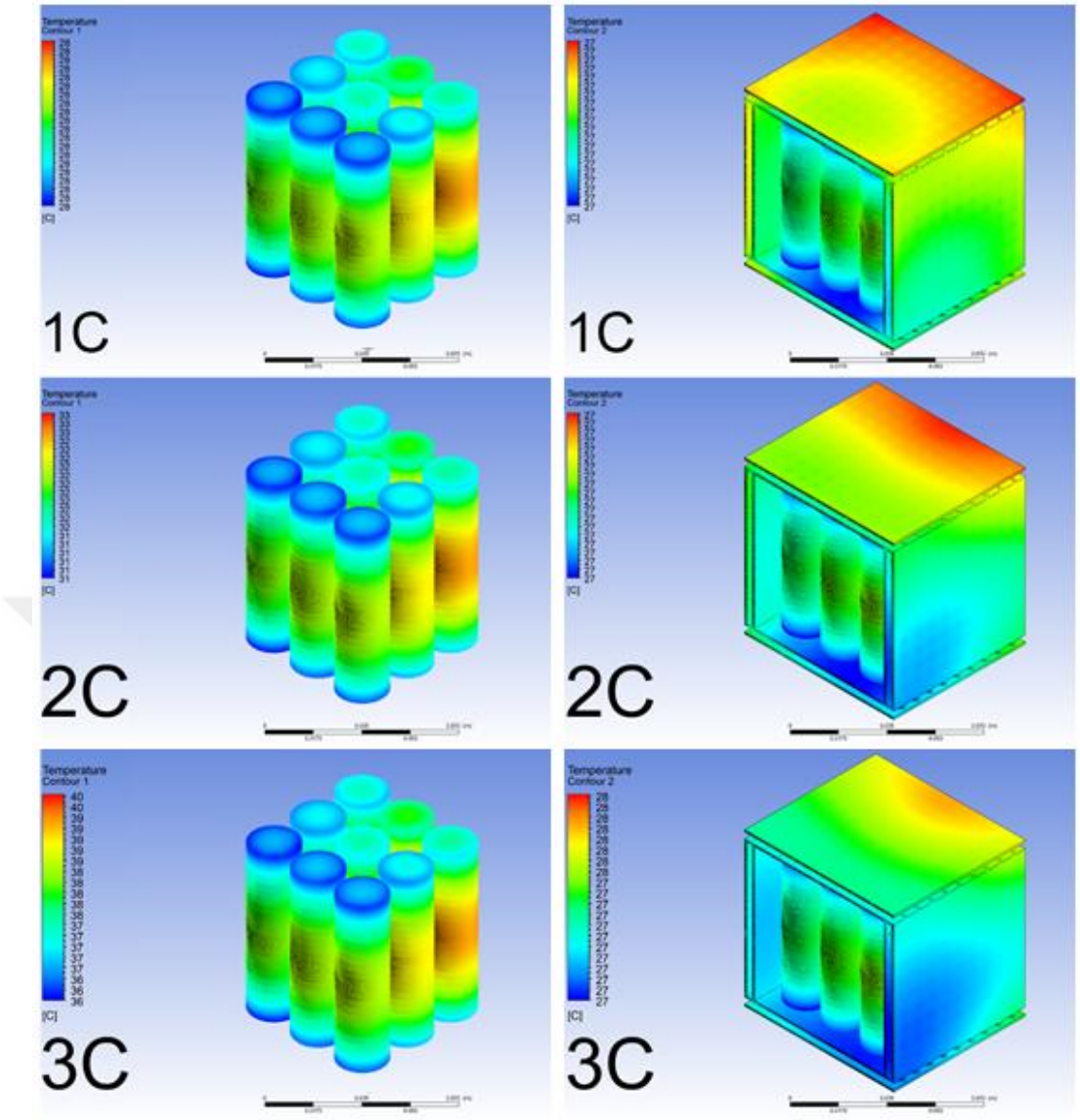

Figure 39. Cells and pack temperature distribution at 2.5 m/s for cross-semicircle battery pack at 1C, 2C and 3C

It is observed that cross-semicircle behaves similar to plainsheet at 1C and 2C but behaves better by 3.7% at 3C, when cooled by 2.5 m/s air speed.

As summarized in table 12, with additional air cooling of 2.5 m/s, all analyzed battery packs (Plain Sheet, 3D Kagome, Honeycomb, and Navtruss) effectively manage to keep temperatures within the optimal range below 60°C at all three discharge rates.

Table 12. Heat transfer at 2.5m/s summary

C-rate	Location	Plain Sheet (°C)	3D Kagome (°C)	Honeycomb (°C)	Navtruss (°C)	Cross Semicircle (°C)
1C	Cell	28	28	28	29	28
	Pack	27	27	27	28	27
2C	Cell	30	30	32	31	33
	Pack	27	29	27	27	27
3C	Cell	33	31	39	37	40
	Pack	27	29	27	28	28

4.2.3 At Velocity 5m/s

Presented are the results obtained when batteries are cooled at 5m/s.

4.2.3.1 Plain Sheet Battery Pack at 5 m/s

The maximum temperatures observed in the cells and the plain sheet battery protection for fan velocity of 5m/s are as shown in Fig.40. For a discharge rate of 1C, the temperatures recorded are 27°C for the cells and 27°C for the battery protection. When the discharge rate is increased to 2C, the temperatures rise to 29°C for the cells and 27°C for the battery protection. At a discharge rate of 3C, the temperatures peak at 31°C for the cells and 27°C for the battery protection. This implies that the cooling process is effective for all three discharge rates at the specific velocity of 5m/s for plain sheet battery pack.

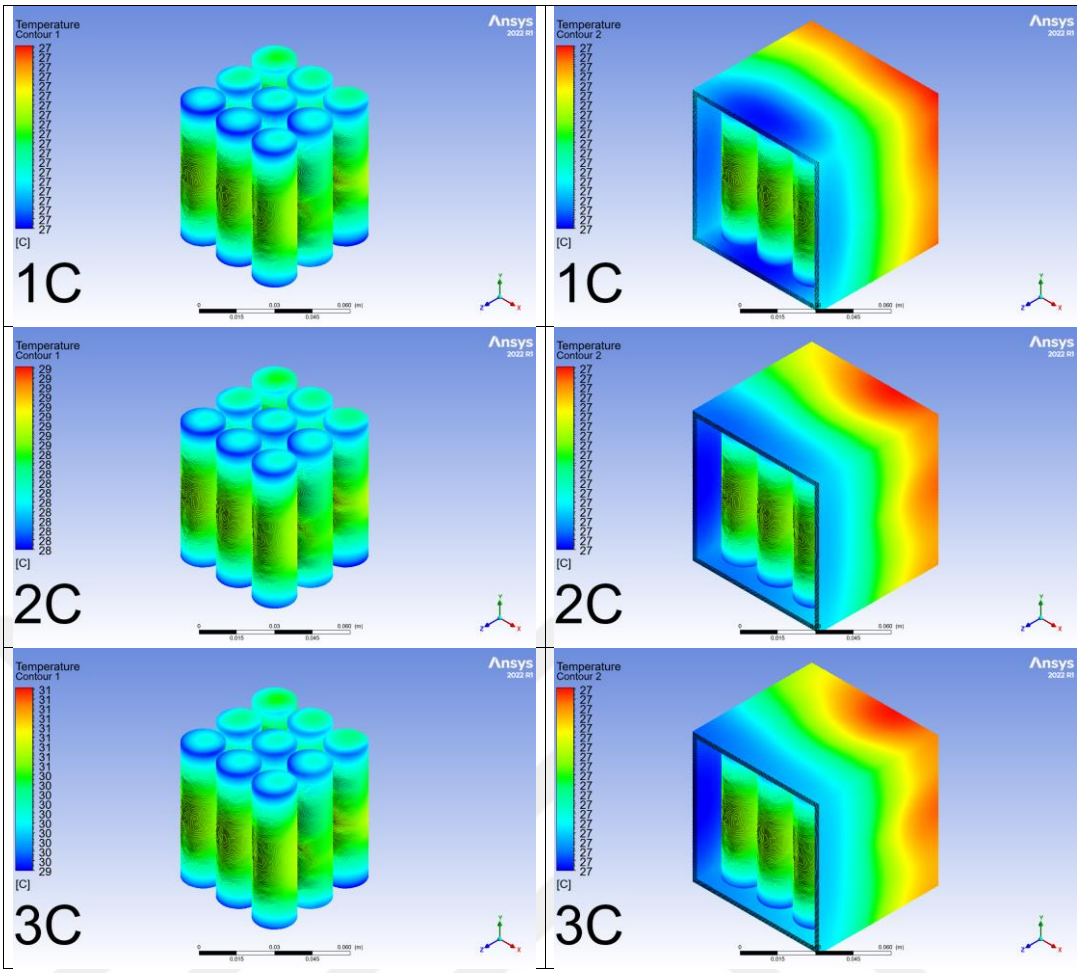

Figure 40. Cells and pack temperature distribution for plain sheet battery pack at 5m/s for 1C, 2C and 3C

The temperature remains uniform across the plain sheet battery protection for all three discharge rates at air velocity of 5 m/s. A stable thermal distribution of 27°C is read throughout the battery protection, mirroring the conditions observed at 2.5 m/s.

4.2.3.2 3D Kagome Battery Pack at 5 m/s

The 3D kagome battery pack at fan velocity of 5m/s exhibits maximum temperatures of 28°C and 27°C at cells and battery protection respectively, during 1C discharge rate. When the discharge rate is increased to 2C, the maximum temperatures escalate to 29°C for the cells and 28°C for the protection. At a 3C discharge rate, the temperatures further increase to 30°C for the cells and 28°C for the protection, as shown in Fig. 41.

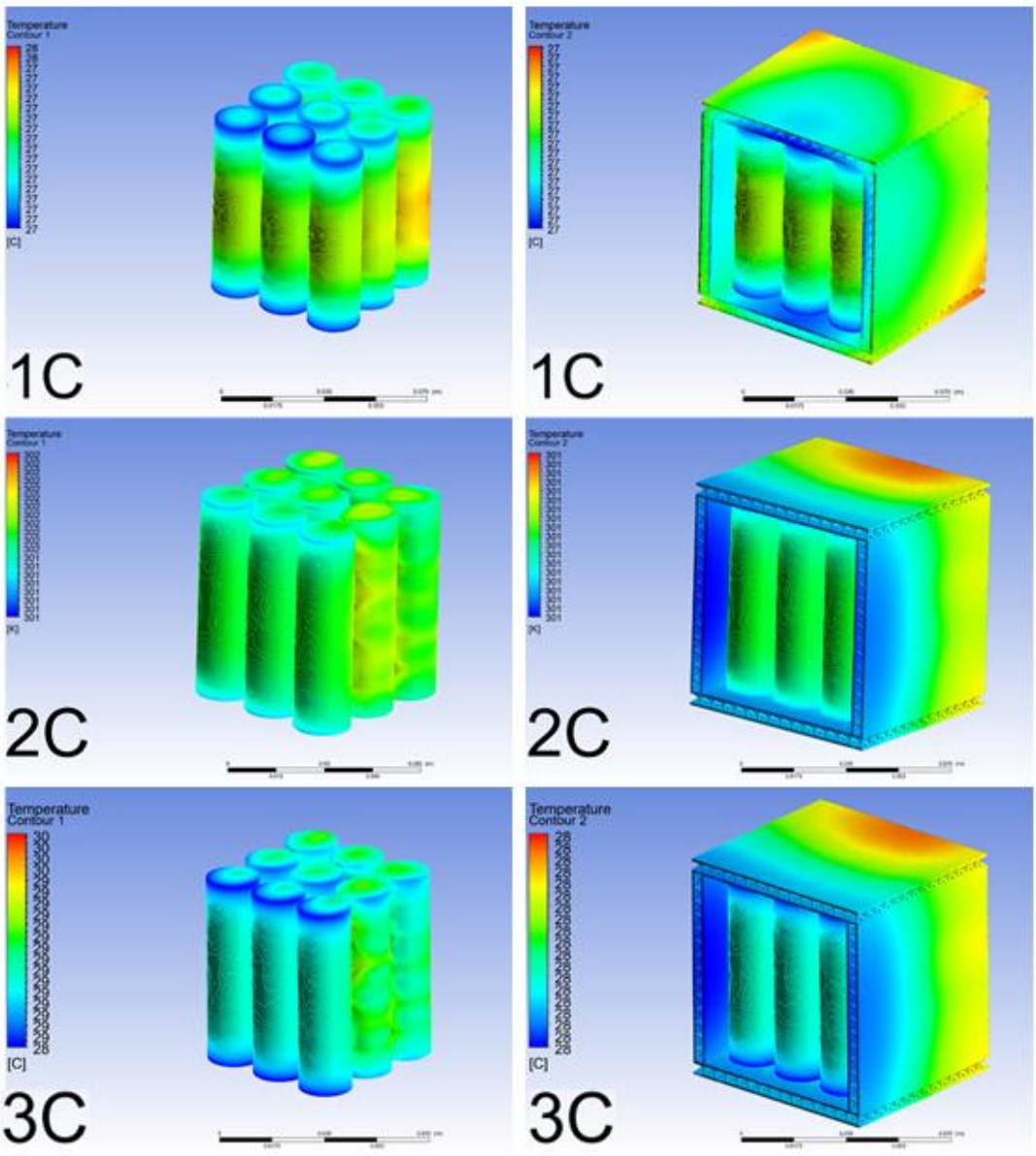

Figure 41. Cells and pack temperature distribution at 5 m/s for 3D kagome battery pack at 1C, 2C and 3C

It can be observed that 3D kagome maintain effective temperature range, and cools appropriately at 5m/s. Also, 3D kagome behaves similar to plainsheet at 1C, and 3.7% at both 2C and 3C when cooled by 5 m/s air speed.

4.2.3.3 Honeycomb Battery Pack at 5 m/s

The simulation of honeycomb battery pack subjected to fan velocity of 5m/s as shown in Fig.42, indicated that the maximum temperatures recorded at the cells and battery

protection were 28°C and 27°C, respectively, at the discharge rate of 1C. With the discharge rate of 2C, these maximum temperatures increased to 32°C for the cells and 27°C for the battery protection. At the discharge rate of 3C, the temperatures further rise to 38°C for the cells and 27°C for the battery protection.

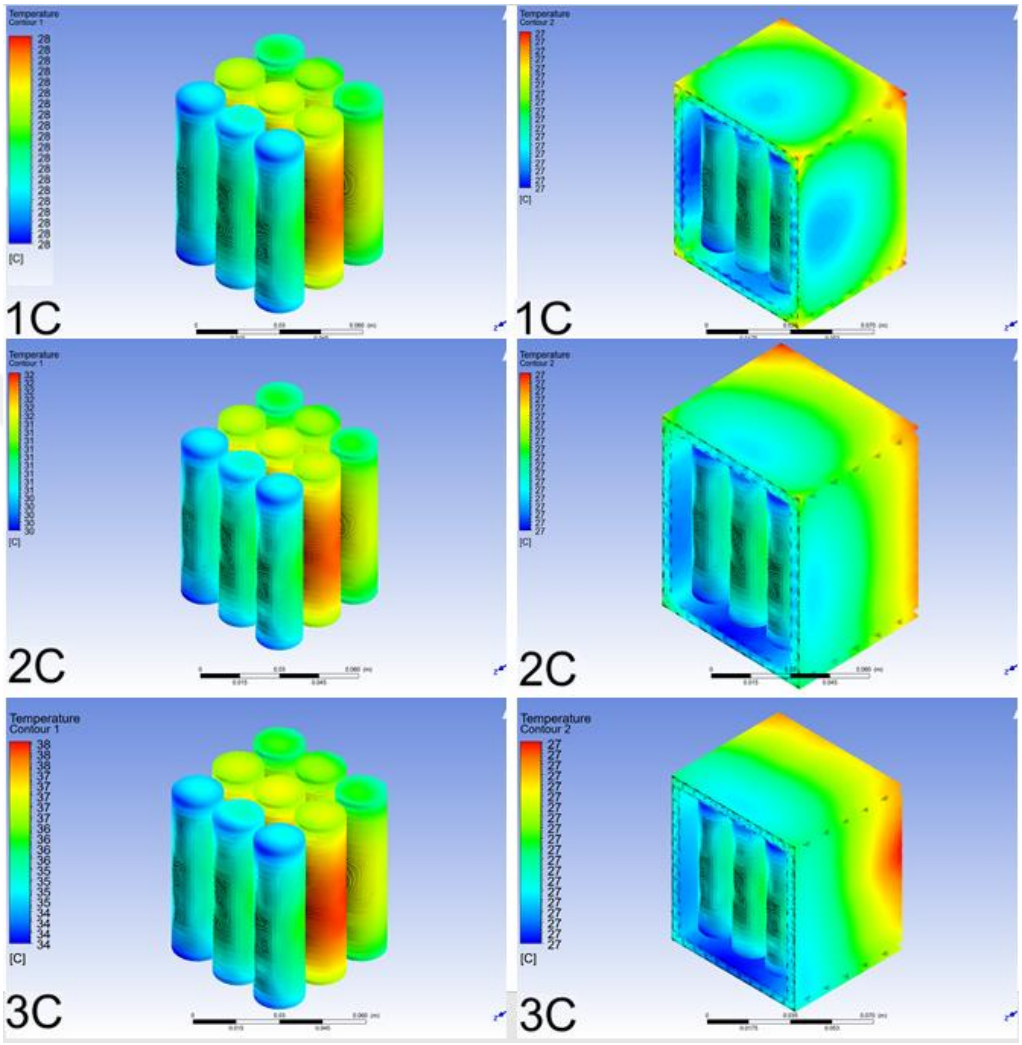

Figure 42. Cells and pack temperature distribution at 5 m/s for honeycomb battery pack at 1C, 2C and 3C

It is observed that honeycomb behaves similar to plainsheet when cooled by 5 m/s air speed at all three discharge rates (1C, 2C and 3C).

4.3.3.4 Navtruss Battery Pack at 5 m/s

The Navtruss battery pack under 5m/s fan velocity recorded maximum temperatures of 29°C in the cells and 28°C in the battery protection at a discharge rate of 1C. Upon

increasing the discharge rate to 2C, the maximum temperatures rise to 31°C for the cells and 27°C for the protection. At a discharge rate of 3C, these values further surged to 36°C for the cells and 28°C for the protection, as shown in Fig.43. This indicates that navtruss battery pack demonstrates effective temperature management at 5m/s, maintaining a stable temperature across different discharge rates.

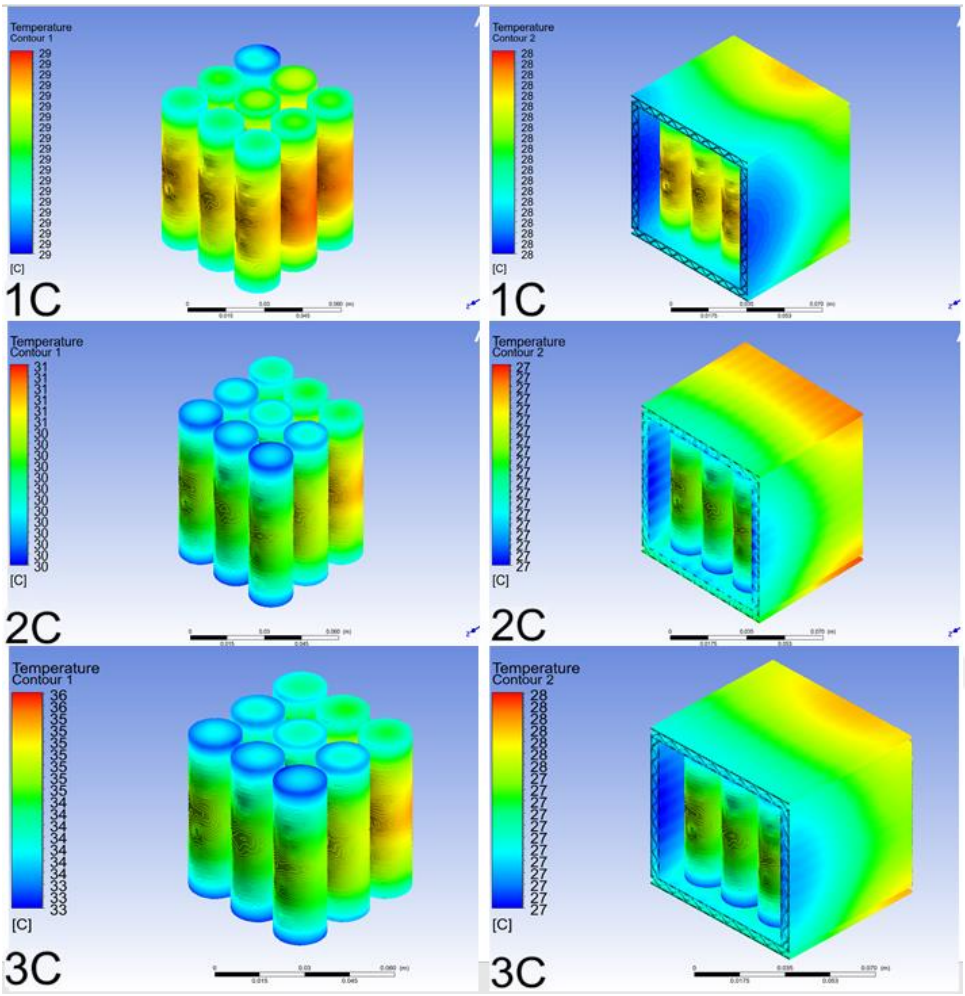

Figure 43. Cells and pack temperature distribution at 5 m/s for navtruss

It is observed that navtruss behaves better than plainsheet by 3.7% at 1C and 3C, but behaves similar to it at 2C when cooled by 5 m/s air speed.

4.3.3.5 Cross-semicircle Battery Pack at 5m/s

The cross-semicircle battery pack under 5m/s fan velocity recorded maximum temperatures of 28°C in the cells and 27°C in the battery protection at a discharge rate

of 1C. Upon increasing the discharge rate to 2C, the maximum temperatures rise to 32°C for the cells and 27°C for the protection. At a discharge rate of 3C, these values further surged to 39°C for the cells and 27°C for the protection, as shown in Fig.44. This indicates that cross-semicircle battery pack demonstrates effective temperature management at 5m/s, maintaining a stable pack temperature of 27°C across different discharge rates.

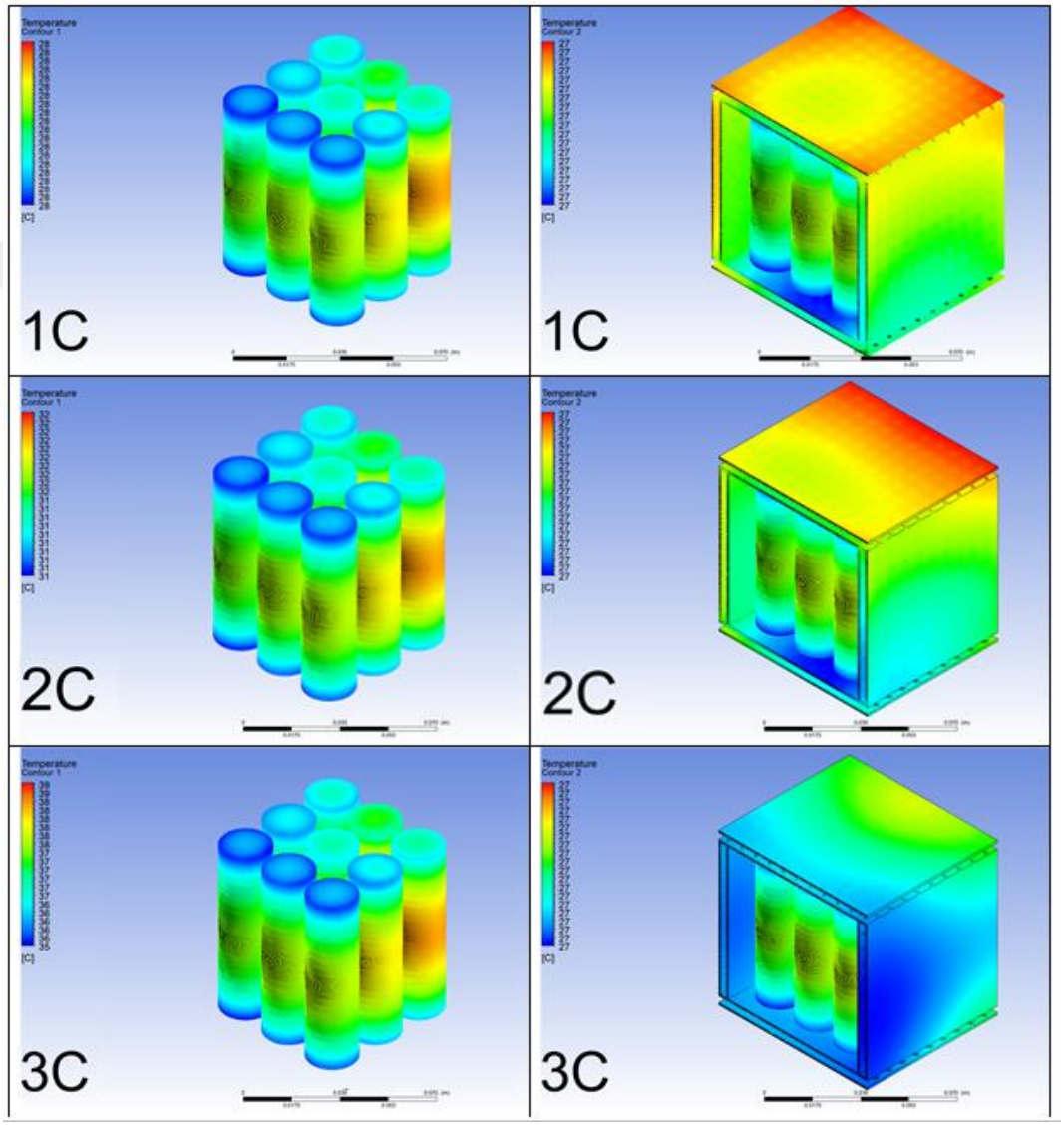

Figure 44. Cells and pack temperature distribution at 5 m/s for cross-semicircle battery pack at 1C, 2C and 3C

It is observed that cross-semicircle behaves similar to plainsheet at all disharge rates (1C, 2C and 3C) when cooled by 5 m/s air speed.

As summarized in Table13, for air velocity of 5 m/s, all battery pack configurations (Plain Sheet, 3D Kagome, Honeycomb, and Navtruss) manage to keep temperatures within the optimal range of below 60°C at all discharge rates effectively.

Table 13. Heat transfer at 5m/s summary

C-rate	Location	Plain Sheet (°C)	3D Kagome (°C)	Honeycomb (°C)	Navtruss (°C)	Cross Semicircle (°C)
1C	Cell	27	28	28	29	28
	Pack	27	27	27	28	27
2C	Cell	29	29	32	31	32
	Pack	27	28	27	27	27
3C	Cell	31	30	38	36	39
	Pack	27	28	27	28	27

CHAPTER 5

EXPERIMENTAL STUDY

Experimental study was only conducted on 3D kagome and plain sheet battery packs, to compare the thermal behavior of lattice-structured battery packs to those of a plain sheet metal.

In material and methods section, we mentioned the expected discharging rates and SOC percentage value for both plain sheet and 3D kagome.

The experiments were initiated with batteries at 95% SOC and were concluded at different SOC levels. The experiments were intentionally stopped at particular SOC points, as represented in Table14, to ensure that the temperature is kept within an appropriate range.

Table 14. SOC start and end levels

				Plain Sheet [%]	3D Kagome	
			SOC [%]			
	Discharge Rate	Fan Velocity [m/s]	Starts	Ends	Ends	Temp Over 60°C
Natural Convection	1C	-	95	12	12	Not
	2C	-		31	33	Excess
	3C	-		38	36	Excess
Forced Convection	1C	1		12	12	Not
		2.5		12	12	Not
		5		12	12	Not
	2C	1		10	10	Not
		2.5		10	10	Not
		5		10	10	Not
	3C	1		40	40	Excess
		2.5		8	7	Excess
		5		3	3	Not

The temperature data are recorded from multiple sensors located at key positions across the battery protection and the cells. The sensor positions at the battery pack includes the front top, middle top, rear top, and right middle positions of the battery protection. It also includes measurements from different positions on the cells such as the front of the first center cell, the front and the rear of the middle center cell, and the rear side of the cell situated at the back center. These readings offer insights into temperature variations and heat dissipation within the battery pack enabling the identification of potential hotspots.

5.1 Natural Convection Heat Transfer

The graphs represents thermal behavior of plain sheet and 3D kagome battery packs during battery discharge at natural convection and different discharge rates. The results obtained during the experiments are shown in figures below.

As depicted in Fig.45, at a discharge rate of 1C, the maximum temperatures observed were 46°C for the cells and 37°C for the battery protection in conventional plain sheet battery packs. In contrast, the 3D kagome packs recorded temperatures of 46°C for the cells and 36°C for the protection. The 3D kagome battery pack demonstrates a lower thermal performance, achieving a temperature of 46°C in just 40 minutes, in contrast to the plain sheet battery pack, which takes 43 minutes to reach the same temperature. In terms of battery protection, the plain sheet pack attains approximately 37°C after 43 minutes, while the 3D kagome pack stabilizes at a marginally lower temperature of 36°C within the 40-minute timeframe during natural 1C discharge rate.

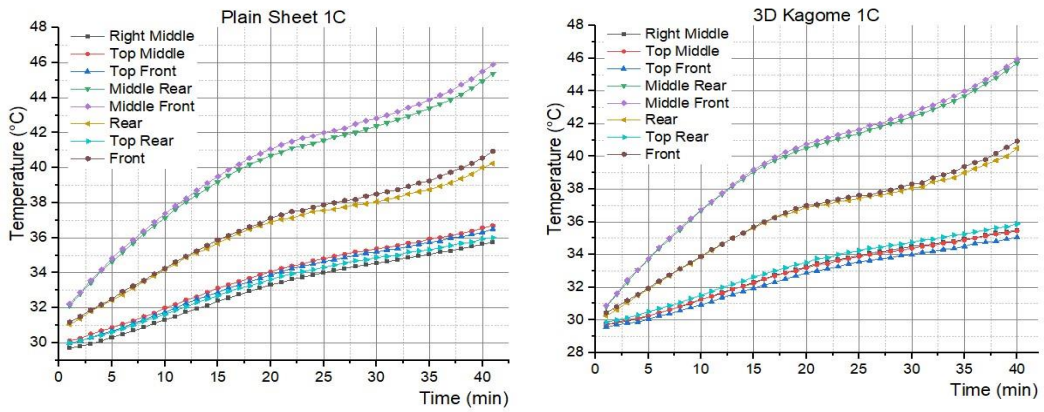

Figure 45. Natural convection heat transfer of plainsheet and 3D kagome at 1C

For 2C natural convection, the results shown in Fig.46 demonstrate that the highest temperatures measured were 60°C for the cells and 42°C for the battery protection in standard plain sheet battery pack, conversely, the 3D kagome battery pack showed the maximum temperature of 57°C for the cells and 39°C for the battery protection. It took 14 minutes for the plain sheet battery pack to discharge to 42°C and 10 minutes for 3D kagome battery pack to discharge to 39°C. When compared to plain sheet, 3D kagome battery pack demonstrates a quicker discharge, but keeps the battery pack at a lower temperature of 37°C compared to 42°C of plain sheet battery pack for approximately same maximum cell temperature.

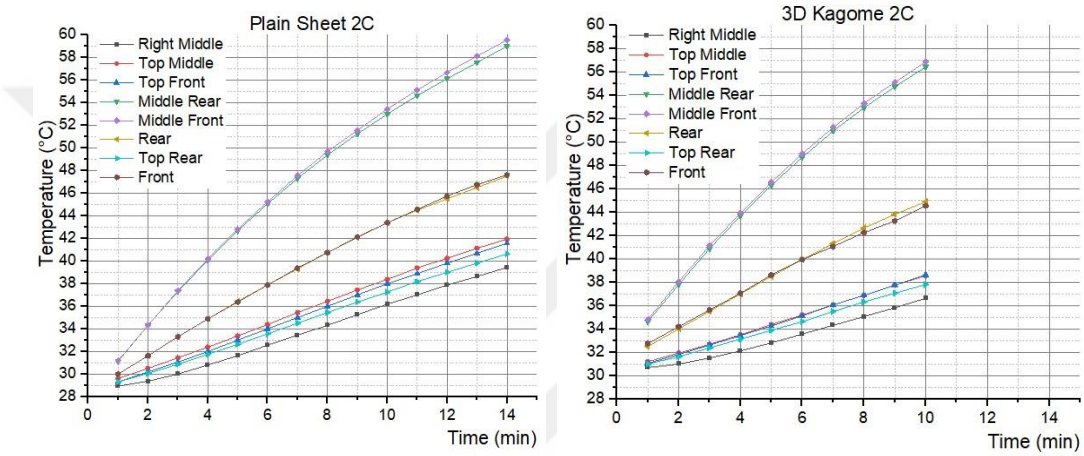

Figure 46. Natural convection heat transfer of plainsheet and 3D kagome at 2C

For the 3C discharge rate, the plain sheet battery pack took 5 minutes to reach maximum cell temperature of 60°C, whereas the 3D kagome battery pack attained 61°C within the same duration. This comparison indicates that the 3D kagome battery pack discharges more swiftly than its plain sheet counterpart. However, it maintains a lower temperature of 42°C, in contrast to the 45°C observed in the plain sheet battery protection, despite both batteries approaching similar maximum cell temperature as shown in Fig. 47.

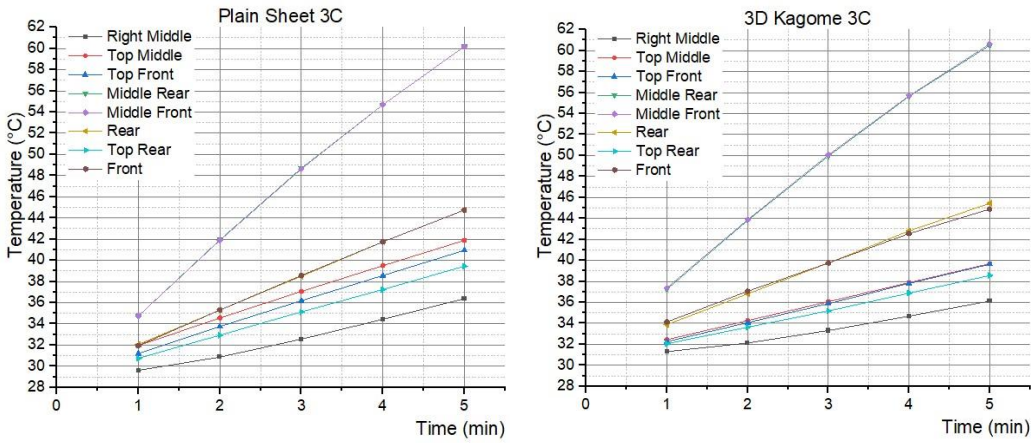

Figure 47. Natural convection heat transfer of plainsheet and 3D kagome at 3C

5.2 Forced Convection Heat Transfer

The graphs represents thermal behavior of battery packs during battery discharge at different air velocities and discharge rates. The results obtained during the experiments are shown in figures below.

5.2.1 At velocity 1m/s

For 1C discharge rate, the plain sheet battery pack took 39 minutes to reach maximum cell temperature of 40°C, whereas the 3D kagome battery pack attained 41°C within the same duration. This comparison indicates that the 3D kagome battery pack discharges more swiftly than its plain sheet counterpart. However, it maintains a lower temperature of 32°C, in contrast to the 31°C observed in the plain sheet battery protection, as shown in Fig. 48.

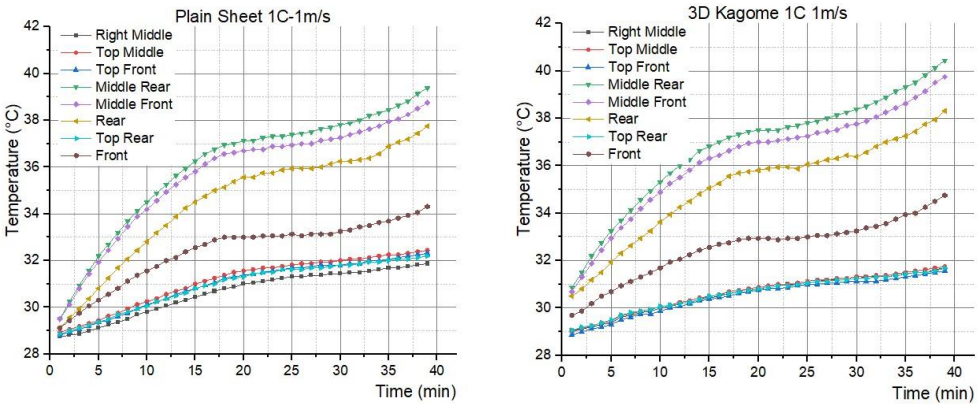

Figure 48. Cells and pack temperatures at specific sensor positions for 1C at 1m/s

At 2C and air velocity of 1m/s, It took 15 minutes for the plain sheet battery pack to discharge to 56°C and 18 minutes for 3D kagome battery pack to discharge to 59°C. When compared to 3D kagome, plain sheet battery pack demonstrates a quicker discharge. 3D kagome keeps the battery protection at a lower temperature of 37°C compared to 40°C of plain sheet battery pack for approximately same maximum cell temperature, as shown in Fig.49.

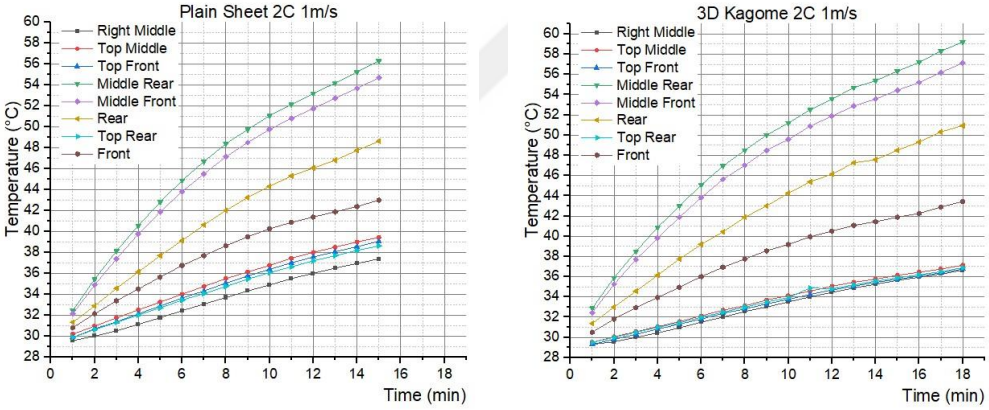

Figure 49. Cells and pack temperatures at specific sensor positions for 2C at 1m/s

For the 3C discharge rate, the plain sheet battery pack took 5 minutes to reach maximum cell temperature of 60°C, whereas the 3D kagome battery pack attained 61°C within the same duration. This comparison indicates that the 3D kagome battery pack discharges more swiftly than its plain sheet counterpart. However, it maintains a lower temperature of 42°C, in contrast to the 45°C observed in the plain sheet battery protection, despite both batteries approaching similar maximum cell temperature as shown in Fig.50.

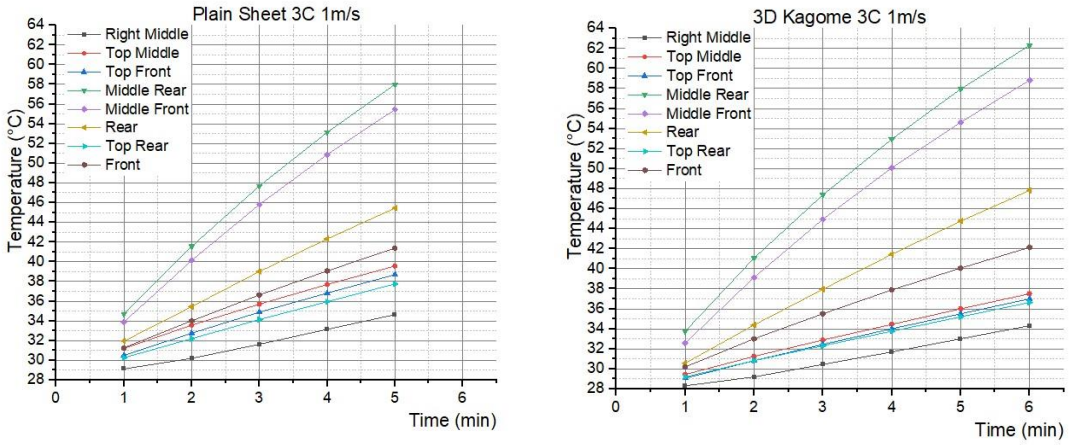

Figure 50. Cells and pack temperatures at specific sensor positions for 2C at 1m/s

5.2.2 At Velocity 2.5m/s

For 1C discharge rate, the plain sheet battery pack took 37 minutes to reach maximum cell temperature of 34°C, whereas the 3D kagome battery pack attained approximately 35°C within 39min. This comparison indicates that the 3D kagome battery pack discharges more swiftly than its plain sheet counterpart. However, it maintains similar maximum cells temperature of 30°C to both plain sheet and 3D kagome, as shown in Fig.51.

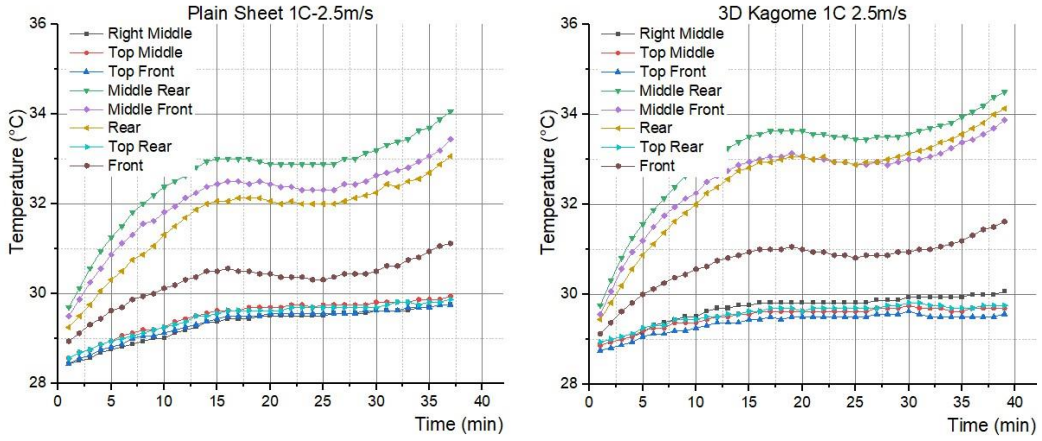

Figure 51. Cells and pack temperatures at specific sensor positions for 1C at 2.5m/s

At 2C and air velocity of 2.5m/s, It took 18 minutes for plain sheet and 20 minutes for 3D kagome battery pack to discharge to 47°C. 3D kagome keeps the battery protection

at a lower temperature of 33°C compared to 35°C of plain sheet battery pack for approximately same maximum cell temperature, as shown in Fig.52.

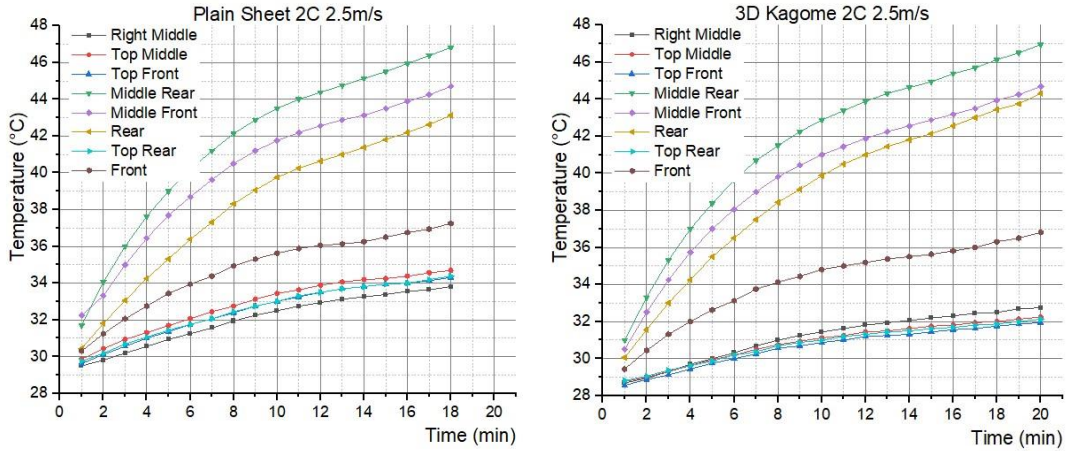

Figure 52. Cells and pack temperatures at specific sensor positions for 2C at 2.5m/s

For the 3C discharge rate, both battery pack cells discharge about 60°C in 10 minutes. 3D kagome protection maintains a lower temperature of 35°C, in contrast to 40°C observed in the plain sheet battery protection, despite both batteries approaching similar maximum cell temperature as shown in Fig.53.

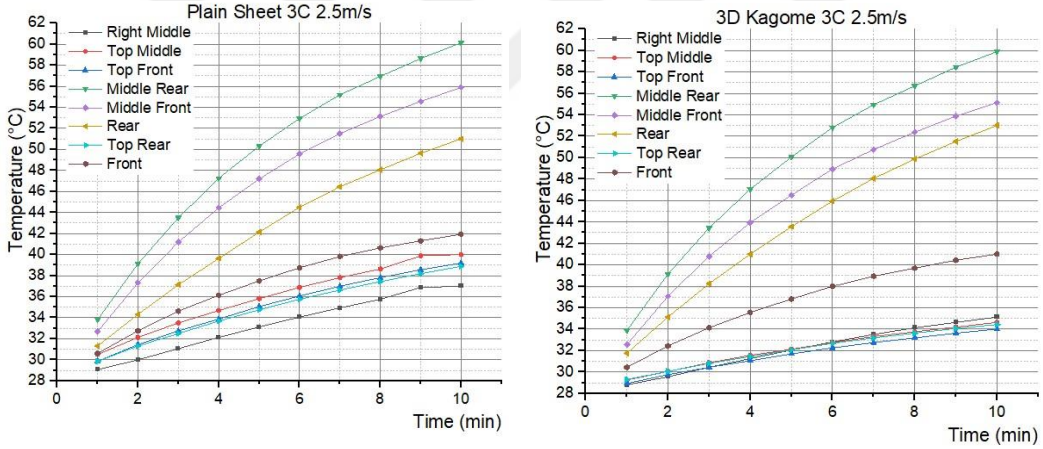

Figure 53. Cells and pack temperatures at specific sensor positions for 3C at 2.5m/s

5.2.3 At Velocity 5m/s

For 1C discharge rate, plain sheet battery pack took 38 minutes to reach maximum cell temperature of 32°C, whereas the 3D kagome battery pack attained it within the 39 minutes. This comparison indicates that the 3D kagome battery pack discharges faster

than plain sheet battery pack. However, it maintains similar pack temperature of 29°C, as shown in Fig.54.

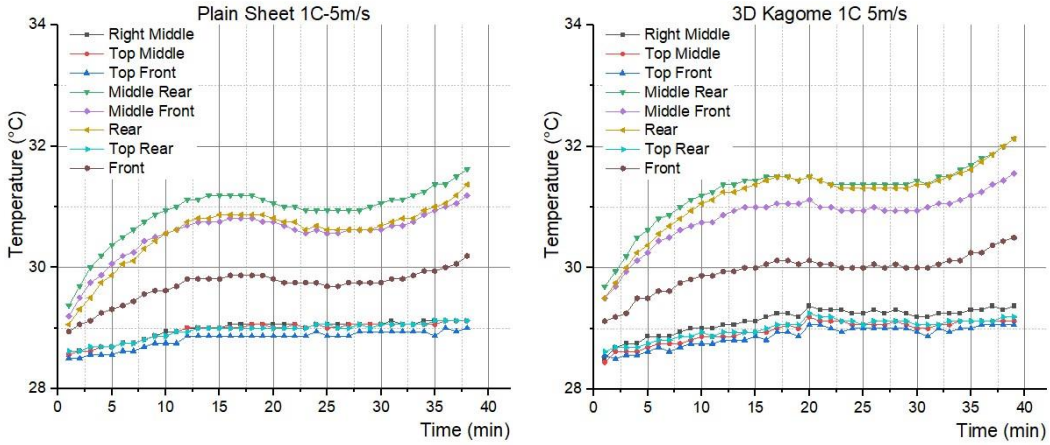

Figure 54. Cells and pack temperatures at specific sensor positions for 1C at 5m/s

At 2C and air velocity of 5 m/s, It took 18 minutes for both battery packs to discharge to 39°C. Within the same time, 3D kagome battery protection maintained 31°C as opposed to 32°C of plain sheet battery pack, as shown in Fig.55.

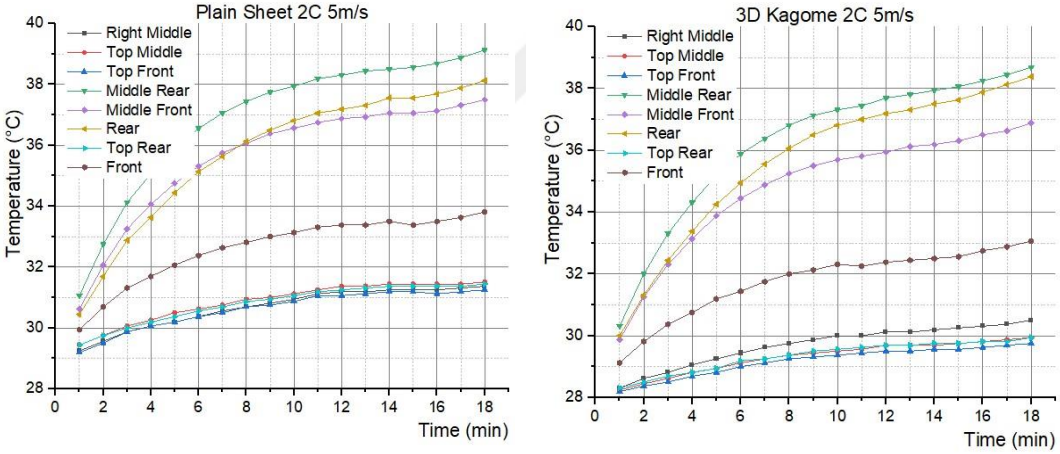

Figure 55. Cells and pack temperatures at specific sensor positions for 2C at 5m/s

For the 3C discharge rate, it took 15 minutes for the plain sheet battery pack to reach maximum cell temperature of 51°C, and 16 minutes for 3D kagome battery pack. It maintains a lower temperature of 33°C, in contrast to the 35°C observed in the plain

sheet battery protection, despite both batteries approaching similar maximum cell temperature, as shown in Fig.56.

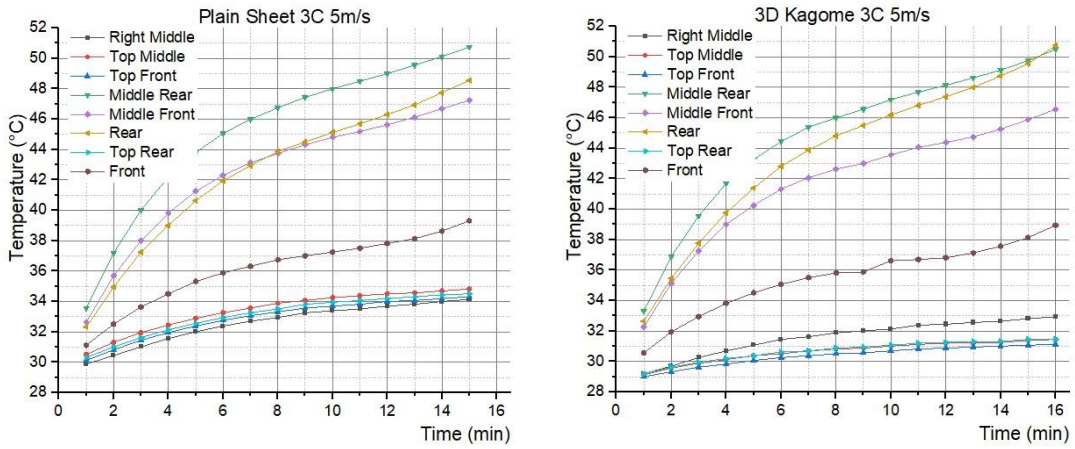

Figure 56. Cells and pack temperatures at specific sensor positions for 3C at 5m/s

CHAPTER 6

CONCLUSION

A research was done to analyze the thermal behavior of an air-cooled battery pack with different lattice structures. Different simulations were conducted to evaluate thermal brhavior of various battery pack configurations such as Plain Sheet, 3D Kagome, Honeycomb and Navtruss at different discharge rates and air velocities. The main objective of these simulations was to determine the ability of each lattice battery pack to dissipate heat under varying conditions compared to the plain sheet battery pack, with emphasis on their ability to maintain temperatures below 60°C the maximum optimal temperature of li-ion cells.

The analysis on the effect of air speed on cooling performance indicates that 3D Kagome and Navtruss consistently achieve a 3.7% improvement over the plain sheet at discharge rates of 2C and 3C, applicable to both 2.5 m/s and 5 m/s air speeds This finding suggests that their performance is stable across varying air velocities. Conversely, Honeycomb and Cross-Semicircle structures exhibit performance levels comparable to the plain sheet at both air speeds and all discharge rates, indicating that these designs do not derive substantial advantages from enhanced air speed.

In the context of performance evaluation across discharge rates, 3D Kagome and Navtruss stand out with a remarkable enhancement, achieving a 3.7% superior performance compared to the plain sheet at discharge rates of 2C and 3C. At a discharge rate of 1C, their performance is either comparable to or marginally better than that of the plain sheet, depending on the air speed conditions. Conversely, Honeycomb consistently reflects the performance characteristics of the plain sheet across all discharge rates and air speeds. The Cross-Semicircle configuration, while exhibiting improved performance at a discharge rate of 3C with an air speed of 2.5

m/s, maintains a performance level similar to that of the plain sheet across all discharge rates when subjected to a 5 m/s air speed.

The general observation relating both the simulation and the experiment is that plain sheet battery protection manage to keep temperatures within an optimal range when increased airflow is applied or at 1C for natural convection. Both analysis highlight that 3D kagome is particularly more effective at maintaining lower temperatures across higher discharge rates with increased airflow.

For future work, a control system can be created to prevent overcharging and over-discharging of battery cells and promote their best performance. This can also help minimize risks associated with extreme charging. Moreover, it is necessary to study other methods of cooling like liquid cooling as well as PCM which can greatly improve thermal management to ensure that temperatures of batteries are kept within safe limits. Also, transient simulation should be done since it will give a better understanding on how different battery systems behave dynamically under various operational conditions which is a more realistic scenario. These studies if implemented will enhance efficiency, safety and durability of batteries used in UAVs.

REFERENCES

[1] X. Zhang, Z. Li, L. Luo, Y. Fan, and Z. Du, “A review on thermal management of lithium-ion batteries for electric vehicles,” 2021.

[2] Q. Wang, B. Jiang, B. Li, and Y. Yan, “A Critical Review of Thermal Management Models and Solutions of Lithium-ion Batteries for the Development of Pure Electric Vehicles.”

[3] X. Feng, M. Ouyang, X. Liu, L. Lu, Y. Xia, and X. He, “Thermal runaway mechanism of lithium ion battery for electric vehicles: A review,” Jan. 01, 2018, *Elsevier B.V.* doi: 10.1016/j.ensm.2017.05.013.

[4] A. B. Al Tahhan, M. AlKhedher, M. Ramadan, A. ElCheikh, D. S. Choi, and M. Ghazal, “Experimental and numerical analysis of a liquid-air hybrid system for advanced battery thermal management,” *Appl Therm Eng*, vol. 253, Sep. 2024, doi: 10.1016/j.applthermaleng.2024.123754.

[5] O. Yetik and T. H. Karakoc, “Thermal management system with nanofluids for hybrid electric aircraft battery,” *Int J Energy Res*, vol. 45, no. 6, pp. 8919–8931, May 2021, doi: 10.1002/er.6425.

[6] M. Coutinho *et al.*, “A review on the recent developments in thermal management systems for hybrid-electric aircraft,” Jun. 05, 2023, *Elsevier Ltd*. doi: 10.1016/j.applthermaleng.2023.120427.

[7] E. J. Adler, B. J. Brelje, and J. R. R. A. Martins, “Thermal Management System Optimization for a Parallel Hybrid Aircraft Considering Mission Fuel Burn,” *Aerospace*, vol. 9, no. 5, May 2022, doi: 10.3390/aerospace9050243.

[8] J. W. Chapman, H. Hasseeb, and S. Schnulo, “Thermal management system design for electrified aircraft propulsion concepts,” in *AIAA Propulsion and Energy 2020 Forum*, American Institute of Aeronautics and Astronautics Inc, AIAA, 2020, pp. 1–23. doi: 10.2514/6.2020-3571.

[9] D. Kim, S. Abdallahh, G. Bosi, and A. Hales, “A Numerical Study of the Suitability of Phase-Change Materials for Battery Thermal Management in Flight Applications,” *World Electric Vehicle Journal*, vol. 14, no. 1, Jan. 2023, doi: 10.3390/wevj14010015.

[10] B. J. Brelje, J. P. Jasa, J. R. R. A. Martins, and J. S. Gray, “C2-Restricted Development of a Conceptual-Level Thermal Management System Design Capability in OpenConcept.”

[11] E. Gültekin and M. Yahşi, “Dynamic compression and impact analyses of the lattice structures for battery safety,” *Proceedings of the Institution of*

Mechanical Engineers, Part D: Journal of Automobile Engineering, vol. 237, no. 5, pp. 930–940, Apr. 2023, doi: 10.1177/09544070221149812.

[12] E. GÜLTEKİN and M. YAHŞİ, "Investigation of Lattice Structures for the Battery Pack Protection," *International Journal of Automotive Science and Technology*, vol. 5, no. 4, pp. 331–338, Dec. 2021, doi: 10.30939/ijastech..1020932.

[13] T. M. O. H. MORIOKA Norikoarch, " Moving to an All-Electric Aircraft System," *IHI Engineering Review*, 2014.

[14] H. Kellermann, M. Lüdemann, M. Pohl, and M. Hornung, "Design and Optimization of Ram Air-Based Thermal Management Systems for Hybrid-Electric Aircraft," 2020, doi: 10.3390/aerospace.

[15] L. Tom, M. Khowja, G. Vakil, and C. Gerada, "Commercial aircraft electrification—current state and future scope," Dec. 01, 2021, *MDPI*. doi: 10.3390/en14248381.

[16] K. Saqli *et al.*, "Electric and Thermal Model of Li-ion battery pack with cylindrical components Electric and Thermal Model of Li-ion battery pack with cylindrical components 1 st Khadija SAQLI 2 nd Houda BOUCHAREB 5 th Mohammed OUDGHIRI." [Online]. Available: https://orcid.org/0000-0002-9485-64294rdAzizNAAMANE

[17] D. Sharma, N. Kachate, and K. Baidya, "Hybrid energy storage system design: Outlier performance improvement of x-EV battery pack," in *Materials Today: Proceedings*, Elsevier Ltd, Jan. 2023, pp. 1643–1649. doi: 10.1016/j.matpr.2022.09.434.

[18] L. H. Saw, Y. Ye, and A. A. O. Tay, "Integration issues of lithium-ion battery into electric vehicles battery pack," Feb. 01, 2016, *Elsevier Ltd*. doi: 10.1016/j.jclepro.2015.11.011.

[19] X. Marcelle Arcila, "Comparative study of three electrochemical cell models for the CFD simulation of a battery module," 2021.

[20] P. N. Halimah, S. Rahardian, and B. A. Budiman, "Battery Cells for Electric Vehicles," 2019.

[21] Q. Huang, M. Yan, and Z. Jiang, "Thermal study on single electrodes in lithium-ion battery," *J Power Sources*, vol. 156, no. 2, pp. 541–546, Jun. 2006, doi: 10.1016/j.jpowsour.2005.05.083.

[22] C. Wu *et al.*, "Experimental and numerical studies on lithium-ion battery heat generation behaviors," *Energy Reports*, vol. 9, pp. 5064–5074, Dec. 2023, doi: 10.1016/j.egyr.2023.04.021.

[23] S. Baazouzi, N. Feistel, J. Wanner, I. Landwehr, A. Fill, and K. P. Birke, “Design, Properties, and Manufacturing of Cylindrical Li-Ion Battery Cells—A Generic Overview,” *Batteries*, vol. 9, no. 6, Jun. 2023, doi: 10.3390/batteries9060309.

[24] A. S. J. van Heerden, D. M. Judt, S. Jafari, C. P. Lawson, T. Nikolaidis, and D. Bosak, “Aircraft thermal management: Practices, technology, system architectures, future challenges, and opportunities,” Jan. 01, 2022, *Elsevier Ltd*. doi: 10.1016/j.paerosci.2021.100767.

[25] J. Li and Z. Zhu, “Battery Thermal Management Systems of Electric Vehicles Space for picture.”

[26] G. Zhao, X. Wang, M. Negnevitsky, and H. Zhang, “A review of air-cooling battery thermal management systems for electric and hybrid electric vehicles,” Jul. 31, 2021, *Elsevier B.V.* doi: 10.1016/j.jpowsour.2021.230001.

[27] Z. Xu, G. Yu, T. Zhang, and R. Wang, “Cooling performance of battery pack as affected by inlet position and inlet air velocity in electric vehicle,” *Case Studies in Thermal Engineering*, vol. 39, Nov. 2022, doi: 10.1016/j.csite.2022.102382.

[28] J. Chaudhari, G. K. Singh, M. K. Rathod, and H. M. Ali, “Experimental and computational analysis on lithium-ion battery thermal management system utilizing air cooling with radial fins,” *J Therm Anal Calorim*, vol. 149, no. 1, pp. 203–218, Jan. 2024, doi: 10.1007/s10973-023-12698-w.

[29] G. Satyanarayana, D. Ruben Sudhakar, V. Muthya Goud, J. Ramesh, and G. A. Pathanjali, “Experimental investigation and comparative analysis of immersion cooling of lithium-ion batteries using mineral and therminol oil,” *Appl Therm Eng*, vol. 225, May 2023, doi: 10.1016/j.applthermaleng.2023.120187.

[30] A. Sarchami, M. Kiani, M. Najafi, and E. Houshfar, “Experimental investigation of the innovated indirect-cooling system for Li-ion battery packs under fast charging and discharging,” *J Energy Storage*, vol. 61, May 2023, doi: 10.1016/j.est.2023.106730.

[31] H. Xu, X. Zhang, G. Xiang, and H. Li, “Optimization of liquid cooling and heat dissipation system of lithium-ion battery packs of automobile,” *Case Studies in Thermal Engineering*, vol. 26, Aug. 2021, doi: 10.1016/j.csite.2021.101012.

[32] A. Wazeer, A. Das, C. Abeykoon, A. Sinha, and A. Karmakar, “Phase change materials for battery thermal management of electric and hybrid vehicles: A review,” *Energy Nexus*, vol. 7, Sep. 2022, doi: 10.1016/j.nexus.2022.100131.

[33] R. Huang, Z. Li, W. Hong, Q. Wu, and X. Yu, “Experimental and numerical study of PCM thermophysical parameters on lithium-ion battery thermal

management," *Energy Reports*, vol. 6, pp. 8–19, Dec. 2020, doi: 10.1016/j.egyr.2019.09.060.

[34] W. Zhuang, Z. Liu, H. Su, and G. Chen, "An intelligent thermal management system for optimized lithium-ion battery pack," *Appl Therm Eng*, vol. 189, May 2021, doi: 10.1016/j.applthermaleng.2021.116767.

[35] B. Ashok *et al.*, "Towards Safer and Smarter Design for Lithium-Ion-Battery-Powered Electric Vehicles: A Comprehensive Review on Control Strategy Architecture of Battery Management System," *Energies (Basel)*, vol. 15, no. 12, Jun. 2022, doi: 10.3390/en15124227.

[36] R. Ranjith Kumar, C. Bharatiraja, K. Udhayakumar, S. Devakirubakaran, K. S. Sekar, and L. Mihet-Popa, "Advances in Batteries, Battery Modeling, Battery Management System, Battery Thermal Management, SOC, SOH, and Charge/Discharge Characteristics in EV Applications," 2023, *Institute of Electrical and Electronics Engineers Inc.* doi: 10.1109/ACCESS.2023.3318121.

[37] C. Kang, J. Yang, X. Yuan, C. Qiu, and Y. Cai, "A novel multilayer composite structure based battery thermal management system," *Front Energy Res*, vol. 11, 2023, doi: 10.3389/fenrg.2023.1187904.

[38] Y. Yu *et al.*, "A Low-Density Polyethylene-Reinforced Ternary Phase-Change Composite with High Thermal Conductivity for Battery Thermal Management," *Energies (Basel)*, vol. 16, no. 9, May 2023, doi: 10.3390/en16093838.

[39] J. Wang, M. Schutzeichel, B. Plaumann, T. Kletschkowski, and A. Panesar, "Multidisciplinary design optimisation of lattice-based battery housing for electric vehicles," *Sci Rep*, vol. 14, no. 1, Dec. 2024, doi: 10.1038/s41598-024-60124-4.

[40] J. Baumeister, J. Weise, E. Hirtz, K. Höhne, and J. Hohe, "Applications of Aluminum Hybrid Foam Sandwiches in Battery Housings for Electric Vehicles," *Procedia Materials Science*, vol. 4, pp. 317–321, 2014, doi: 10.1016/j.mspro.2014.07.565.

[41] C. Alaoui, "Solid-state thermal management for lithium-ion EV batteries," *IEEE Trans Veh Technol*, vol. 62, no. 1, pp. 98–107, 2013, doi: 10.1109/TVT.2012.2214246.

[42] L. Zhu and C. E. Christoffersen, "Transient and steady-state analysis of nonlinear RF and microwave circuits," *EURASIP J Wirel Commun Netw*, vol. 2006, 2006, doi: 10.1155/WCN/2006/32097.

[43] O. Kalkan, “Thermal performance improvement of an air-cooled 18650 NMC battery module: A novel busbar design that acts as a turbulator,” *J Energy Storage*, vol. 88, May 2024, doi: 10.1016/j.est.2024.111613.

[44] “Aluminum 6061-T6; 6061-T651.”

[45] GAZI UNIVERSITY ADDITIVE MANUFACTURING TECHNOLOGY APPLICATION AND RESEARCH CENTER EKTAM, “Concept Laser M2 Cusing SLM Machine,” https://ektam.gazi.edu.tr/view/page/247540/concept-laser-m2-cusing-slm-machine.

[46] “RAPID PROTOTYPE LAB”.

[47] “A28_Public_Datasheet”.

[48] Den kotov, “Skywalker X8,” https://grabcad.com/library/skywalker-x8-2.